

# THE RADIO AND ELECTRONIC ENGINEER

## The Journal of the British Institution of Radio Engineers

FOUNDED 1925 INCORPORATED BY ROYAL CHARTER 1961

*"To promote the advancement of radio, electronics and kindred subjects by the exchange of information in these branches of engineering."*

---

VOLUME 27

FEBRUARY 1964

NUMBER 2

---

### COLD CATHODE TUBES AND THEIR APPLICATIONS

FOR the past decade solid-state circuits have captured the imagination of the design engineer—the invention of the transistor has, in fact, revolutionized the art of radio and electronic engineering. Inevitably this concentration on the exploitation of a versatile new technique has tended to overshadow developments in the older and more established fields. Improvements, in both thermionic valves and gas discharge tubes have, nevertheless, gone on apace—maybe spurred on by competition from the semi-conductor itself! Today the experienced design engineer is realizing that valves and semi-conductors are, to a large extent, complementary and that he must keep abreast of developments in both fields.

Of all the tubes now available, perhaps those bracketed under the broad heading 'Cold Cathode' have been given least attention of late. It is with this particularly in mind that the Institution's Programme and Papers Committee has set out to acquaint engineers generally with recent developments in the design and application of gas discharge devices by arranging a three-day Symposium on "Cold Cathode Tubes and Their Applications" to be held at Cambridge from 16th–19th March. It would be a mistake to assume that the original proposal was greeted with unanimous enthusiasm: doubts were expressed as to the possibility of obtaining a sufficient number of worthwhile papers to occupy even a day's meeting! In the event however, the response from designers of cold cathode tubes and circuits from all over the world has considerably exceeded that for any comparable Institution Symposium—nearly sixty papers were offered and the Organizing Committee had the invidious task of selecting a balanced programme which could reasonably be presented in the time available.

Some thirty contributions will be presented in the course of three whole-day sessions on "Physics of Operation and Tube Development", "Circuit Design and Reliability" and "Applications of Cold Cathode Tubes". As will be seen from the lists of papers and synopses elsewhere in this issue, coverage is very wide and international in character—seven countries are represented. An innovation in this Symposium Preview issue of *The Radio and Electronic Engineer* is the publication of an introductory paper on Cold Cathode Discharge Tubes, which gives a good idea of the potentialities of the devices, and thus of the value of the Symposium.

All papers to be presented will be preprinted thus enabling the discussion periods to be more fruitful, and many of the papers will be supported by demonstrations in a laboratory close to the lecture theatre of the Cavendish Laboratory where the meetings are being held. The social programme which has become a traditional feature of Brit.I.R.E. Conventions and Symposiums will include a reception on the evening before the Symposium starts and a Dinner in Downing College where many of the delegates who are in Cambridge for the whole period will be able to stay.

The programme of the Symposium has been arranged to give the opportunity for tube designers, circuit engineers and those concerned with applications to come together and examine a broad class of electronic devices which already find considerable use in many fields and which have valuable possibilities in other applications.

A. G. W.

## INSTITUTION NOTICES

### Symposium on 'Cold Cathode Tubes and their Applications'

This issue of *The Radio and Electronic Engineer* gives a preview of the arrangements for the Symposium on 'Cold Cathode Tubes and their Applications' which is to be held in Cambridge from 16th to 19th March next. On pages 117-124 will be found the outline programme and synopses of the papers.

Registration forms for the Symposium were sent out in the January issue and those intending to take part are urged to return completed forms without delay, especially if residential accommodation at Downing College is required since this will be strictly limited. Further copies of the registration form may be obtained from the Institution on request.

All papers are being preprinted but sets of the preprint volumes will *only* be sent beforehand to those who have registered to attend the Symposium. An announcement will be made in the April issue of *The Radio and Electronic Engineer* regarding the wider availability of the papers.

### Symposium on 'Electronics in the Automobile Industry'

The Institution's West Midland Section is joining with the Electronics Section of the South Midland Centre of the Institution of Electrical Engineers in holding a one-day Symposium on the above subject at the University of Birmingham on Tuesday, 7th April.

Further details and registration forms may be obtained from Mr. G. K. Steel, D.I.C., A.M.I.E.E., College of Advanced Technology, Department of Electrical Engineering, Gosta Green, Birmingham, 4.

### Symposium on Microminiaturization

A three day Symposium on Microminiaturization will take place in Edinburgh at the Heriot-Watt College from Friday, 3rd April, to Sunday, 5th April 1964, under the joint sponsorship of the Scottish Section of the British Institution of Radio Engineers and the Electronics and Measurements Section of the Scottish Centre of the Institution of Electrical Engineers.

Further information and registration forms should be requested from the Honorary Secretary of the Brit.I.R.E. Scottish Section, Mr. R. D. Pittilo, B.Sc., A.M.Brit.I.R.E., 35 Crawford Road, Burnside, Glasgow.

### Joint Computer Conference

Sir Edward Playfair, K.C.B., President of the British Computer Society, will present the opening address at the Joint Computer Conference to be held at the Heriot-Watt College, Edinburgh from Tuesday, 31st March to Friday, 3rd April 1964.

The conference which has the theme of 'The impact of users' needs on the design of data processing systems'—is being arranged jointly by the Institution of Electrical Engineers, the British Computer Society and the British Institution of Radio Engineers under the aegis of the United Kingdom Automation Council. Some 40 contributions have been offered for the conference which has been divided into four sessions:

- Programming and operating systems;
- Storage technology and organization;
- Maintenance;
- Input, output and man-machine communications.

The full texts of the contributions will be published in the Conference publication, which will be sent to all who register to attend the conference at least one week before the conference. Registration forms are now available on application to the Secretary, The Institution of Electrical Engineers, Savoy Place, W.C.2.

### E.O.Q.C. Conference—1964

The German Society for Statistical Quality Control will be host Organization to the eighth Annual International Conference on Quality Control to be held from 9-11th September 1964, in Baden-Baden. The theme for this Conference will be: 'Quality Appraisal and Quality Incentives'.

Further particulars may be obtained from The British Productivity Council, Vintry House, Queen Street Place, London E.C.4.

### Correction

The following correction should be made to The Presidential Address published in the January 1964 issue of *The Radio and Electronic Engineer*.

Page 6, 2nd column: after the seventh paragraph add the following paragraphs:

This form of collaboration fosters technical understanding but between all the Institutions, another and more important understanding needs to be fostered: the understanding of the effects of these new advances in technology upon people. This is not the time nor the occasion to embark on a philosophic discourse but we would do well to remember that today we stand on the brink of the second industrial revolution. A technological revolution that can, and will, change the pattern of our lives.

Man, by nature, dislikes change. By nature we associate unchanging conditions with safety and security and likewise we associate change with insecurity and danger. All through life we retain this fear of the dangers of the unknown; our apprehension of the things we do not understand.

*Correction slips may be obtained from the Institution on request.*

# A Survey of Cold Cathode Discharge Tubes

By

D. M. NEALE, B.Sc.†

*This survey is published as an introduction to the Symposium on "Cold Cathode Tubes and their Applications" which is being held in Cambridge in March 1964.*

**Summary:** From the first neon discharge tubes of 1910, a range of devices has evolved covering a remarkable diversity of applications. Voltage regulators and reference tubes are available for voltages from 55 V–27 kV and currents from 1  $\mu$ A–100 mA. Relay tubes offer current gains between  $10^6$  and  $10^{12}$  and provide continuous control of loads of up to 2 kW or switch peak loads of 10 MW. The stepping tube has been developed to provide highly reliable counting at frequencies up to 1 Mc/s.

Electronic flash tubes provide high-intensity light flashes of 1  $\mu$ s–1 ms duration with colour closely approximating daylight. A diversity of gas-filled indicators and register devices provides on-off and in-line digital display of high reliability and long life.

An outline of the historical development of cold cathode tubes is followed by a discussion of the leading characteristics of each class of tube currently available.

## 1. Introduction

It is not practicable in a short survey paper to describe adequately the physical processes involved in the various forms of gas discharge tube. Parker<sup>1</sup> has already covered this ground admirably. It is proposed instead to outline the history of the cold cathode tube and then to indicate some of the distinctive features of the remarkable range of corona, glow and arc discharge tubes now available.

## 2. History

### 2.1. The Neon Lamp

The majority of cold cathode tubes use a gas filling of which neon is the principal constituent. Development of the modern cold cathode tube may thus be said to date from 1898, the year in which Sir William Ramsay discovered neon. Ten years later Georges Claude began to isolate substantial quantities of a helium-neon mixture and in 1910 Claude exhibited two 38-ft neon tubes. These were the precursors of the familiar neon sign and decorative lighting tube of today, in which the light comes principally from the long positive column.

Filament lamps and electric power were both expensive at that time. There was accordingly a strong incentive to develop a cheap and robust lamp of low power consumption and suitable for use on domestic supply voltages. Professor H. E. Watson<sup>2</sup> has described the work which led to the appearance of the domestic neon lamp, first in Germany in 1918 and later in Holland. Once sputtering had been substan-

tially reduced, the design of a 'beehive' neon for 220 V supplies presented few problems. For 110 V supplies, however, an alloy or activated cathode was required in order sufficiently to reduce the cathode fall. The successful development of such a tube by Philips in Holland stimulated renewed activity in the U.S.A. and eventually, in 1929, the General Electric Co. produced a miniature neon indicator. The annual consumption of this type of small tube is now estimated at some 70 million.<sup>3</sup>

### 2.2. Voltage Stabilizers and Trigger Tubes

Work on the neon lamp produced, as a by-product, the voltage stabilizer or regulator. Gradually a range of tubes was developed in which, by choice of electrode materials, geometry and gas-filling, a variety of anode-maintaining voltages was available in the range 50 V to 150 V. Higher voltages were obtained by arranging several gaps in series within one envelope.

By using a corona discharge instead of a glow discharge, still higher voltages were obtained. Today corona stabilizers are available for any voltage between 340 V and 27 kV.

Bell Telephone Laboratories announced the first cold cathode trigger tube in 1936.<sup>4</sup> Using an activated cathode, the 313-A set the pattern for a number of trigger tubes made in Europe during the next two decades. The activated cathode led to anode maintaining and critical trigger voltages each of the order of 70 V. Whilst this relatively low voltage was attractive from the aspect of power economy, it was attended by disadvantages also. The cathode surface was subject to contamination and ageing and the

† Research Department, Ilford Ltd., Brentwood, Essex.

tube characteristics changed accordingly. Triggering was uncertain in complete darkness and spontaneous in bright sunlight.

In 1946, the Philips Research Laboratories described<sup>5</sup> a cathode prepared by a technique conferring life and stability greatly superior to the best obtainable with activated cathodes. Sputtering, which had hitherto led to destruction of the cathode and 'clean-up' of the gas-filling, was used to advantage in the new technique. After the tube was sealed, a pure molybdenum cathode was subjected to heavy sputtering to expose a clean electrode surface. The sputtered-off molybdenum largely cleaned-up gas impurities and, deposited on the envelope, 'gettered' any contaminants released by outgassing of the glass. The lesser degree of sputtering produced during life maintained the tube in a 'new' condition until the cathode was almost completely eroded.

The first commercial tube to use the new technique was the 85A1. It could be used as a stabilizer controlling the voltage appearing across a fluctuating shunt load. Operating at constant current, on the other hand, it provided an altogether new degree of stability and with its descendants, became known as the 'voltage reference tube'.

During the next ten years the same technique was applied to the manufacture of high-stability trigger tubes.<sup>6</sup> Photo-emission could no longer be relied upon to produce primary ionization and the new tubes were accordingly provided with a continuous priming discharge. This slight complication was offset by complete insensitivity to the level of ambient illumination.

Independently, Standard Telephones and Cables had also developed<sup>7</sup> a trigger tube using a pure metal cathode and priming discharge. In this case the objective was the production of a high-speed tube. Rapid deionization was assisted by introducing hydrogen into the gas-filling and also by using an electrode geometry including an additional 'shield' electrode between anode and cathode.

In recent years shield electrodes have been used in a variety of trigger tubes to provide a substantially increased anode breakdown voltage.

### 2.3. Stepping Tubes

The first published account<sup>8</sup> of a multi-cathode stepping tube described a tube developed in America by Remington Rand. The first tubes to be widely used, however, were made in England by S.T.C. and by Ericsson Telephones. For some ten years following its introduction in 1949,<sup>9</sup> the Ericsson 'Dekatron' became practically synonymous with the cold cathode stepping tube. The original double-pulse 'Dekatron' was followed in 1952 by the single-pulse tube<sup>10</sup> operating up to 20 kc/s. Routing guides were added

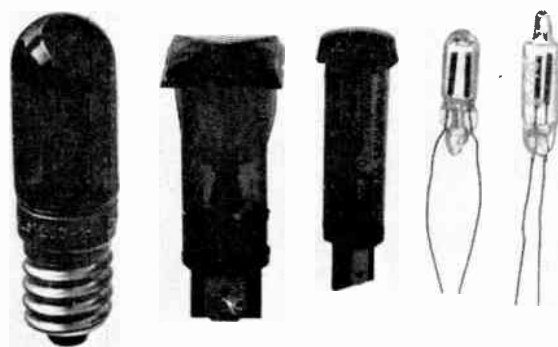


Fig. 1. Indicator diodes. Right to left:—Hivac NT2 and lens-ended version, two Cerberus neon tubes with series resistor enclosed in coloured plastic case, Cerberus diode with coloured fluorescent coating inside envelope.

in 1955 to simplify the construction of reversible scalars.<sup>11</sup> In 1962 auxiliary-anode tubes were introduced from which numerical indicators could be driven directly.<sup>12</sup>

Over the last few years other manufacturers have produced stepping tubes many of which have distinctive features. Elesta announced in 1960<sup>13</sup> a miniature tube operating at up to 1 Mc/s and in 1963<sup>14</sup> a more advanced tube easily driven by transistors, requiring no power supply stabilization and providing a high level output. These improvements are the outcome of unconventional methods of tube construction and operation. By comparison with the conventional stepping tube, the Elesta ECT100 is 'inside-out'; instead of a central disk, the common anode takes the form of a ring outside the star-shaped cathodes.

A new Japanese tube<sup>15</sup> 'inverts' the conventional electrode arrangement. Using a common cathode surrounded by a ring of rod anodes, this tube requires only about half the guide pulse amplitude of a conventional tube. Also it produces less sputtering and can apply the whole of the cathode current directly to a numerical indicator tube.

### 2.4. Numerical Display Tubes

At quite an early date, neon tubes were made with cathodes in the form of letters or other shapes of artistic or advertising value. It is only in the last five years, however, that tubes have been made containing several such cathodes mounted in close super-position and arranged so that any cathode may be chosen to carry the current from a common anode. One of the first such tubes, the S.T.C. GN-1 was designed for operation on a.c. or d.c. More recent designs<sup>16</sup> have all been for d.c., although the tubes are often operated on rectified, unsmoothed a.c. in order to obtain extended life.

Most numerical indicator tubes require a potential difference of at least 40 V between conducting and non-conducting cathodes. As this is an inconveniently large voltage to obtain from most transistor circuits, special indicators have been devised for use with semiconductors. Philips developed in 1959 a numerical indicator<sup>17</sup> providing a display resembling a clock face in which one or more numbers could be illuminated in response to 5 V input signals. The Japanese company, Fujitsu, announced in 1962 a small on-off indicator<sup>18</sup> requiring an input of only 5 V and hence suitable for transistor flip-flops as well as other applications.

### 2.5. Arc Discharge Tubes

Development of the cold cathode arc discharge tube was initiated by Edgerton, Germeshausen and Grier at Massachusetts Institute of Technology. Their work culminated in 1936 in the 'Strobotron'.<sup>19</sup> This tube, like similar tubes produced in this country, was a tetrode in which a discharge between two control electrodes was used to trigger the discharge of a capacitor connected between anode and cathode. It could be used as a stroboscopic light source and also for generating electrical impulses.

Shortly after, further work at M.I.T. led to the high-intensity flash tubes now widely used for photographic purposes.<sup>20</sup> Argon and xenon-krypton gas fillings were chosen to produce a substantially white flash when loaded to an instantaneous dissipation of up to 1 MW.

During the 1940's the properties of the flash discharge tube were studied and developed<sup>21, 22</sup> for possible use in motion picture studios. Some promising results were obtained, but two drawbacks were never overcome: noise and flicker. Each discharge produces an audible click due to the abrupt pressure changes within the tube. Also the high mean power dissipations called for tubes with forced ventilation. Together, these factors were not easily reconciled with the need for a small, silent lamp. At the frequency of flashing corresponding to maximum efficiency of light utilization, i.e. at 24 c/s, the flicker also proved so objectionable that actors were unable to perform well.

A more successful development has been the pulsed xenon arc lamp used in cinema projectors, notably Philips and Bauer. A high proportion of new installations are using machines equipped with these lamps. A high efficiency of light utilization is achieved by switching the lamp on only while the projector shutter is open.

In the development of photographic flash tubes, much was learnt which proved applicable to the design of arc discharge switching tubes capable of holding off up to 50 kV and carrying currents up to about

10 kA for intervals measured in microseconds. It was not until 1961, however, that arc discharge switching tubes were described<sup>23</sup> capable of sustaining continuous currents of several amperes and peak currents of more than 100 A. These arc thyratrons ('Arcotrons') are a product of the Swiss firm, Cerberus. The same company announced a glow thyatron<sup>24</sup> in the following year. Both types of tube were based on the controlled introduction of ions into the main gap rather than the controlled multiplication of primary ionization continuously present.

Even though semiconductors now predominate in certain applications for which cold cathode tubes were at one time considered to show great promise, it would not appear that the gas discharge tube is in any danger of being displaced entirely. On the contrary, the variety of new developments which have occurred since 1960 suggest that cold cathode tube design has now been refined to the point at which new types may be produced with reasonable confidence to meet almost any need.<sup>25</sup>

## 3. Currently Available Tubes

In describing some of the principal types of cold cathode tube currently available, a degree of selection is inevitable. Recently compiled tables<sup>26</sup> list data on over 450 corona and glow-discharge tubes of various kinds. Even these tables exclude most of the several hundred character display tubes which have been manufactured by Burroughs in the U.S.A. Nor do they include arc discharge tubes. Extensive use is also being made of c.c.t.'s in the U.S.S.R.<sup>27</sup> but data on Russian tubes is not available. The world total of cold cathode tube types may therefore be estimated to exceed 1000.

### 3.1. Diodes

#### 3.1.1. Glow discharge tubes

The c.c.t. most widely used today is still the miniature neon indicator. Much was learnt in the development of this tube and much more in attempts to use it in applications for which it was not designed. Specialized tubes have since been developed to meet these applications. Thus, whereas the typical indicator neon has an anode-ignition voltage ( $V_{IG}$ ) of about 75 V and an anode-maintaining voltage ( $V_M$ ) of 55 V, 'difference diodes' have been produced for which the corresponding figures are of the order of 170 V and 60 V. Such tubes provide more reliable operation in logical circuits since the change in anode potential is much greater between the 'off' and 'on' conditions.

Most miniature neon indicators are designed to operate at about 0.5 mA. Voltage stabilizing diodes have been developed for continuous currents of up to 80 mA. Commonly used combinations of cathode and gas filling give maintaining voltages of approxi-

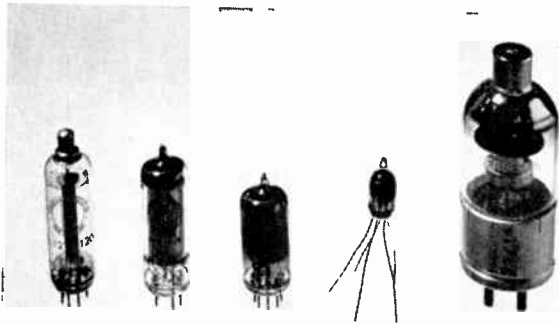


Fig. 2. Corona, glow and arc discharge tubes. Left to right:—English Electric 1200 V corona stabilizer, QS1218/1200; Ericsson 150 V glow stabilizer, GD150M/S; Ericsson 85 V voltage reference tube, GD85M/S; Mullard subminiature twin-trigger tube, Z700W; Cerberus 3A arc thyatron, BT15.

mately 55, 60, 75, 85, 108 and 150 V. In all, about 150 tubes are listed as current types<sup>26</sup> although a proportion of these are direct equivalents.

In general, the activated cathodes used for low-voltage tubes cannot be expected to result in close tube tolerances or in good stability through life. For voltage stabilization, therefore, increasing use is made of the sputtered molybdenum cathode.<sup>5</sup> Voltage reference tubes combine this technique with a geometry designed to minimize temperature coefficient and voltage jumps such as occur spontaneously or with change in current. In the 83A1 the temperature coefficient is  $-0.003\%$  per deg C and voltage jumps are less than  $0.0015\%$  over the current range 3.5 to 6.0 mA. During the first 10 000 working hours the total excursion of  $V_M$  does not exceed the limits  $-0$  to  $+0.4\%$ . Even this performance is bettered considerably during the 2000 hours following an initial burning-in period of 300 hours.

Through a combination of precisely controlled manufacture and accelerated life tests, it has been shown<sup>28</sup> possible to predict the life of cold cathode tubes with a high degree of confidence. For both activated and pure-metal cathodes, the life bears an inverse power law relation to the operating current. At full rated current, the 75C1 provides an estimated life of 10 years. At lower currents this will be greatly extended.

Reference tubes are best operated at constant current and it is thus common practice to obtain a stabilized supply from a diode stabilizer having a higher value of  $V_M$ . Unless a much higher voltage is available from which this additional tube may be operated, difficulty in striking may arise, particularly in the dark. A radioactive isotope may be included in the tube to provide primary ionization assisting striking. When this is done, the anode breakdown

voltage is the same in light or dark. Solid isotopes constitute a slight health hazard in the event of tube breakage and for this reason a gaseous isotope such as tritium is commonly used.

Even when the tube contains a radioactive substance, difficulty is often experienced in striking a stabilizer under on-load conditions. This is due to the potentiometer action of the series ballast resistance and shunt load. A number of tubes are accordingly provided with a priming anode which may be returned through a high resistor to the h.t. supply. The discharge between priming anode and cathode produces ionization in the main discharge gap sufficient to ensure breakdown at a voltage not much above  $V_M$ .

The incremental resistance of a glow discharge stabilizer or reference tube is usually in the range 100 to 400 ohms. Impedance is a function of frequency however. The effective inductance of the tube is greatest at about 100 c/s, but its effect is not significant at frequencies below 500 c/s. Benson has studied and reported on these effects in detail.<sup>29</sup>

The neon-filled tube using a pure molybdenum cathode normally provides a value of  $V_M$  in the range 83 to 85 V. It is, of course, possible to operate two or more tubes in series, but where substantially higher voltages are to be controlled corona discharge tubes are normally employed.

### 3.1.2. Corona discharge tubes

These take the form of a central wire anode surrounded by a cylindrical cathode, the electrode assembly being enclosed in an atmosphere of pure hydrogen. Using a standard electrode assembly, the manufacturer can control the stabilizing voltage by adjusting the pressure of gas-filling, to which it is substantially proportional. Whereas glow discharge stabilizers operate at a relatively small number of arbitrary voltages, therefore, corona stabilizers can be offered for a wide range of uniformly-spaced voltages. Moreover, any intermediate value can be met to special order. Alternative combinations of electrode dimensions may be used in order to avoid the need for pressures above atmospheric.

The problems of initiating a discharge under on-load conditions are not so serious with a corona tube since an excess of only about 50 V is required above the stabilizing voltage.

A minimum current of a few microamperes must be carried by the corona discharge if it is to be self-maintaining.

The maximum current is limited by the danger of breakdown into the glow discharge mode. An increase in tube length provides a proportional increase in maximum current. The manufacturer's maximum rating may also be governed by considerations of tube

life. This is usually limited by the rise in maintaining voltage,  $V_M$ , occurring as gas clean-up occurs. Cohen and Jenkins<sup>30, 31</sup> quote test data suggesting a rise of  $2\frac{1}{2}\%$  in the value of  $V_M$  for a 2 kV tube operated for 10 000 hours at 300  $\mu$ A.

The characteristics of currently-available corona tubes range between 350 V tubes for 1 to 100  $\mu$ A and a 27 kV tube for 50 to 1000  $\mu$ A. A slope resistance of about 100 k $\Omega$  is typical for fluctuations in tube current at or above 50 c/s. For slower changes in tube current, thermal effects in the tube can produce lower, and even negative, values of slope resistance.

### 3.2. Relay Tubes

#### 3.2.1. Trigger glow tubes

When a gas discharge passes from the corona to the glow mode, the effect of space charge provides a positive feedback mechanism leading to an abrupt increase in current of as much as six orders of magnitude. In a trigger tube, two such processes are cascaded so that an even greater current amplification is possible. In a widely used modern tube, the Mullard Z803U, the ratio of anode current to pre-strike trigger current is approximately  $10^6$  to  $10^8$ , depending on whether or not the priming gap is used. A power gain of  $10^{10}$  is possible without exceeding the continuous current rating. An electrometer tube, the Cerberus GR19, draws a pre-strike current of less than  $10^{-12}$  A, provides a current gain of about  $10^{10}$  and a power gain of about  $10^{12}$ . For switching purposes, the cold cathode trigger tube thus fulfils two requirements of a switching device: a high ratio of 'off' to 'on' impedances and a high power gain.

An ideal switch produces no voltage drop during conduction. Bearing this in mind it is understandable

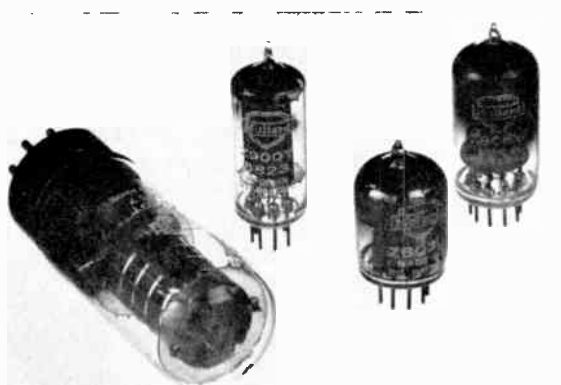


Fig. 3. Mullard trigger tubes. Left to right:—Z300T/1267 and Z900T activated-cathode tubes, Z803U sputtered molybdenum-cathode tube, Z806W sputtered molybdenum-cathode, shielded-anode, close-tolerance tube.

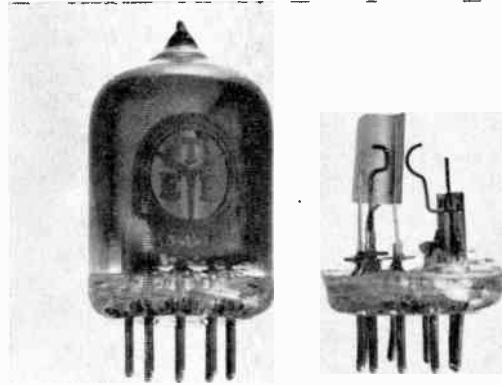


Fig. 4. Molybdenum-cathode trigger tube, CV2434, intact (left) and opened (right) to show (left to right) priming anode, curved cathode plate, curved trigger and straight anode wires. Note washers preventing bridging of insulation between pins by sputtering during manufacture.

that early cold cathode trigger tubes were designed to use the activated cathode with which a relatively low anode maintaining voltage,  $V_M$ , is obtained. For many applications, it is a valuable feature of the trigger tube that the critical trigger voltage,  $V_T$ , provides a built-in voltage reference which is independent of anode supply voltage. When a pure metal cathode is used, both  $V_T$  and  $V_M$  can be held to a closer tolerance and show better stability through life. For such applications, therefore, and particularly for logical circuits involving the interconnection of tubes, the benefits of the pure metal cathode outweigh the disadvantage of its increased power dissipation. Realization of this fact has led to the withdrawal of many trigger tubes using activated cathodes, although some of the more successful designs are still listed.

For at least one application, the activated-cathode remains the better choice. This is for the 'touch-button' tube used for lift call buttons and similar purposes. As this is an 'on-off' application,  $V_T$  need not be particularly stable. On the other hand, if  $V_T$  is low the caller need only become part of a relatively low-voltage circuit.

The majority of modern trigger tubes now use the sputtered molybdenum cathode. Typically this leads to an anode breakdown voltage,  $V_{IG}$ , of about 300 V, an anode maintaining voltage,  $V_M$ , of 100–115 V and a critical trigger voltage,  $V_T$ , of 120–140 V. Maximum continuous current ratings range from 2 to 40 mA, but the larger tubes can sustain peak currents in excess of 2 A for short intervals. Because the work function of a pure metal cathode is not sufficiently low, visible light penetrating the glass envelope will not produce primary ionization by photo-emission. A radioactive isotope assists triggering, but still leaves

a significant statistical delay. The majority of molybdenum cathode tubes are therefore provided with an additional electrode gap in which a discharge of about  $10 \mu\text{A}$  is maintained continuously. Ions or photons from this discharge continuously supply primary ionization of the trigger-cathode gap and so permit of triggering in a time limited only by the formative times of the trigger-cathode and anode-cathode gaps.

Higher values of anode-cathode breakdown voltage,  $V_{IG}$ , are possible in a tube including an intermediate shield electrode held at 50 to 75% of the anode voltage. A number of such tubes provide values of  $V_{IG}$  up to 450 V. They may therefore be used on unsmoothed, rectified a.c. supplies of up to 300 V r.m.s. Not only does this provide a simplification in power supply, but also it allows the circuit to return to the 'off' condition when the trigger potential is reduced, since the tube deionizes each time the anode potential falls to zero.

Two tubes manufactured by Elesta, the ER2 and ER32, have shield electrodes, the potential of which is set by the plasma. The need for external connection is thus eliminated.

Most trigger tubes may not be operated with a negative anode potential exceeding  $-V_M$ . Both Cerberus and Elesta, however, manufacture tubes for operation with raw a.c. anode supplies. The GR16 and ER21A fire with trigger positive, the GR17 and ER22 with trigger negative.

For applications requiring a stable value of  $V_T$ , it is necessary with many tubes to avoid the passage of reverse trigger current. If the trigger serves, even briefly, as a cathode, it will sputter contaminating materials on to the main cathode. As a result the value of  $V_T$  will be raised. This is a problem which is solved by careful circuit design. There is, however, an effect occurring within the tube which leads to a temporary

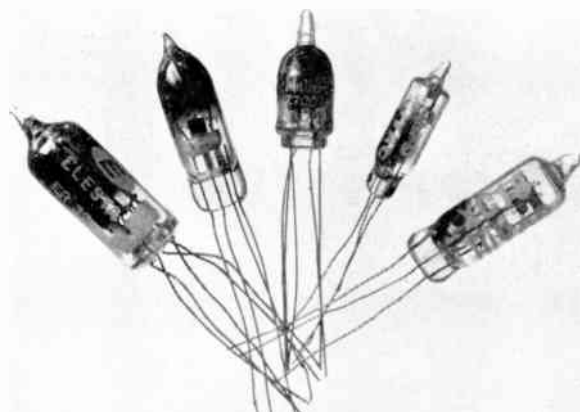


Fig. 5. Subminiature trigger tubes. Left to right:—Elesta ER32, Ericsson GTE120Y, Mullard Z700W, Hivac XC26 and XC18.

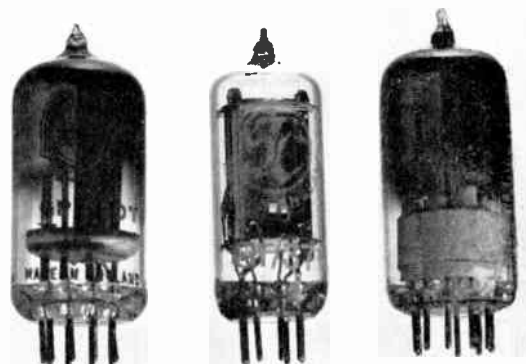


Fig. 6. Shielded-anode trigger tubes. Left to right:—Ericsson GPE120T close-tolerance tube, S.T.C. G1/371K high-speed tube, Elesta ESR2 which contains two 97V stabilizing diodes in the same envelope as the trigger tube.

reduction in  $V_T$  after passage of anode current. This 'trigger hysteresis' is due to electrode heating. In the CV2434 it is of the order of 8 V for an anode current of 25 mA. The formative and recovery time-constants are somewhat below and above 10 seconds respectively. In the Ericsson GPE 120T and the Mullard Z806W, particular care has been taken to minimize trigger hysteresis and the effect is less than 2 V at the worst. Both tubes use shields between anode and cathode.

The total ionization time  $T$ , of a trigger tube is indefinitely long at  $V_T$ , but decreases when an over-voltage is applied to the trigger. In the CV2434,  $T$  is 2 ms for an over-voltage of 0.5 V, but falls to 20  $\mu\text{s}$  for an over-voltage of 10 V.

Deionization time is less easily reduced, since it depends on tube geometry and gas-filling. The choice of gas-filling in turn restricts the choice of electrode materials. In the S.T.C. G1/371K these factors have been adjusted to produce a deionization time of only 30  $\mu\text{s}$ . This is about one-twentieth of the value for a typical trigger tube. The G1/371K can thus be used for high-speed logic circuits. Using this tube, ring counters have been constructed operating at up to 1 Mc/s.

To simplify the construction of RC timing circuits stabilized against supply voltage variations, Elesta produce a tube comprising a trigger tube and two 97 V stabilizing diodes in a single envelope. This tube, the ESR2, requires a minimum of external wiring and accordingly very high values of timing resistance may be used. Time intervals of several hours are thus controlled with high accuracy.

### 3.2.2. Glow thyratrons

In the trigger tubes described above, breakdown of the main anode-cathode gap results from heavy

local ionization consequent on breakdown of the trigger-cathode gap. A glow thyratron produced by Cerberus, the GT21, operates on a different principle and accordingly possesses distinctive characteristics. A small negative voltage ( $\sim 5$  V) applied to a perforated control grid prevents ions in a priming discharge from entering the main anode-cathode gap. When the grid bias is removed or made positive, ions enter the gap and breakdown occurs. As in a conventional trigger tube, the discharge may be extinguished only by reducing the anode-cathode voltage for a time exceeding the deionization time.

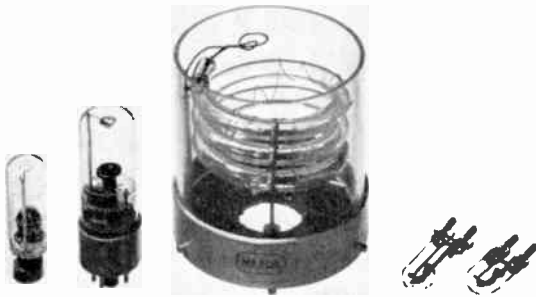


Fig. 7. Arc discharge tubes for stroboscopic and photographic applications. Left to right:—Ferranti EN15 and NSP2, Mazda SFE21, FA27 and FA10.

The small control voltage for a glow thyratron may readily be provided by transistors and it is in fact preferable to connect the grid to a circuit of less than 1 megohm impedance. A high anode breakdown voltage, ( $\sim 450$  V), coupled with a maximum sustained current of 40 mA, allows the tube to control a load of nearly 15 W. For certain bridge and timing circuits it is an advantage to have a control voltage almost at cathode potential: the built-in voltage reference of a conventional trigger tube is not always welcome. It will thus be seen that glow thyratrons and trigger tubes are complementary rather than competitive.

### 3.3. Arc Discharge Tubes

If the current in a glow discharge is progressively increased beyond the region of normal glow, the discharge will eventually move abruptly into the arc mode, i.e. it will concentrate on a small part of the cathode area. The high current density ( $100\text{--}1000$  A/cm<sup>2</sup>) will rapidly destroy a cathode not suited to this mode of operation. Various arc discharge tubes have been developed, however, most of which are intended to carry high or very high currents for short periods.

#### 3.3.1. Switching tubes

Once an arc is established, the voltage across a tube comprises a cathode fall of about 20 V and an  $IR$  drop due to the effective resistance of the positive column. A switching tube is therefore designed to have a short positive column so that the power dissipated in the tube is minimized. In some diodes (e.g. the Ericsson GD2V) the breakdown voltage is controlled to within 5%. Applications include surge arresting and capacitor switching for high-voltage testing. Breakdown voltages up to 2 kV are available and maximum peak current ratings of 10 000 A. On a high-voltage tube, the switching efficiency is over 99%.

Arc trigger tubes of comparable rating are available also. The Cerberus tubes use a priming discharge gap.

The Ferranti neon, argon and xenon-filled arc tetrodes are sometimes used as switching devices. Like the Sylvania 'Strobotron', however, they are primarily designed as stroboscopic light sources.

#### 3.3.2. Flash and stroboscopic tubes

If an arc discharge tube is designed to have a long positive column, the impedance of the positive column is increased proportionately. A storage capacitor connected in parallel with the tube will then deliver more than 90% of its energy into the positive column. Relatively little energy will be wasted in the connecting leads or in the cathode fall. The instantaneous loading of the positive column so achieved can be as high as 1 MW and the intense ionization of the gas filling produces a brilliant flash of light. Argon and xenon-krypton fillings are commonly used for the photographer's so-called electronic flash tube as these fillings provide light of substantially the same quality as daylight.

In order to provide a sufficiently long discharge path, photographic flash tubes commonly take the form of a U or helix. The impedance of the positive column is about 3 ohms and hence the flash duration (in seconds) is about three times the storage capacitance (in farads). If the resistance and inductance of the leads are kept to a minimum, flashes of less than 1  $\mu$ s are possible. For photographic flash tubes operating at about 2 kV, flash durations of 30 to 100  $\mu$ s are more typical. Over the last few years, tubes operating at about 250 V have become popular. These produce a flash of the order of 1 ms.

With a single flash, an efficiency of 50 lumens/watt may be attained. In a stroboscopic flash lamp, however, the loading per flash must be reduced to avoid overheating. The efficiency may then fall to 20 or 30 lumens/watt at about 25 flashes per second.

The flash tubes discussed above are essentially diodes with an externally wrapped trigger lead. A pulse of approximately 10 kV applied to the trigger

produces sufficient distortion of the potential gradient within the tube to initiate breakdown.

In the Sylvania 'Strobotron'<sup>19</sup> and similar tubes made by Ferranti, two additional electrodes are provided within the envelope. Triggering may be effected by a relatively small pulse ( $\sim 30$  V), applied between these two electrodes or by breakdown between any two of the four electrodes. Once the tube is triggered, it is important that the current in the main anode-cathode gap be allowed to increase rapidly so that the discharge moves immediately into the arc mode. The tube is damaged if the discharge is restricted to the glow mode. As with the other arc discharge tubes mentioned above, the main gap extinguishes when the capacitor has discharged to slightly below the arc maintaining voltage ( $\sim 20$  V). When internal electrodes are provided, however, it is necessary to ensure that discharges between other electrode pairs extinguish also.

### 3.3.3. Arc thyratrons

An interesting development in arc discharge tubes is the Cerberus 'Arcotron' which can sustain continuous currents of several amperes. The largest tube in the range, the BT14, can carry 6 A continuously or 100 A peak. The anode breakdown voltage is over 900 V and firing is controlled by an input of 40 V to the grid.

In principle, the 'Arcotron' is very similar to the Cerberus glow thyratron described already. A small priming arc of 20 mA is maintained between an auxiliary anode and main cathode. When the negative bias ( $\sim 40$  V) on the control grid is removed, a discharge occurs from main anode, through the perforated grid, to cathode. The arc drop is about 20 V. The efficiency, though high, is thus not as good as that of a silicon controlled rectifier. On the other hand the gas-filled device has an ionization time of the order of 100  $\mu$ s. As this is some two orders larger than the equivalent figure for a semiconductor device, the 'Arcotron' is correspondingly less vulnerable to supply-borne transients. Moreover, a protective stack of Zener diodes may be used if necessary with confidence that the surge will be carried by the protective device rather than the arc tube. With silicon controlled rectifiers the same protection is difficult to obtain.

### 3.4. Stepping Tubes

Recent developments in cold cathode stepping tubes have increased the difficulty of defining concisely the nature of such a tube. The classical design comprises a central anode surrounded by a ring of 10 index cathodes, usually in the form of nickel rods. Between adjacent pairs of index cathodes are further, similar guide cathodes. These are interconnected to

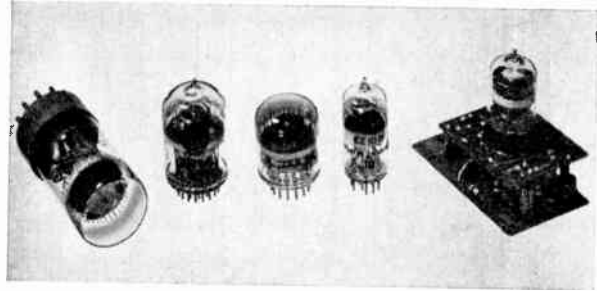


Fig. 8. Stepping tubes. Left to right:—Ericsson GS10D reversible selector, Ericsson GSA10G reversible selector with auxiliary anodes and routing guides, Mullard Z505S reversible 50 kc/s selector, Elesta EZ10B non-reversible 1 Mc/s selector, Elesta ECT100 reversible 1 Mc/s selector shown mounted on transistor flip-flop plug-in module.

form one or more rings and are biased to some +50 V so that the anode current will normally be carried by one of the index cathodes. Stepping of the discharge from one index cathode to the next is effected by depressing the potential of an adjacent guide so that it accepts the discharge. The guide potential is later raised so that the discharge moves on to the next index cathode, its position being indicated by the cathode glow. Maximum stepping rates range from 1 kc/s for the Ericsson GS10J low-voltage tube to 1 Mc/s for the Elesta EZ10B and ECT100.

In the original Ericsson 'Dekatron',<sup>9</sup> two rings of guides are used. By pulsing the two rings in staggered phase relationship the discharge is caused to step preferentially in a direction determined by the sequence in which the pulses are applied. The single-pulse Dekatron dates from 1952.<sup>10</sup> It contains three rings of guides, but only one of these need be pulsed. The direction of stepping cannot readily be reversed, however.

S.T.C. and Elesta have both produced non-reversible tubes in which the direction of stepping is determined by electrode geometry. They combine simplicity of construction with simplicity of operation.

For reversible counters, problems of inter-stage coupling are simplified by the provision of separate connections to the guides between cathodes 9 and 0.<sup>11</sup> Two recently-introduced Ericsson tubes, the GCA10G and GSA10G, are additionally provided with 10 auxiliary anodes disposed between the main anode and index cathodes. From the auxiliary anodes outputs may be taken of an amplitude exceeding the 40 V which can at best be obtained from an index cathode. Moreover, the output is of the polarity required for direct operation of a numerical display tube.

Even larger outputs are provided by probes adjacent to the index cathodes of the Elesta ECT100. Ionic coupling holds a probe at the potential of the virtual

anode surrounding a conducting cathode. Outputs of up to 200 V are thus available and a trigger tube may be operated directly and reliably. The ECT100 combines a number of novel features from which it is claimed<sup>14</sup> substantial benefits derive. Index cathodes and guides are formed as four star-shaped stampings mounted co-axially within an anode ring. The stampings are insulated from each other but the tips of the arms are bent to lie in the same plane. A transistor flip-flop is used to hold the 'odd' index cathodes 60 V above or below the 'even' cathodes. The two stampings representing the 'odd' and 'even' guides are capacitor-coupled to the two index cathode stampings. When the transistor flip-flop reverses state, therefore, the potential of one guide rises and the other falls. There is thus a very positive transfer of the discharge in the appropriate direction and onto the index cathode which has just assumed the lower potential. This hydrogen-filled tube can operate at up to 1 Mc/s, requires no closely regulated h.t. supply and is claimed to be free from 'sticking', i.e. reluctance to step after being left operating in a static condition.

A recently described Japanese tube<sup>15</sup> resembles a conventional stepping tube in appearance, but operates with the opposite polarity. Because the anode fall is less than the cathode fall, the drive required by the guide anodes is about half that required by a tube using guide cathodes. The tube may thus be driven by transistors. It is claimed that because there is a single cathode, sputtering does not produce 'sticking'. The index anodes may also be connected directly to the cathodes of a numerical indicator tube. The whole cathode current of the stepping tube is then drawn from the indicator tube. The visible glow in the stepping tube is of course on the large common cathode, but in the published description it is not mentioned whether this is still useful as an indication of state of count.

### 3.5. Register and Display Tubes

The cathode glow surrounding a conducting cathode has been used to provide a range of numerical indicators fulfilling a variety of needs.

#### 3.5.1. 'On/off' indicators

For binary stages it is necessary only to have a two-state display. Tung-sol make a range of small cold cathode thyatrons which may be used as indicators. The control voltages are easily provided by transistors, but extinction requires depression of the anode supply voltage.

The Fujitsu TG121A is a two-cathode tube operating at about 300  $\mu$ A. One cathode is visible, the other shielded from view. An input of only 5 V is sufficient to produce transfer of the glow from one to the other. Although transfer cannot occur at extremely high speeds, it is claimed the tube has no detrimental

effect on transistorized computer flip-flops to which it may be connected.

#### 3.5.2. Glow-position register tubes

The Ericsson GR10A and Mullard Z503M resemble conventional stepping tubes without guides. If one cathode is held at least 24 V below any other, it will preferentially accept the discharge. Such a tube may be used as a display for transistorized or hard-valve counters.

#### 3.5.3. "Clock-face" tubes

The Burroughs B9012 and Mullard Z550M indicators each have the numerals 0-9 perforated in a mask plate. A 5 V bias applied to any of 10 trigger electrodes directs the discharge to one of 10 cathodes, the glow from which is visible through the perforations of one

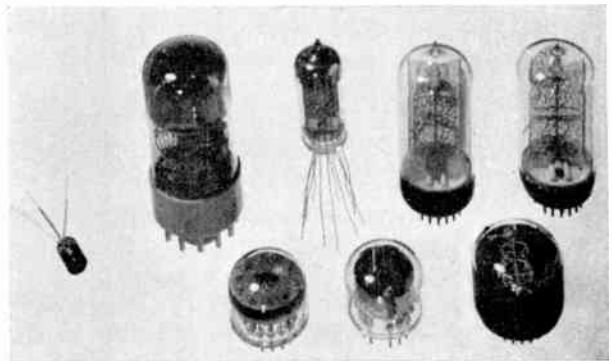


Fig. 9. Register and numerical display tubes. Left to right:—Fujitsu TG121A "on-off" indicator, Mullard Z503M glow-position indicator, Z550M "clock-face" tube, Hivac XN1 wire-ended side-view number tube, Mullard Z520M with mercury addition and orange-dipped envelope, Ericsson GR10G side-view and GR10K end-view numerical indicators, Ericsson GR4G side-view tube for  $\frac{1}{2}$ ,  $\frac{1}{3}$ ,  $\frac{1}{4}$  and 1.

numeral. The display thus resembles a clock face on which one number is a luminous red-orange. Normally the tube is supplied with rectified, unsmoothed a.c. so that the display will change with changes of input. This type of tube is easily operated by transistors and is rather more easily read than the glow-position register tube.

#### 3.5.4. In-line numerical display tubes

During the last decade there has been a rapid increase in the use of instruments and equipment with in-line digital displays. Many display devices have evolved, but one of the most successful is undoubtedly the cold cathode numerical display tube. It combines long life, ruggedness, and economy with legibility over wide viewing angles and in high light intensities. Moreover it can be operated by thermionic valves, cold cathode tubes or semiconductors.

A typical numerical display tube comprises 10 cathodes stamped from sheet nickel in the shapes of the numerals 0–9. They are mounted one behind the other, about 1 mm apart and surrounded by a wire mesh anode. A multi-pin base or flying leads provide separate connections to the individual cathodes and the anode. The tube contains neon; it has been found that the inclusion also of a trace of mercury greatly increases tube life although the explanation of this is a little obscure.

When current passes from the anode to one of the cathodes, the cathode is surrounded by the negative glow to a depth of about 1 mm. As the cathode stampings have a width of about 0.4 mm, the total width of the glow is 2.4 mm and the obscuration produced by cathodes in front is quite small. Sufficient current must be passed to fill the whole cathode area and this implies that operation is entering on the abnormal glow mode. If excessive current is passed, tube life is reduced and sputtering may cause bridging of the insulators between cathodes. The areas of numerals are often made equal by adjusting the widths of their limbs. Nevertheless, these considerations dictate that the cathode current be held within rather narrow limits, usually in the ratio 2 to 1.

Tubes are made with character heights ranging from 8 to 60 mm and drawing nominal cathode currents from 1 to 7 mA. For a given size of numeral, the space between adjacent numerals is less for side viewing tubes than for the type viewed through the end of the circular envelope. The end-view arrangement simplifies tube replacement from the front of the instrument, however, and Burroughs have combined the virtues of both tube types by producing an end-view tube with flattened sides to the envelope.

Most manufacturers now make long-life tubes. The inclusion of mercury produces a blue haze within the tube but this is rendered invisible by dipping the tube envelope in a red or yellow lacquer.

All current tubes are designed for operation on d.c. It is not practicable to extend life by reducing cathode current because the numerals would then be incompletely filled. A commonly-used alternative is to operate the tube from a pulsating supply, e.g. half-wave rectified, unsmoothed a.c. While conducting, the tube carries sufficient current to fill the cathode completely, but the average current is reduced by a factor of at least three and the life is correspondingly increased. Even without these precautions, most modern tubes provide a life of at least 5000 hours under the most severe conditions, i.e. with the display static on a single number.

The cathode required may be selected by direct mechanical switching. The other cathodes, if left disconnected, will then assume a potential intermediate between anode and the conducting cathode. Most

tubes are designed also for operation by the application of a 'pre-bias', i.e. the cathode which is to conduct is held 40–100 V negative with respect to the others. If the pre-bias is insufficient, anode current will be shared to a significant extent between the chosen cathode and adjacent cathodes. When this happens, the clarity of the display is impaired. It happens that the minimum pre-bias of 40 V can be provided by almost all types of active element at present in use.

Display tubes are available also in which the cathodes take the form of letters and symbols. Burroughs have specialized in this field and produce tubes with twin characters and also a 13-bar alphanumeric matrix.

#### 4. Conclusions

The cold cathode tube has been developed for a diversity of applications, each of which it fulfils with conspicuous success despite strong competition from semiconductor devices. Apart from high voltage applications, for which it has not yet been challenged, the cold cathode tube offers greater precision as a voltage reference and greater simplicity as a counting device (albeit with transistor drive). Its limited speed of response is an advantage in medium and low-speed applications subject to supply-borne interference.

The reliability, consistency and stability of cold cathode devices are, in general, very good. Practical difficulties are more often than not the result of inadequate circuit design.

#### 5. Acknowledgment

The author wishes to thank the Directors of Ilford Limited for permission to publish this paper.

#### 6. References

1. P. Parker, "Electronics". (E. Arnold, London, 1950.)
2. H. E. Watson, "The development of the neon glow lamp (1911–61)", *Nature*, **191**, No. 4793, pp. 1040–1, 9th September 1961.
3. "From small beginnings", *Brit. Commun. Electronics*, **8**, No. 9, p. 655, September 1961.
4. S. B. Ingram, "The 313-A vacuum tube", *Bell Lab. Rec.*, pp. 114–6, December 1936.
5. T. Jurriaanse, F. M. Penning and J. H. A. Moubis, "The normal cathode fall for molybdenum in mixed gases", *Philips Res. Reports*, **1**, No. 16, pp. 225–30, 1946.
6. C. H. Tosswill, "Cold-cathode trigger tubes", *Philips Tech. Rev.*, **18**, No. 4/5, pp. 128–41, 1956/7.
7. G. H. Hough and D. S. Ridler, "Some recently developed cold cathode glow discharge tubes and associated circuits", *Electronic Engng*, **24**, Nos. 290, 291, 292, pp. 152–7, 230–5, 272–6, April, May, June 1952.
8. J. J. Lamb and J. A. Brustman, "Poly-cathode glow tube for counters and calculators", *Electronics*, **22**, No. 11, pp. 92–6, November 1949.
9. R. C. Bacon and J. R. Pollard, "The dekatron—a new cold cathode counting tube", *Electronic Engng*, **22**, No. 267, pp. 173–7, May 1950.
10. J. R. Acton, "The single-pulse dekatron", *Electronic Engng*, **24**, No. 288, pp. 48–51, February 1952.

11. L. C. Bramson, "Reversible dekatron counters", *Electronic Engng*, 27, No. 328, pp. 266-8, June 1955.
12. D. Reaney, "A new dekatron for direct operation of digitrons", *Electronic Engng*, 34, No. 412, pp. 372-6, June 1962.
13. K. Apel, "A gas-filled decade counting tube for counting speeds up to 1 Mc/s", *Elektron. Rundschau*, 14, No. 10, pp. 405-8, October 1960.
14. K. Apel, "ECT100, a new circuit element for counting techniques", *Elektron. Rundschau*, 17, No. 2, pp. 57-61, February 1963.
15. Y. Hatta, H. Mase and M. Sugawara, "A new poly-anode counting tube, the 'polyatron'", *The Radio and Electronic Engineer (J. Brit. I.R.E.)*, 26, No. 5, pp. 383-7, November 1963.
16. N. McLoughlin, D. Reaney and A. W. Turner, "The digitron: A cold cathode character display tube", *Electronic Engng*, 32, No. 385, pp. 140-3, March 1960.
17. T. P. J. Botden, "A gas-discharge indicator tube for transistorized decade counting circuits", *Philips Tech. Rev.*, 21, No. 9, pp. 267-75, 1959/60.
18. Y. Fukukawa and T. Nakajo, "Indicator tube for transistor circuits", *Electronics*, 35, No. 14, pp. 64 and 66, 6th April 1962.
19. K. J. Gerneshausen and H. E. Edgerton, "The strobotron", *Electronics*, 10, No. 2, pp. 12-14, February 1937 and No. 3, pp. 18-21, March 1937.
20. P. M. Murphy and H. E. Edgerton, "Electrical characteristics of stroboscopic flash lamps", *J. Appl. Phys.*, 12, No. 12, pp. 848-55, December 1941.
21. R. S. Carlson and H. E. Edgerton, "The stroboscope as a light source for motion pictures", *J. Soc. Motion Picture Televis. Engrs*, 55, No. 1, pp. 88-100, July 1950.
22. H. N. Olsen and W. S. Huxford, "Electrical and radiation characteristics of flashlamps", *J. Soc. Motion Picture Televis. Engrs*, 55, No. 3, pp. 285-98, September 1950.
23. H. Seifert, "Cold cathode thyratrons for continuous currents of several amperes", *Elektron. Rundschau*, 15, No. 1, pp. 7-10, January 1961.
24. J. Henry, "Glow thyratrons", *Electronique Industrielle*, Nos. 54 and 55, pp. 195-9, 239-43, June and July/August 1962.
25. W. F. Feist and G. Wade, "Are hot cathodes on the way out?", *Electronics*, 36, No. 23, pp. 39-45, 7th June 1963.
26. D. M. Neale, "Cold Cathode Tube Circuit Design". (Chapman and Hall, London, 1964.)
27. S. Ramsey, "Why Soviets talk up cold-cathode tubes", *Electronics*, 35, No. 47, pp. 54-5, 23rd November 1962.
28. M. E. Bond, "The life expectancy of cold cathode tubes", *Electronic Engng*, 34, No. 418, pp. 798-803, December 1962.
29. F. A. Benson, "Impedance/frequency characteristics of glow-discharge reference tubes", *Proc. Instn Elect. Engrs*, 107, Pt.B, No. 32, pp. 199-208, March 1960.
30. E. Cohen and R. O. Jenkins, "The characteristics and applications of corona stabilizer tubes", *Electronic Engng*, 32, No. 383, pp. 11-15, January 1960.
31. E. Cohen and R. O. Jenkins, "The corona discharge and its application to voltage stabilization", *Proc. Instn Elect. Engrs*, 107, Pt.B, No. 33, pp. 285-94, May 1960.

*Manuscript received by the Institution on 21st December 1963. (Paper No. 880.)*

© The British Institution of Radio Engineers, 1964

## STANDARD FREQUENCY TRANSMISSIONS

(Communication from the National Physical Laboratory)

Deviations, in parts in  $10^{10}$ , from nominal frequency for  
January 1964

January 1964	GBR 16kc/s 24-hour mean centred on 0300 U.T.	MSF 60 kc/s 1430-1530 U.T.	Droitwich 200 kc/s 1000-1100 U.T.	January 1964	GBR 16 kc/s 24-hour mean centred on 0300 U.T.	MSF 60 kc/s 1430-1530 U.T.	Droitwich 200 kc/s 1000-1100 U.T.
1	—	- 150.7	+ 26	17	- 150.1	- 150.6	+ 1
2	- 151.1	- 150.9	+ 27	18	- 150.7	- 150.0	+ 1
3	- 151.1	- 150.1	+ 26	19	- 150.5	- 151.7	+ 1
4	- 151.0	- 150.0	+ 30	20	- 151.6	- 151.9	+ 3
5	- 151.4	- 150.6	—	21	- 152.0	- 151.2	+ 3
6	- 151.0	- 151.8	- 4	22	- 151.5	- 151.7	+ 4
7	- 151.7	- 152.1	- 3	23	- 152.0	- 151.1	+ 5
8	- 151.0	- 149.7	- 3	24	- 151.3	- 151.3	+ 4
9	- 150.5	- 151.1	- 2	25	- 150.9	- 151.1	+ 5
10	- 149.9	- 149.2	- 2	26	- 150.7	- 150.1	+ 5
11	- 150.4	- 149.6	- 1	27	- 150.9	- 150.5	+ 4
12	- 149.8	- 149.9	—	28	- 150.8	- 150.8	+ 5
13	- 150.2	- 149.5	0	29	- 150.5	- 150.2	+ 6
14	- 149.6	- 150.3	0	30	- 150.9	- 150.8	+ 6
15	- 150.3	- 149.7	+ 1	31	- 150.9	- 150.7	+ 6
16	- 150.4	- 150.0	+ 1				

*Nominal frequency corresponds to a value of 9 192 631 770 c/s for the caesium  $F_{1,m}(4,0)-F_{1,m}(3,0)$  transition at zero field.  
Note: The MSF/GBR frequency offset was adjusted to  $-150 \times 10^{10}$  at 0000 U.T. on the 1st January 1964.*

# of current interest . . .

## The British Space Research Programme

In reply to a Parliamentary question on 5th December seeking information on the progress of the British space programme, the Minister of Aviation, the Rt. Hon. Julian Amery, stated that his Department was carrying out a programme of research into the technology required for the civil and military exploitation of space, supplemented by work carried out in industry. The programme was currently being reviewed. He continued:

"The design study of a communications satellite, announced in the debate on 29th March, has been completed. Its implications are now being studied. Twenty separate systems including 15 types of satellite were considered in a co-operative study undertaken by my Establishments, the Post Office and industry. Discussions are in progress with Europe for British participation in a satellite communications system. These will be followed by talks with the United States and other countries. We are keeping in close touch with the Commonwealth.

"We are continuing to play our part in the negotiations for setting up the European Space Research Organization. The Preparatory Commission of the Organization has placed contracts for two preliminary satellite design studies on the Ministry of Aviation. We are also to supply a number of *Skylark* sounding rockets.

"We are developing *Blue Streak* as part of the ELDO programme. The first *Blue Streak* will be launched from Woomera, probably in April 1964.

"Under the scientific space research programme, for which the Minister for Science is responsible, the second Anglo-American scientific satellite awaits launching in the United States. My Department has placed a contract for the third satellite in the programme which will be the first British-made satellite. It should be ready for launching by the United States in about three years' time. Development of a stabilized version of the *Skylark* sounding rocket has reached an advanced stage."

## Developments in Swept-Frequency Radar Technique

Work has been going on for the past six years at the Marconi Research and Development Laboratories on the design of a special type of radar aerial head. As is well known, the conventional method of establishing the height of an aircraft is to employ a separate height-finding device, the information from which is co-ordinated with range and bearing information derived from other equipments.

The type of height-finder which is in general use employs a narrow radio-frequency beam of fixed frequency which is directed along the general bearing

of the target aircraft by a parabolic reflector or kindred device. The height finding facility is achieved by arranging that the whole aerial structure (the array and its reflector) shall tilt or nod in the vertical plane. Having scanned to its target from information derived from the surveillance radar, the height-finding beam is tilted to establish the angle which gives the maximum return signal. This angle is (subject to certain corrections) a function of the aircraft height for a given range. The system is reasonably accurate but has its limitations; notably that the speed of height-taking is bounded by the mechanical process of nodding, and also that very powerful motors and elaborate control gear are essential.

One approach to the problem of providing an alternative is that of using some form of stacked aerial array and comparing the strengths of signal returns from aeriels of differing heights. Such a system was used in wartime CH radar and has recently been revived in more sophisticated form.

An alternative is to retain the nodding aerial in principle, but to nod the beam electronically, and it was long ago realized that this could be done by varying the frequency of the radiated beam. The real problem was to accomplish this without degrading the radiation pattern of the aerial, particularly the level of the sidelobes.

Several possible techniques were investigated and of these, two were selected for further study. The most promising one uses a helically-wound waveguide 12 ft 6 in (4 m) in length as a delay line which illuminates a duralumin cylindrical parabolic reflector. A full-size S-band (10 cm) swept-frequency radar aerial has been built and successfully tested up to 3 mW peak power. The whole aerial head is quite light in weight (approx. 900 lb (450 kg) overall). Rotation of the head in the horizontal plane is carried out in the usual way, for while it is feasible to achieve horizontal rotation electronically there are no significant advantages in so doing.

Some aspects of the system are still subject to classification. Of the aerial arrangements however, it can be said that experimental figures have been obtained of sidelobes 32 dB down compared with the main beam. (25 dB is considered good on height-finders.) Scans of up to 70 deg vertical arc have been obtained and this is by no means the limit. The beam shape at all relevant frequencies is substantially constant. The accuracy is as good as that obtained with the best mechanical noddors of similar aperture, whilst the data-rate is much higher by reason of the inertia-free tilt facility and there is no loss of time involved in separate orientation as with a mechanically nodding height-finder.

# The Design of Second-harmonic Detector Heads and their Application to the Reading of Digital Information and the Measurement of Low Speeds of Rotation

By

D. B. G. EDWARDS,  
Ph.D., M.Sc.,†

E. M. DUNSTAN, M.Sc., Ph.D.,†  
AND

C. J. TUNIS, Ph.D.‡

*Presented at the Conference on "Signal Recording on Moving Magnetic Media" in Budapest from 15th–18th October 1962.*

**Summary:** Two applications of the second harmonic principle are outlined and the design of suitable detector heads is detailed.

The first application relates to the detection of binary recorded information on magnetic tape. The detector head described provides an output signal which is a direct measure of the flux linking the head at any instant and does not depend for its output signal on relative motion between the head and the source of flux. The design and construction of such a head is considered and the results of an approximate analysis of its operation are compared with the actual performance of a practical head. The head is capable of resolving digits at packing densities in excess of 100 per inch. A double head arrangement consisting of a writing head separated from a flux-sensitive head by a digit separation is also described. This makes it possible to record digits at a constant packing density irrespective of tape speed and also can be used to provide character by character checking of the information being recorded.

The second part of the paper considers a detector head suitable for detecting a d.c. magnetic field of the order of 10 millioersteds in space in the presence of another d.c. field at right angles and several orders of magnitude greater. A theoretical analysis of the operation of the device is presented and the results are in good agreement with the performance of a practical head. The detector head is intended to measure the 'cross field' generated when a cylindrical conducting rotor is rotated in a primary d.c. field. This cross field is proportional to the angular velocity of the rotor. The combination provides a basis for a commutatorless and brushless d.c. tachogenerator having a very low noise content.

## 1. Introduction

The principle of the second-harmonic magnetic modulator has already been applied to the amplification of small d.c. signals,<sup>1</sup> measurement of small magnetic fields such as the Earth's field in geomagnetic surveys<sup>2</sup> or the field in magnetic specimens tested in permeameters,<sup>3</sup> and the reproduction of very-low-frequency sinusoidal signals recorded on magnetic tape.<sup>4,8,9</sup>

Devices designed for these applications depend for their operation on the disturbance of the odd symmetry of the  $B$ - $H$  characteristic of a sample of magnetic material which occurs when a d.c. field is applied to the specimen.

Figure 1(a) shows an ideal  $B$ - $H$  characteristic of a specimen of soft magnetic material. Consider the application of a triangular wave (for ease of explanation)

of magnetic field (modulation) having a peak value  $\hat{H}$  greater than that required to saturate the material ( $H_{\text{sat}}$ ) (Fig. 1(b)). In the absence of any d.c. biasing field this will produce a flux density in the material as shown in Fig 1(c) (solid line) which results in the voltage pulse train of Fig 1(d) at the terminals of a 'read' winding wound on the specimen. The flux waveform is symmetrical and the pulse train will, therefore, only contain odd harmonics of the excitation frequency.

If a positive d.c. bias field  $H$  is applied, saturation in the positive direction will start earlier and finish later than in the absence of  $H$ , whilst that in the negative direction will correspondingly start later and finish earlier. This results in the output pulse train shown by the dotted line in Fig. 1(d) and containing a second harmonic component. For small values of  $H$ , this component is proportional to  $H$  and has a phase with respect to the fundamental which is independent of  $H$ , unless this reverses sign in which case its phase changes by 180 deg.

† Electrical Engineering Laboratories, University of Manchester.

‡ Formerly at the Electrical Engineering Laboratories, University of Manchester; now with International Business Machines, Inc., Endicott, New York.

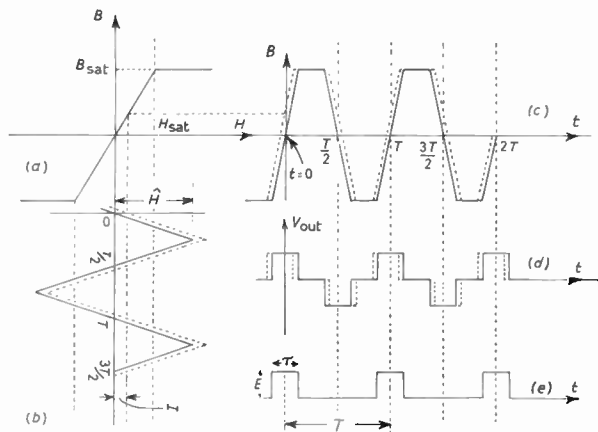


Fig. 1. Idealized operation.

- (a) Idealized  $B-H$  characteristic.
- (b) Modulation field waveform.
- (c) Flux waveform.
- (d) Output voltage from 'read' winding.
- (e) Positive pulse train component ( $H = 0$ ).

In this paper two applications of the second harmonic modulator principle are outlined and the design of suitable detector heads is detailed. The first application relates to the detection of binary recorded information on magnetic tape.

Reproduction of such digits is normally achieved by moving the tape past a head so designed that some of the leakage flux from the tape links with a coil wound on the head. The voltage developed in this coil is proportional to the rate of change of flux linking it ( $d\phi/dt$ ) and in this instance clearly depends on the tape speed. In the head to be described, however, the leakage flux from the tape generates a field in the magnetic material of the head, which is detected, as already explained, as a voltage having a component at twice the modulation frequency. This component is proportional to the generated field, and therefore to the leakage flux from the tape.

The magnetic-tape system is of moderate performance and is designed to provide the input/output medium for a medium-speed digital computer. It is also intended for use 'off line' to convert information into a paper medium, or *vice versa*. In this latter application the 'read' heads are important, since they provide a constant amplitude of signal over the wide speed range necessary to match the information rate of the magnetic tape and the various paper equipments. For example, at a teleprinter speed of 10 characters per second the magnetic tape on which the packing density is typically 100 digits per inch, is only moving at 1/10 in per second. Alternatively, when reading information into the computer the character rate is 1000 per second, i.e. 10 in/s.

A further development allows a 'write' head to be placed one digit separation (0.010 in) away from the 'read' head. This permits information to be written on magnetic tape and then read off and checked prior to the writing of the next information, even at a packing density of 100 bits/inch. This technique is developed in the system to enhance its reliability.

The second development was to provide a commutatorless and brushless d.c. tachogenerator which would produce a d.c. signal proportional to angular velocity but with a very low noise content. Conventional d.c. tachogenerators suffer from noise components, in particular commutator ripple, which are of the order of 3% of the generator output. At low speeds, difficulties arise as commutator ripple and rotational-frequency noise components have a period which is of the same order as the servo response time so that the system is capable of following these noise components, thus resulting in uneven rotation. If adequate smoothing of the output is provided, the servo response time is increased and, in particular, friction and 'stiction' effects which are no longer reduced by the inertia of the system become important, causing uneven rotation due to lack of loop gain at rotation frequency. Methods of reducing the effective tachogenerator noise exist,<sup>5,6</sup> but these are either unsuitable at low speeds or yield a very small output.

In the brushless tachogenerator<sup>7</sup> a cylindrical conducting rotor is rotated in a primary d.c. field. The currents induced in the rotor create a d.c. magnetic field at right angles which is proportional to the angular velocity of the rotor and is measured using the second harmonic head described in Section 3.

## 2. The Design of a Variable-reluctance Detector for use with a Digital Tape System

### 2.1. Detail of the Digital Read Head

The form of this head is shown in Fig. 2. It consists of a thin strip of soft magnetic material (Permalloy C) which has a small hole punched centrally at A, the strip itself being bent into the shape of a conventional 'read' head with a 'read' gap at B. In operation a sine wave of current, frequency  $f = 150$  kc/s, is made to flow in the modulation winding C which is wound on the small toroid formed by the hole in the strip. The modulation current causes flux to circulate round this small toroid and at the current peaks will tend to saturate the material. Because of the way in which the modulation coil is wound the flux is ideally balanced with respect to the main loop of the reading head formed by limbs X and Y and the 'read' gap. Thus the head will have no effect on the information recorded on the tape. The 'read' winding D is wound as shown around the limbs X and Y.

When a region of leakage flux on the tape is situated in the vicinity of the read gap, then some flux will

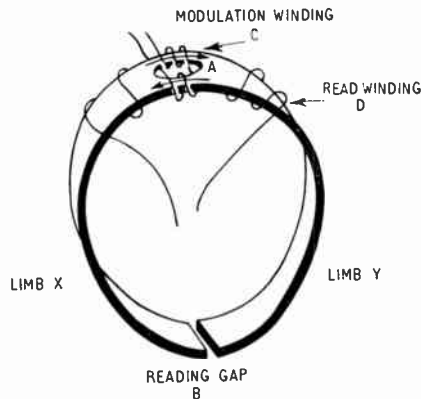


Fig. 2. Digital 'read' head.

tend to pass around the head. The exact proportion will depend on the relative reluctance of the path around the head and that of the 'read' gap. The head reluctance is essentially that of the modulation section which is saturated twice per cycle of modulation current. This approach to the operation of the head rather than that adopted in the introduction is taken because it is more amenable to analysis. As already explained, the signal induced in the 'read' winding will have a large  $2f$  component. It is locked in phase to the modulation current and is altered by 180 deg when the direction of flow of flux around the head is reversed.

If there is zero external flux in the vicinity of the 'read' gap B, then theoretically there should be zero output voltage in the read winding. In practice, however, some flux due to the modulation current links the read coil, for the modulation circuit cannot be perfectly balanced. This introduces a component of voltage at the fundamental frequency.

Furthermore, since saturation of the modulation toroid occurs, non-linearities will introduce odd-harmonic components, mainly third. Thus there are at least three major component frequencies present in the voltage induced in the 'read' coil. This voltage is fed into an amplifier tuned to the  $2f$  component (300 kc/s), which has adequate rejection at the fundamental and third-harmonic frequencies.

The variable-reluctance head is sensitive to any magnetic field in its vicinity whether alternating or static and so a second-harmonic signal can be derived from the following sources:

- (a) Flux from digital information on the tape which provides the desired output signal.
- (b) Flux due to remanence in the 'read' head itself. This can be minimized by a suitable choice of magnetic material, but in practice it is possible to eliminate this signal by a small d.c. current in the read winding, D.

- (c) External flux sources, such as the Earth's field or mains transformers. The effect of these sources can be reduced in two ways: by making the physical dimensions of the head small and by screening techniques. The latter method has proved to be adequate,<sup>4</sup> but in practice is very inconvenient. However, the need for screening can be almost eliminated if the former method is adopted. The type of head to be described is suited to a small construction and, for example, the Earth's field gives approximately 1/20 of the signal obtained from a digit on tape.
- (d) Any second-harmonic component of the modulation current. This second-harmonic signal can have a phase which is different from that due to any of the above flux sources and cannot be entirely eliminated by the use of a d.c. current in the 'read' coil. It is thus desirable to have a modulation current which is as free as possible from second-harmonic components. A second-harmonic component of 0.1% in the modulation current gives rise to an output signal equivalent to one hundredth of a digit.

Although the head has been made as small as possible in order to minimize external field effects, other factors, such as material used, physical shape and gap width are determined by much the same considerations as for a more conventional reading head.<sup>10</sup> The common aim is to intercept a maximum of leakage flux from the tape.

#### 2.1.1. Read head construction

The principal defect of the reading head described in Ref. 8 was the lack of uniformity in characteristics between individual heads. The use of the present method of construction has improved this situation. A significant reduction in head size has also been achieved which permits eight such heads, each 0.040 in wide, to be accommodated across  $\frac{1}{2}$ -in magnetic tape, and eliminates the need for magnetic screening in most cases.

A lamination of 0.002 in thick Permalloy C, in an annealed condition, and of the form shown in Fig. 3(a) forms the basis of the read construction. Through the hole in the centre of this strip 4 turns of 40 s.w.g. wire are wound, two on either side of the hole as shown in Fig. 3(b).

To eliminate the tendency for the wire to short-circuit with the Permalloy strip, wire with a heavy covering of plastic insulation is used. The modulation current flows in this winding and the winding direction is such that the flux follows a path around the toroid formed by the hole. The mean path length for the flux is well defined by this hole and the Permalloy strip and thus will be similar for all such strips. A six-turn 'read' winding of 40 s.w.g. is wound, in two

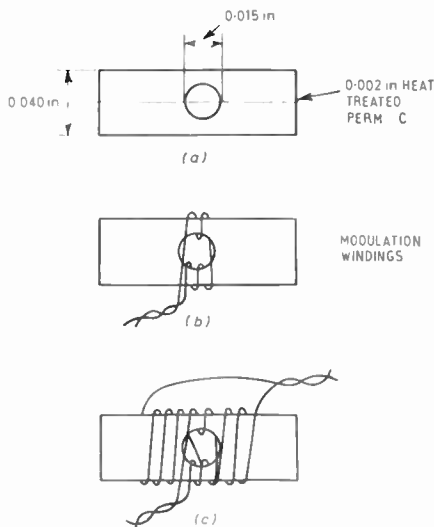


Fig. 3. Construction of the variable-reluctance head.

halves, adjacent to the modulation winding, as shown in Fig. 3(c). Six turns was considered to be a reasonable number during the construction of the first heads, but there is no basic reason why many more turns of a finer wire could not be accommodated whilst maintaining the small head size.

The strip is now bent to form a small head basically shaped about the windings on the lamination itself. The long limbs of the head facilitate its manipulation while it is being fitted into its brass holder (Fig. 4). A brass shim is inserted between the limbs to define the 'read' gap and then the screw S is tightened, clamping the head between the two jaws of the holder. The excess metal of the head is then cut away and the surface of the holder is carefully lapped until the distance  $d$  is approximately 0.010 in. The head is then finally secured with a 'loaded' Araldite resin.

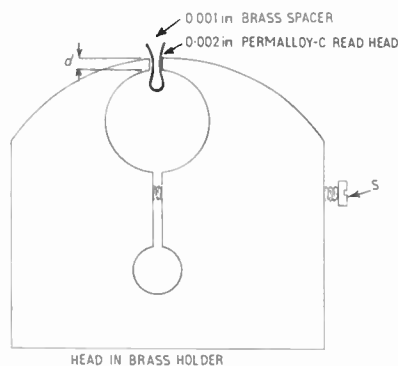


Fig. 4. Construction of the variable-reluctance 'read' head.

A number of 8-head blocks were made in a similar manner and Fig. 5 shows a completed block which was manufactured in this way. However, to facilitate assembly and test and to accommodate a variety of tape widths and the possibility of head replacement, manufacture is now finished in a single-channel form. These heads can be stacked according to requirements, with the gaps aligned to the necessary accuracy. In practice the modulation sections of a multi-channel head are all connected in series.

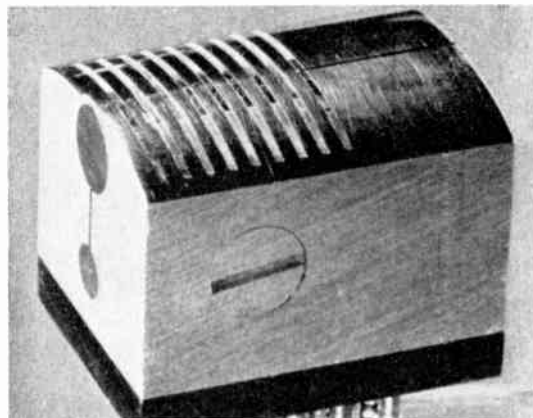


Fig. 5. Complete 8-track head block.

### 2.2. Approximate Analysis of Head Operation

The leakage flux from the tape in the vicinity of the head is presented with two alternative paths; it may jump the air-gap or it may pass around the head itself. Division of the flux along these two paths depends upon the respective reluctance of each path and  $\phi_H$  the flux circulating around the head is given by:

$$\phi_H = \phi_T \frac{R_g}{R_g + R_H} \quad \dots\dots(1)$$

where  $\phi_T$  is the total leakage flux from the tape

$R_g$  is the reluctance of the air-gap

$R_H$  is the reluctance of the main path around the head.

The reluctance of this main path  $R_H$  is determined mainly by that of the modulating section which, from Fig. 6, can be seen to be approximately

$$R_H = \frac{L}{2\mu A} \quad \dots\dots(2)$$

where  $L$  is the length of one half section of the toroid.

$A$  is the cross-sectional area of a half section.

$\mu$  is the incremental permeability of the modulating section material.

Therefore

$$\phi_H = \phi_T \cdot \frac{1}{\left(1 + \frac{L}{2\mu AR_g}\right)} \dots\dots(3)$$

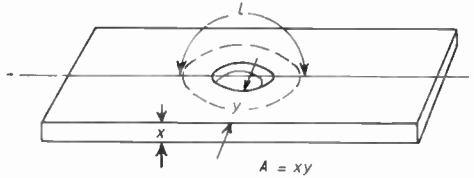


Fig. 6.  $L$  and  $A$  of the 'read' head.

A practical plot of incremental permeability against polarizing field for Permalloy C obtained from Ref. 11 indicates that the curve approximates a rectangular hyperbola. Therefore the assumption is made that

$$\mu H = K' \dots\dots(4)$$

where  $K'$  is a constant.

This equation implies that at very small values of  $H$ ,  $\mu$  tends to infinity, but in practice, of course,  $\mu$  will tend to  $\mu_0$  the initial permeability. This serious deviation between the practical result and the assumed theoretical curve is of no importance here, however, because flux changes around the head only occur at relatively high polarizing fields.

The polarizing field in this case is the sinusoidal modulation current, so that eqn. (4) becomes:

$$\mu I |\sin \omega t| = K \dots\dots(5)$$

where  $K$  is a new constant.

The magnitude of the sine function is taken as it is assumed that the incremental permeability is a function only of the magnitude and not of the direction of the applied field.

Therefore combining eqns. (5) and (3)

$$\phi_H = \phi_T \cdot \frac{1}{1 + \frac{LI |\sin \omega t|}{2AKR_g}} \dots\dots(6)$$

and if

$$b = \frac{L}{4AKR_g} \dots\dots(7)$$

$$\phi_H = \phi_T \cdot \frac{1}{1 + 2bI |\sin \omega t|} \dots\dots(8)$$

Differentiation of eqn. (8) yields an expression for the induced voltage  $E_R$  in the 'read' coil:

$$E_R = \frac{2\phi_T \omega b I \cos \omega t}{1 + 2bI |\sin \omega t|} \dots\dots(9)$$

In Fig. 7 eqns. (8) and (9) have been plotted throughout one cycle of the modulation frequency to illustrate

the theoretical form of the flux linking the 'read' turns and the voltage induced therein. These are very similar to the practical waveforms obtained despite the assumptions made in deriving the theoretical expressions.

In practice an amplifier tuned to the second harmonic of the modulation frequency provides the output signal. The second-harmonic component of the total flux linking the head is thus of interest and by Fourier analysis this can be shown to be

$$\phi_{2f} = \left[ \frac{4\phi_T}{\pi} \int_0^{\pi/2} \frac{\cos 2\omega t d(\omega t)}{1 + 2bI |\sin \omega t|} \right] \cos 2\omega t \dots\dots(10)$$

The peak value  $\hat{\phi}_{2f}$  of this flux can thus be determined and is given by the following expression:

$$\hat{\phi}_{2f} = \frac{4\phi_T}{\pi} \left[ -\frac{1}{bI} + \frac{\pi}{4b^2 I^2} + \left(1 - \frac{1}{2b^2 I^2}\right) \cdot \frac{1}{\sqrt{(4b^2 I^2 - 1)}} \cdot \log \frac{(1 + 2bI) + \sqrt{(4b^2 I^2 - 1)}}{(1 + 2bI) - \sqrt{(4b^2 I^2 - 1)}} \right] \dots\dots(11)$$

where  $4b^2 I^2 > 1$ .

The peak value of the second-harmonic voltage induced in a 'read' winding of  $N$  turns can be evaluated from the formula

$$E = N \frac{d\phi}{dt} \times 10^{-8} \text{ V} \dots\dots(12)$$

and is equal to  $2\omega N \hat{\phi}_{2f} \times 10^{-8}$  V. If  $E_{2f}$  is defined as the peak-to-peak magnitude of the second-harmonic voltage to conform with the practical measurements then

$$E_{2f} = 32N\phi_T f \cdot F(b, I) \dots\dots(13)$$

where  $N$  is the number of turns on the 'read' coil.

$\phi_T$  is the leakage flux from the tape.

$f$  is the frequency of the modulation current.

$F(b, I)$  is a function of  $b$  and  $I$ .

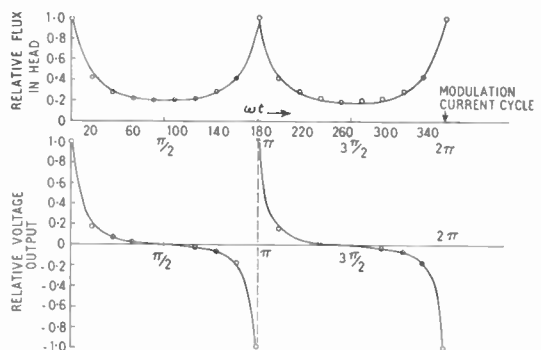


Fig. 7. Theoretical flux and voltage waveforms.

$I$  is the peak amplitude of the modulation current.

$b$  is a function of the head parameters. (See eqn. (7).)

In order to evaluate eqn. (13) the principal unknowns, namely,  $R_g$  and  $\phi_T$  were determined experimentally. Then assuming that all the leakage flux from the tape links the head and a digit of optimum length, recorded on a background of oppositely saturated magnetic tape, the second-harmonic signal is calculated to be 180  $\mu\text{V}$  peak per turn of 'read' winding. Experimentally the voltage is 110  $\mu\text{V}$  peak per turn, which represents a considerable agreement with the theoretical value.

These results were taken at 50 kc/s modulation current so that the effects of eddy currents were not important. (See Section 2.2.2.)

2.2.1. Sensitivity vs. modulation current

Equation (13) gives the amplitude of the second-harmonic voltage output of the head. The expression involves a term dependent on  $b$  and  $I$ , the modulation current amplitude. The value of  $b$ , which is a function of head parameters, may be calculated. Figure 8 shows the theoretical curve of signal output versus modulation current taken at the value of  $b$  corresponding to the heads in current use. Also shown on this graph is the experimental curve normalized to the same maxima in order that the relative shapes of the curves can easily be compared.

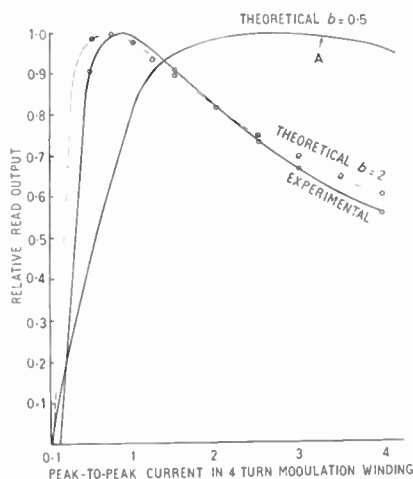


Fig. 8. Signal output vs. modulation current.

Both curves are essentially similar, each displaying a 'steep linear' region for small modulation currents, a 'saturation' region, and finally, a 'fall-off' region for increasingly high currents.

It will be noted that the theoretical curve passes through the origin of the axes, whereas the experimental curve displays zero output at a modulation current of 0.1 A peak-to-peak. For the purposes of the analysis of head operation, a continuous variation of permeability with modulation current was assumed. The experimental curve indicates that this is not the case, and that no variation in permeability occurs below currents of 0.1 A.

As the current increases above this value, reluctance modulation occurs and, during each current cycle, the leakage flux passing around the 'read' head is as shown in Fig. 7.

For increasing currents the minimum flux passing around the head becomes lower at the current peaks, more net change of flux occurs and the voltage induced in the 'read' winding has a larger second-harmonic component. Under these conditions the linear portion of the signal/modulation-current curve is traversed.

Further increases in current do not affect the amount of flux being changed, but merely alter the fraction of the current cycle during which this flux is changed. Although the amplitude of the voltage induced in the 'read' winding is larger, its second harmonic component begins to decrease, causing the 'fall-off' portion of the signal/modulation-current curve. The precise nature of this curve depends on the factor  $b$ . For example, if  $R_g$  was to be increased and hence  $b$  reduced to, say, 0.5, then the curve alters to that shown at A in Fig. 8. For maximum flux change to occur during a current cycle the value of  $R_H$  must be changed from much less than  $R_g$  to greater than  $R_g$ , since leakage-flux circulating the head is proportional to  $R_g/(R_g + R_H)$ . If the head has a large value of  $R_g$  then  $R_H$  must itself become large and this demands high modulation currents. This explains the shift of the curve to A in Fig. 8. Conversely, if  $R_g$  is reduced then the peak of the curve moves to the left. It must be stated, however, that the curves for very small gap sizes ( $R_g < 0.25$ ) will be inaccurate. This is because these curves display maximum sensitivity at low values of modulation current and the assumption  $\mu H = K'$  is most inaccurate in this region. It appears, however, to be quite satisfactory for the practical gap sizes considered as evidenced by the close agreement between experimental and theoretical data.

2.2.2. Sensitivity and frequency

Equation (13) which gives the expression for the signal output voltage of the head, displays a linear dependence on  $f$ , the frequency of the modulation current. Deviations from a linear dependence would be expected, however, due to the presence of eddy-current losses in the magnetic material of the head. These losses have not been taken into account in the theoretical development of eqn. (13).

Figure 9 shows the variation of output signal with frequency for the heads in use. The curve has been taken at a constant value of modulation current. It is closely linear up to a frequency of 50 kc/s. Beyond this there is still an increased signal to be obtained by an increase in frequency, trebling the modulation frequency of 50 kc/s results in increasing the available signal by a factor of 2.0, but subsequently the dependence rapidly departs from linearity and there would seem to be no advantage in using modulation frequencies greater than 200 kc/s.

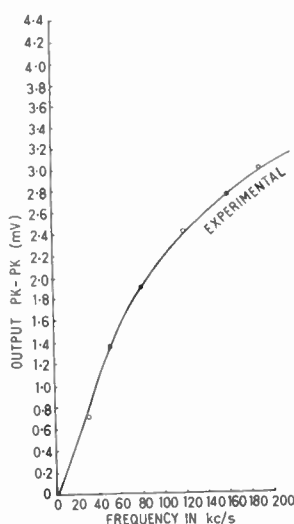


Fig. 9. Signal vs. frequency of modulation current.

The net effect of the flow of eddy currents is to prevent fields from penetrating immediately to the interior of the material, and when the applied field is varying continually the field strength in the interior of the material may never be more than a small fraction of the field strength at the surface.

Since the penetration of the field due to the modulation current is not complete at high frequencies, the effective area and permeability of the modulation section of the head will be reduced. The resultant variation in head reluctance is extremely difficult to calculate, but the factor  $b$  will tend to increase as eddy-current losses become more significant.

### 2.2.3. Step-function response

An understanding of the nature of the response of the magnetostatic 'read' head to digits recorded on tape can be obtained by examination of the 'read' head response to an isolated step change in the direction of magnetization of the tape. Figure 10 is a graph of the 'read' head output as the head position is moved toward and past a point on the tape where the magnetization changes from one saturated state to the

other. In the immediate region of the step change there is a concentration of leakage flux.

When the head is a long way from the change of magnetization it intercepts no leakage flux and there is zero output. At distances comparable with the overall head size, leakage flux will be intercepted and the signal will begin to rise as the head approaches the position of the step change. Assume that flux will flow through the head from limb X to limb Y. This will give rise to an output signal having some fixed phase relationship with respect to the modulation current. This phase has been defined as negative, as shown in Fig. 10.

The negative-phase signal continues to increase as the head approaches the step. When the head is over the step, although relatively large amounts of flux are flowing in limbs X and Y, these are flowing in opposite directions and the net flux flowing through the head begins to diminish. In fact, when the head is symmetrically placed with respect to the step change, the net flux flowing through it will be zero and there will be no output signal. As the head moves further to

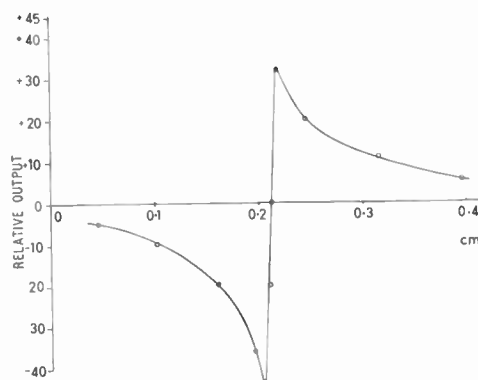


Fig. 10. Head response to step change.

the right, a relatively large amount of flux will circulate in the direction of limb Y to limb X and give rise to an output signal which is 180 deg out of phase with the initial signal. This is the positive-phase output signal shown in Fig. 10. This signal reaches a peak and then diminishes to zero as the head recedes from the step change. The response is fairly symmetrical. The graph of Fig. 10 is taken for the transition from the saturated state A to the saturated state B. If similar data were taken for the transition from state B to state A, the observed signals would be first of positive phase and then negative.

### 2.2.4. Digit response

For a recording system the digit signifying a '1' could be a short section of tape magnetically saturated in a direction opposite to that of the remainder of the

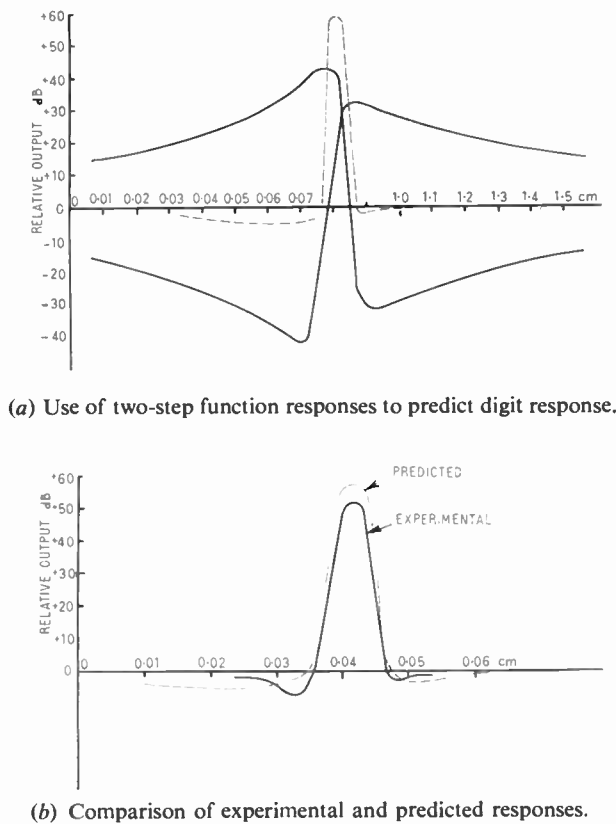


Fig. 11. Digit response.

tape. The digit, then, consists of two consecutive step changes of magnetization, the first being from state A to state B and the second from state B to state A. The response of the 'read' head to the digit may be deduced by the addition of the two individual step responses in appropriate positions. Using the step response of Fig. 10, the response to a digit of 0.010 in was calculated; the actual and predicted curves are compared in Fig. 11.

For a given head design there is clearly an optimum digit length to provide maximum digit signal. For lengths greater than the optimum the positive-phase signals of the two step responses are displaced and maximum reinforcement does not occur. For lengths shorter than the optimum the two step functions are tending to cancel each other. The optimum length of digit is approximately that at which the head just spans the digit, collecting leakage flux from both points at which the direction of magnetization changes.

The static reading head uses 0.002-in thick Permalloy C with a reading gap established by a 0.001-in brass spacer. It spans a digit of length 0.005 in, therefore, the reading of changeovers in the magnetic state spaced by 0.005 in is possible. The

experimental response to a single '1' digit of this size is shown in Fig. 12.

A 'zero' digit is indistinguishable from the background noise of the tape and is ideally represented by zero output signal. However, the magnitude of this 'zero' signal is determined by such factors as the remanence of the head itself, unbalanced modulation current and stray magnetic fields. Because of the very small size of the head, the effects of stray fields are sharply minimized. It is possible to obtain a modulation current relatively free of second harmonic, and remanence in the head may be eliminated by passing a small direct current (1mA) through the 'read' winding. The resultant 'zero' signal obtained is less than 1/50 of the signal obtained for a '1' digit.

### 2.3. Reading Head Characteristics

A summary of the dimensions and characteristics of the head for the system in use is given below.

Head material	Annealed Permalloy C
Width	0.040 in
Thickness	0.002 in
Hole size	0.015 in
Modulation current	0.8 A peak-to-peak
Modulation turns	2+2
Reading turns	3+3
Reading gap	0.001 in
Overall head size	0.050 in
Output signals	110 $\mu$ V peak per turn at a modulation frequency of 50 kc/s, 220 $\mu$ V at 150 kc/s.

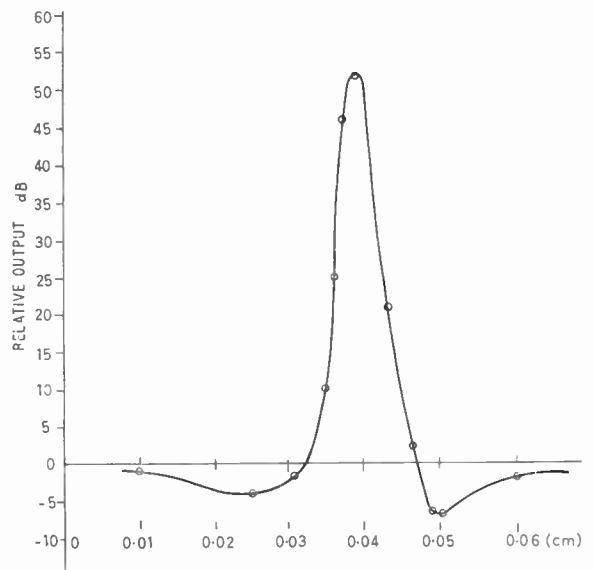


Fig. 12. Experimental response to a single '1' digit 0.005 in long.

2.4. *Combination Read-write Unit*

A useful magnetic component results from combining a static reading head and a writing head in close proximity. The arrangement is shown in Fig. 13. Naturally when writing, the field due to the writing current is detected by the 'read' head. For this reason the 'write' head is provided with a wide gap and a 0.005-in digit is written by applying a short current pulse (10 μs) to the write head. The digit length is determined by the mechanical structure of the head rather than the amount of tape movement in 10 μs. In this way the interference signal is small and has time to decay (100 μs) prior to the occurrence of the 'read' signal. At 10 in/s there is a 1-ms delay between writing and reading.

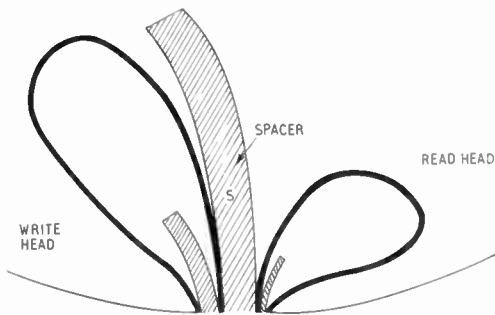


Fig. 13. Close-proximity read-write head.

This type of head permits the recording of information on tape over a wide range of speeds at a packing density independent of tape speed and depending only on the mechanical structure of the head. It also permits information to be written character by character on magnetic tape, each character being checked by reading from the tape before the writing of the remainder is permitted. A system operating on this principle and including arrangements for identifying good or bad characters has been built and has been operational for about 18 months. The system uses erased tape magnetized in one direction to represent a '1'. Whilst this results in half the output signal from the read head, it guards against drop-outs due to pin-holes in the oxide coating which will now look like erased tape.

2.5. *Conclusions*

A number of multi-track 'read' only and 'read'/'write' heads have been made in the last 18 months and have been operating successfully and reliably; generally in such a digital system they do not need any screening. The worst signal/noise ratio experienced in operation is of the order of 7 : 1. Reading and recording is 'in contact' and the 'read' head would appear to have the same separation loss of 55 dB per wavelength as a normal head. Whilst the performance

is low (for example, 100 digits/in and 10 in/s) in comparison with magnetic-tape systems employed as backing stores the scheme is satisfactory for many medium-speed digital computers. Also, there are indications that the system packing could be improved to about 200 digits/in, whilst the tape speed could also be increased by a factor of at least three without any change in the modulation frequency or the present bandwidth of the 'read' amplifier which is 14 kc/s centred at 300 kc/s.

3. **The Design of a Detector for use with the Brushless D.C. Tachogenerator**

3.1. *Principle of Operation of Tachogenerator*

Figure 14 illustrates the principle of operation of the brushless tachogenerator. A cylindrical conducting rotor A is placed in a d.c. magnetic field  $H_0$ . Rotation of the rotor in this primary magnetic field causes currents to flow in the rotor which produce a field with a component  $H$  at 90 deg to  $H_0$ .

Neglecting second-order effects and assuming the conductivity of the rotor is constant then

$$H = k\sigma\omega H_0$$

where  $\omega$  is the angular velocity of the rotor,  $\sigma$  is the conductivity of the rotor material and  $k$  is a constant depending on the geometry of the rotor.

The field  $H$ , which is proportional to the angular velocity of the rotor, is detected and can be measured by the second-harmonic modulator-detector D. In operation, the field set up by the rotor current is balanced by that of a current in the feedback windings W placed so that ideally the current distribution is exactly equivalent to that in the rotor. The detector D is then used as an error detector in conjunction with a suitable feedback system to maintain the difference between these fields within prescribed limits. The current in the feedback windings can then be used as a direct indication of rotor speed.

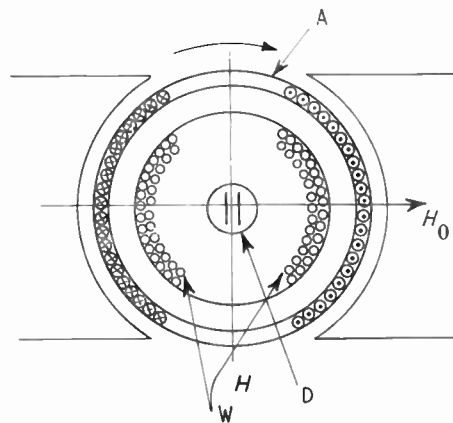


Fig. 14. Principle of operation of the brushless tachogenerator.

This form of tachogenerator seems capable of combining the low-noise properties of a brushless system with the excellent sensitivity afforded by the second-harmonic detector enabling quite low speeds to be measured. In addition, the linearity associated with a feedback system gives promise of a good performance in the high speed range.

3.2. Design of the Magnetic Circuit

In operation, the head must detect a field  $H$  of the order of 10 millioersteds in the presence of a field  $H_0$  at right angles without loss of sensitivity. It must also have a sufficiently small residual when  $H$  is zero.†

The value of  $H_0$  varies with the physical layout of the tachogenerator and typical values could be 2000 oersteds if the detector is in the body of the primary field (as in Fig. 14) or 1 to 10 oersteds if the head is screened.

Now it can be shown that the performance of the head is not much affected by the presence of  $H_0$  provided that:

- (a) The flux lines due to  $H_0$  are, at all times, at right angles to the direction of detection, otherwise conditions for a residual will be created.
- (b) The field strength created in the strip by  $H_0$  does not approach too near the saturation value for the magnetic material. (See Appendix.)

These requirements preclude the use of complete magnetic circuits such as those shown in Figs. 15(a), 15(b) and 15(c). Thus, in the circuit of Fig. 15(a), although a zero net-flux linkage with the read winding due to  $H_0$  can be achieved by suitable orientation of the head, flux densities in the  $y$  direction may easily approach saturation. The circuits of Figs. 15(b) and 15(c) are improved in as much as there is no tendency for flux lines from  $H_0$  to flow in the  $y$  direction provided the plane of the head is set accurately at

right angles to  $H_0$ . This adjustment, however, is very critical and in addition the circuit of Fig. 15(b) allows fields to be created by  $H_0$  in the material which may exceed saturation.

On the other hand, the open construction of the circuit of Fig. 15(d) does not encourage flux lines from  $H_0$  to flow in the  $y$  direction in the circumstances described above and adjustment of the head about the  $z$  axis is the only critical one. The orientation of the strips with the thin dimension parallel to  $H_0$  also satisfies the second requirement.‡

Although, in principle, such a magnetic circuit could and has been made to work in the presence of a right-angle field up to 1600 oersteds, in practice mechanical tolerances, the difference between the magnetic properties of the strips, and non-uniformity of the field, are such that condition (a) cannot be adequately satisfied. Thus it is necessary to operate the detector in a region where the right-angle field is small (<10 oersteds) to obtain an adequately small residual.

3.3. Detector Construction

Figure 16(a) shows the detector in skeleton form. A-A are two strips of annealed Permalloy C of rectangular cross section with windings M-M arranged so as to produce modulation fields in opposite directions in the two strips. 'Read' winding R encompasses both strips so that, in principle at least, there is zero coupling between the modulation and 'read' windings; this reduces the selectivity required in the 'read' amplifier to reject fundamental and odd harmonics and reduces the effect of any second harmonic in the modulation waveform. Even harmonic components of the flux in the strips which are generated by a d.c. bias field along the length of the strips produce e.m.f.s which are additive.

The use of annealed magnetic material is essential for the reduction of remanence and noise in the detector. A modulation-current frequency of 50 kc/s is employed which represents a compromise between adequate sensitivity (this is still increasing at 150 kc/s for the strips used in practice) and the requirement

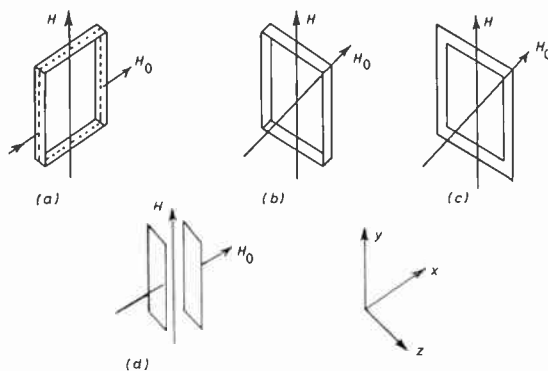
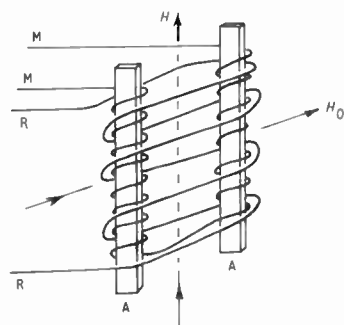


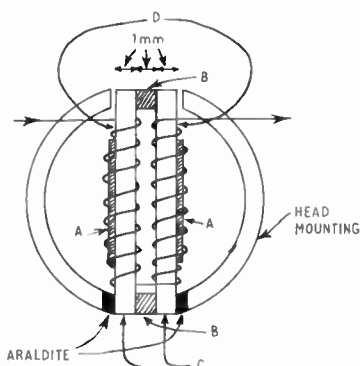
Fig. 15. Configurations of the detector magnetic circuit.

† The existence of a residual can be explained if it is assumed that the 'zero' is obtained by balancing two (or more) fairly large second-harmonic signals generated in different parts of the head by components of the field  $H_0$  which act in different directions in the different parts. This condition would arise if the detector were distorted or if  $H_0$  were not uniform and parallel. If now the different parts of the head have slightly different widths of hysteresis loop or are subject to different values of modulation field, then the phases of the second-harmonic components generated in the different parts will differ slightly resulting in the residual.

‡ It is relevant to note that for a strip 1 cm long, 2 mm wide and 0.015 mm thick, the value of  $B/H$  is 1.008 in a direction parallel to the 0.015 mm dimension and 135 parallel to the 2 mm dimension.



(a) Theoretical construction.



(b) Mechanical construction showing modulation winding (32 turns). The 'read' winding (not shown) has 43 turns.

Fig. 16. Second-harmonic flux detector construction.

that the modulation must saturate the body of the strip to secure a very low remanence figure.

A form of construction based on the ideas expressed in the previous section and used for the prototype tachogenerator is shown in Fig. 16(b). The former is fabricated from sections C cut from 1-mm microscope-slides. These are cemented together with suitable spacers B to form the rectangular structure shown and are ground to ensure that the surfaces D-D are parallel. Two identical strips of Permalloy C (A-A) are then cemented to C-C as shown. The dimensions are such that the modulation windings extend past the ends of the strips to reduce the decrease of field strength which occurs near the end of a solenoid.

The assembly is mounted in the holder shown at one end only to permit free longitudinal expansion; experience has shown that potting is undesirable as this increases the temperature rise and, consequently, mechanical distortion and produces distortion on its own account due to uneven contraction of the Araldite on setting.

This construction ensures that the detector occupies a small volume, thereby assisting the creation of a

uniform field for the head to operate in. A further improvement can be obtained by cementing the magnetic material on the inside faces of the sections C, but this increases the problem of ensuring that the faces are parallel.

The operation of the detector head is now considered in more detail and the result of the analysis is used to choose the optimum dimensions of the strips.

### 3.4. Detector Operation when the Magnetic Circuit is Incomplete

It has been shown (Sect. 3.2) that to detect a small magnetic field in the presence of a large one acting at 90 deg an open type of detector-head construction is required. This results in demagnetization effects. Thus if, for instance, a single strip of rectangular cross section is magnetized, poles appear at the ends creating a demagnetizing field  $H_D$  within the strip. This field is related to the intensity of magnetization  $I$  by

$$H_D = LI$$

where  $L$  is the demagnetization coefficient and is a constant determined by the strip dimensions. Now

$$B_i = H_i + 4\pi I$$

(where  $i$  refers to internal values), so that

$$H_D = (L/4\pi)(B_i - H_i)$$

Thus the external value of the magnetic field  $H_e$  necessary to create a field  $H_i$  in the material is given by

$$H_e = H_i + H_D$$

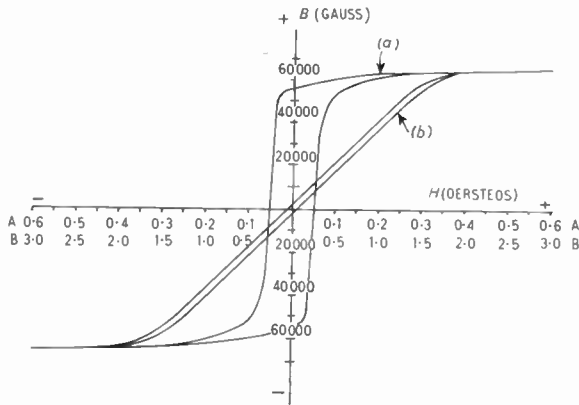
or

$$H_e = H_i(1 - L/4\pi) + (L/4\pi)B_i$$

and for the cases of interest  $1/500 > L/4\pi > 1/10\,000$ , so that  $L/4\pi \ll 1$  and  $H_e \approx H_i + (L/4\pi)B_i$ .

Consider now the effect of demagnetization on the hysteresis loop shown in Fig. 17(a), which is typical of materials in the Permalloy C class. The effective loop can be constructed by selecting values of  $H_i$ , reading off values of  $B_i$  from the loop and adding the quantity  $(L/4\pi)B_i$  on to  $H_i$  to obtain  $H_e$ . Thus, for the case where  $L/4\pi = 1/4000$  the 'sheared' loop takes the form shown in curve (b) of Fig. 17. This shows that the width of the loop is now small compared with the fields necessary to reach the 'saturation knee', so that the  $B/H$  characteristic now closely approximates to the idealized one assumed in the introduction except for the slope of the characteristic for values of field greater than saturation which is not zero. This will modify the shape of the voltage pulses at the output of the 'read' winding and hence the second-harmonic content.

However, assuming that the sheared  $B/H$  characteristic obtained in practice is the same as the ideal one, it is possible to evaluate the maximum second-



(a) Normal loop (scale A).  
(b) Sheared loop (scale B).

Fig. 17. Effect of demagnetization on hysteresis loop.

harmonic output and peak-modulation field required provided that the value of  $H_{sat}$  used is that relevant to the sheared  $B/H$  characteristic. If  $H'_{sat}$  is the required value, then

$$H'_{sat} = H_{sat} + (L/4\pi)B_{sat}$$

In the Appendix the peak value of second-harmonic output is calculated. This has a maximum value of

$$8NAB_{sat} \cdot f \times 10^{-8} \frac{H}{H'_{sat}} \dots\dots(14)$$

which occurs at a modulation field of amplitude  $\hat{H}$  such that

$$\frac{\hat{H}}{H'_{sat}} = \sqrt{2} \dots\dots(15)$$

3.5. Choice of Strip Dimensions

Normalizing eqn. (14) to  $N = 1$  and  $H = 1$ :

$$V_{2f} = \frac{8AfB_{sat} \times 10^{-8}}{H_{sat} + (L/4\pi)B_{sat}} \dots\dots(16)$$

and occurs when the peak value of the sinusoidal modulation field is

$$\hat{H} = \sqrt{2}[H_{sat} + (L/4\pi)B_{sat}] \dots\dots(17)$$

Consider now these expressions applied to a single strip of material of rectangular section and of length  $a$ , width  $b$  and thickness  $c$ . The demagnetizing factor  $L/4\pi$  is a function of the dimensional ratios  $b/a$  and  $c/a$ , so that it is convenient to rewrite eqn. (16) in the form

$$\frac{V_{2f}}{a^2} = \frac{8 \cdot b/a \cdot c/a \cdot f \cdot B_{sat} \times 10^{-8}}{H_{sat} + (L/4\pi)B_{sat}}$$

and to consider  $V_{2f}/a^2$  as the relevant quality rather than  $V_{2f}$ .

The detailed variations of  $L/4\pi$  with  $c/a$  and  $b/a$  have been calculated and the results used to determine

corresponding variations of  $V_{2f}/a^2$  per turn per oersted and the peak exciting field subject to the assumptions that:

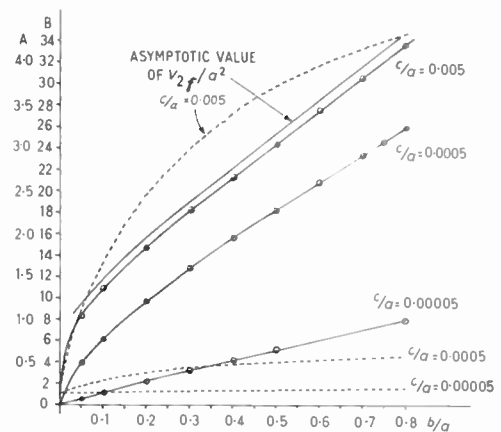
- (a)  $B_{sat} = 6400$  gauss; this represents a typical value and is approximately the average of the practical measurements obtained testing strips (Table 1).

Table 1

$B_{sat}$ for different strips			
Strip dimension		$B_{sat}$	
cm	mm	mm	
1	2	0.015	5460
1	4	0.015	5270
1	2	0.03	5850
1	4	0.03	6200
1	2	0.044	7300
1	4	0.044	7290
2	2	0.015	5760
2	4	0.015	5730
2	2	0.03	6360
2	4	0.03	6620
2	2	0.044	7850
2	4	0.044	7650

- (b)  $H_{sat} = 0.8$  oersted. This value is greater than that quoted for fully annealed material (0.2 oersteds), but measurements using a hysteresis loop tester show it to be typical of a specimen of annealed Permalloy C after cementing to the glass structure.

Figures 18(a) and 18(b) show the results of the above calculations plotted as families of curves.



Scale A ——— Variation of  $V_{2f}/a^2$  (mV peak).  
Scale B - - - - Variation of  $\hat{H}$  (oersteds).

Fig. 18. Variation of  $V_{2f}/a^2$  and  $\hat{H}$  with strip dimensions where  $a$  is the strip length.

3.6. Choice of Strip Length

This has to satisfy two conflicting requirements:

- (a) The strip should be as long as possible for maximum sensitivity and minimum modulation requirements.
- (b) The detector head should operate in a region where  $H$  is reasonably uniform; this implies small dimensions.

The final choice is somewhat arbitrary, but a value of  $a$  between one-fifth and a half the rotor diameter seems reasonable depending on the physical layout and therefore the resulting uniformity of the field.

3.7. Choice of  $b/a$  and  $c/a$

Reference to Fig. 18 shows that for all the values of  $b/a$  a considerable gain in sensitivity is obtained by increasing  $c/a$  from  $5 \times 10^{-5}$  to  $5 \times 10^{-4}$  at the expense of a similar increase in modulation requirements. However, the gain obtained by increasing  $c/a$  by a further factor of ten is very limited, whilst the necessary modulation field has increased out of proportion.

Thus a value of  $c/a$  of the order of  $5 \times 10^{-4}$  is indicated, whilst the value of  $b/a$  should be made as high as is consistent with ease of construction and availability of material.

It is interesting to note that for most practical sizes of strip the value of  $(L/4\pi)B_{sat}$  is much greater than  $H_{sat}$ , so that the performance depends on the strip dimensions rather than the state of the material.

Thus for the prototype detector, the strip is 0.5 in long, 0.25 in wide and 0.5 mil. thick; therefore  $c/a = 0.001$   $b/a = 0.5$ , which yields a value of  $L/4\pi B_{sat} = 4$  oersteds compared with the value of  $H_{sat} = 0.8$  oersteds.

3.8. Performance of Practical Detector

The performance of the detector head used in the prototype tachogenerator is summarized below:

- Maximum sensitivity = 0.19 mV p-p/millioersted in phase signal.†
- Modulation current for maximum sensitivity = 750 mA peak-to-peak
- Power dissipated in modulation windings = 150 mW
- Residual
  - (a) In 35-oersted field at 90 deg = 0.76 mV quadrature
  - (b) In 1-oersted field at 90 deg = 0.04 mV quadrature

† This figure is less than twice the theoretical value for one strip as in practice the 'read' winding is not in close proximity to the Permalloy strips so that it does not link all the flux. There is also some interaction between the strips.

- Remanence = 0.1 millioersteds
- Noise = 0.03 millioersteds
- Coupling, between modulation and 'read' windings, is such that second-harmonic suppression in the oscillator for an equivalent error 0.1 of the polarization error =  $\frac{1}{2300}$

3.9. Schematic of Prototype Tachogenerator System

As a conclusion to this section of the paper a simplified description of a prototype tachogenerator system is given which employs the form of the second-harmonic detector just considered. Figure 19 shows a block schematic of the complete tachogenerator system.

A sinusoidal current at a frequency of 50 kc/s is fed from the oscillator O to the modulation windings of the flux gate detector D. This produces, at the output of the 'read' windings, a second-harmonic voltage at 100 kc/s whose amplitude is proportional to the d.c. magnetic field created by the rotor currents and whose phase with respect to the fundamental is independent of the magnitude of the field unless it reverses sign, in which case the output changes in phase by 180 deg. This voltage is fed to a band-pass a.c. amplifier A1 tuned to 100 kc/s whose output is converted by a phase-sensitive rectifier into a balanced d.c. potential whose magnitude and sign depends on the magnitude and direction of the field at the detector. This potential is fed via a stabilizing network to a d.c. current amplifier A2 which in turn feeds the split feedback winding F1F2.

If these windings are connected in the proper sense, any increase of magnetic field caused by rotation of the rotor causes an output from the detector resulting in a current change in the feedback windings which annuls the field created by the rotor.

The change of current is determined by measuring the differential voltage  $V$  across the resistors R1 and R2. These resistors are proportioned so that if the sensitivities of the two windings F1 and F2 are respectively  $k_1$  and  $k_2$  oersteds per unit current then:

$$\frac{k_1}{k_2} = \frac{R_1}{R_2}$$

The second-harmonic reference voltage for the phase-sensitive detector is derived from the oscillator via a frequency doubler and an adjustable phase shifter.

Figure 20 illustrates the complete assembly, including the excitation magnet (A), the slotted rotor (B) and the detector zeroing adjustment (C).

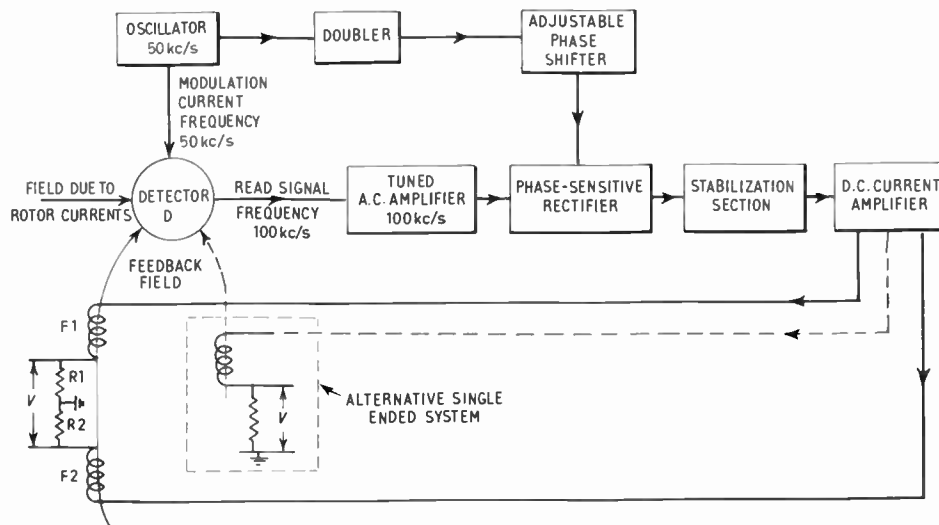


Fig. 19. Block diagram of prototype tachogenerator.

In Fig. 21 the rotor has been removed, revealing the feedback windings (D). It can be seen that the distribution of these windings is similar to the distribution of field (and therefore the current in the rotor) promoted by the pole pieces (E) in conjunction with a central iron core (not visible).

The axial position of the detector head indicated by the arrow in Fig. 21 was chosen in the prototype so as to remove the very sensitive detector from the vicinity of the powerful excitation field and hence improve the zero error and residual. Associated with this decision is the necessity for slotting the rotor to force currents induced in the excitation region of the rotor into the vicinity of the detector head.

Performance tests on the prototype showed that a zero stability of the order of  $<0.1$  rev/min could be expected under laboratory conditions. Above 100 rev/min the output signal at constant speed was a function of time, as a result of a change of rotor conductivity due to the heating effect of the induced currents. This effect provides an upper limit to the speeds which can be measured with this type of tachogenerator system.

#### 4. Acknowledgments

The authors wish to acknowledge Professor F. C. Williams and Professor T. Kilburn for the initial conceptions of the two devices described in this paper. They also acknowledge Mr. T. Zombory-Moldovan for his work on the construction of the heads and all members of the Electrical Engineering Department of the University of Manchester for their co-operation in the preparation of this paper.

#### 5. References

1. F. C. Williams and S. W. Noble, "The fundamental limitations of the second-harmonic magnetic modulator as applied to the amplification of small d.c. signals", *J. Instn Elect. Engrs*, 97, Part II, p. 445, 1950.
2. E. P. Felch *et al.*, "Airborne magnetometer", *Electrical Engineering*, 66, p. 680, July 1947.
3. C. Q. Adams, "New flux-gate magnetometers for use with single strip permeameters", Navord Report 6835, U.S. Naval Ordnance Laboratory, White Oak, Maryland, May 1960.
4. E. D. Daniel, "A flux-sensitive reproducing head for magnetic recording systems", *Proc. Instn Elect. Engrs*, 102, Part B, p. 442, July 1955.
5. J. C. West and T. W. Hey, "Elimination of brush ripple in d.c. tachometer generators", *J. Sci. Instrum.*, 28, p. 18, 1951.
6. C. C. Johnson, "A homopolar tachometer for servomechanism application", *Proc. Inst. Radio Engrs*, 40, p. 158, 1952.
7. "Brushless Tachometer Generator", U.K. Patent Application No. 28181/56.
8. T. Kilburn, G. R. Hoffman and P. Wolstenholme, "The reading of magnetic records by reluctance variation", *Proc. Instn Elect. Engrs*, 103, Part B, Supplement No. 2, 1956.
9. L. W. Ferber, "Flux-responsive magnetic heads for low-speed read-out of data", *Inst. Radio Engrs Conv. Rec.*, Part 4, 1958.
10. E. D. Daniel, P. E. Axon and W. T. Frost, "A survey of factors limiting the performance of magnetic recording systems", *Proc. Instn Elect. Engrs*, 104, Part B, p. 158, March 1957.
11. S. E. Buckley, "Permalloy", reprinted from "Steels in Modern Industry", Standard Telephones and Cables Ltd., 1951.
12. J. A. Osborn, "Demagnetizing factors of the general ellipsoid", *Physical Review*, 67, Nos. 11 and 12, June 1st-15th 1945.

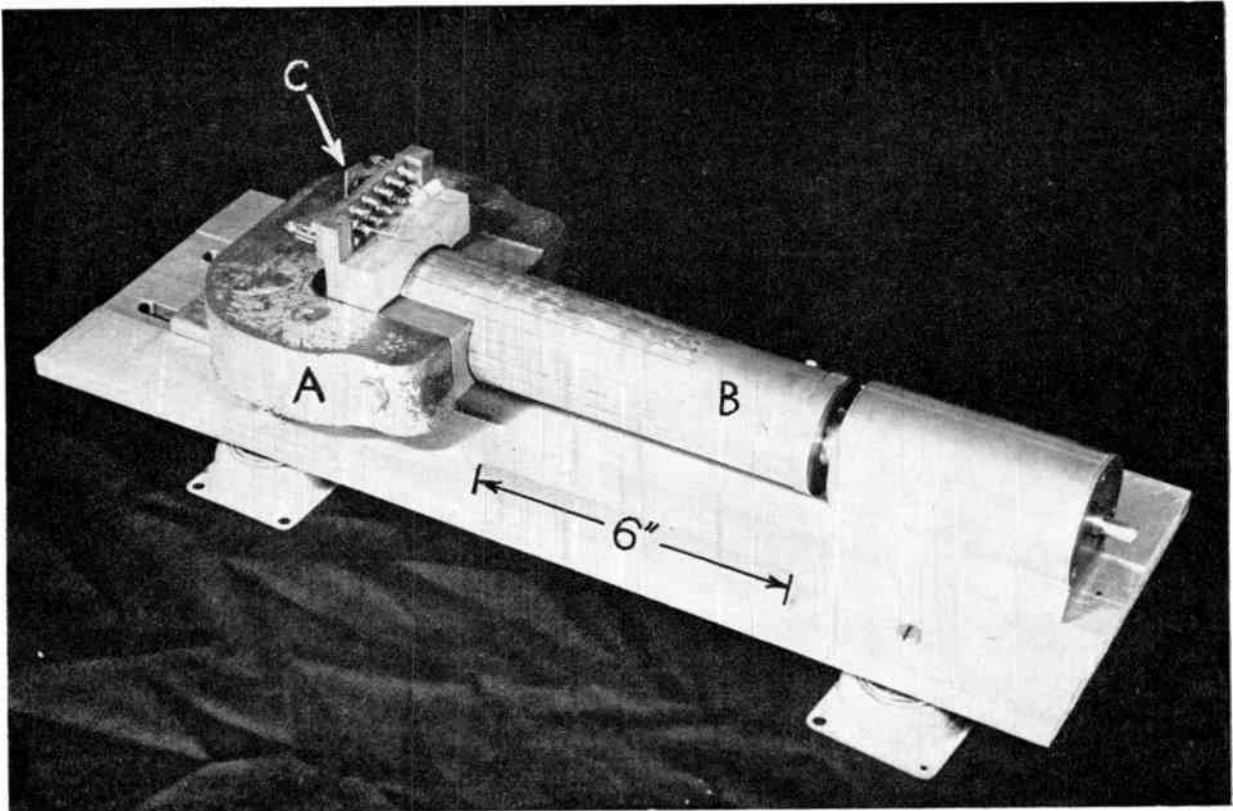


Fig. 20. Complete assembly of the tachogenerator.

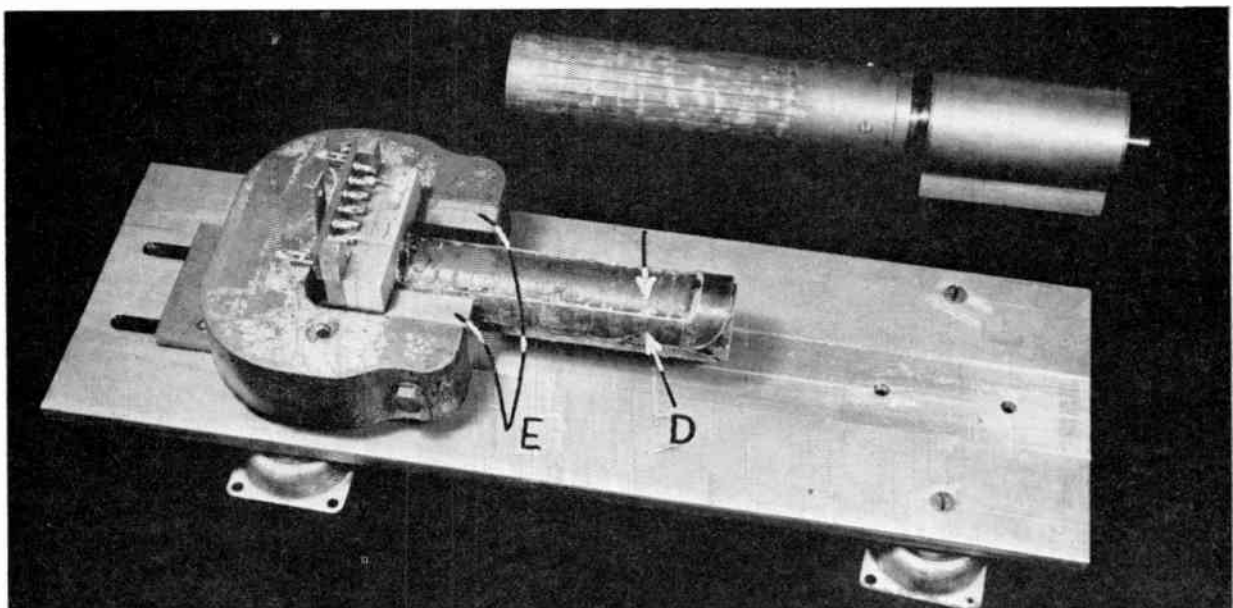


Fig. 21. Tachogenerator with the rotor removed to show the feedback windings.

### 6. Appendix

Returning now to Fig. 1 and replacing the value of  $H_{sat}$  by  $H'_{sat}$ , it is convenient to consider the positive pulses of the train as constituting one waveform and the negative pulses another and then to add these waveforms to obtain a resultant.

Now it can be shown that for the pulse train shown in Fig. 1(e) with peak amplitude  $E$ , period  $T$ , and pulse width  $\tau$ , the amplitude of the second-harmonic component is given by:

$$V_{2f} = \frac{E}{\pi} \sin \left[ 2\pi \frac{\tau}{T} \right]$$

Rewriting this equation:

$$\begin{aligned} V_{2f} &= E\tau \cdot \frac{2}{T} \cdot \frac{\sin [2\pi(\tau/T)]}{2\pi(\tau/T)} \\ &= (\text{area under pulse}) \cdot \frac{2}{T} \cdot \frac{\sin 2\pi(\tau/T)}{2\pi(\tau/T)} \quad (18) \end{aligned}$$

Thus, it can be seen that the amplitude of the second-harmonic component of the pulse train depends, for a given repetition rate, only on the area under the pulses and their width.

Returning now to the case in hand, and assuming  $\hat{H}/H'_{sat} \geq 1$  it can be seen from Fig. 1(b) that:

$$\frac{\tau}{T} = \frac{H'_{sat}}{2\hat{H}} \quad \dots\dots(19)$$

whilst the area under the pulse is just equal to the switched flux linkages with the 'read' windings:

$$= 2NAB_{sat} \times 10^{-8} \quad \dots\dots(20)$$

where  $N$  is the number of turns on the 'read' winding and  $A$  is the cross-sectional area of the specimen. Combining eqns. (18), (19) and (20), the amplitude of the second-harmonic components of the positive- and negative-pulse trains  $V_{2f+}$  and  $V_{2f-}$  is given by

$$V_{2f+} = V_{2f-} = 4NAB_{sat}f \times 10^{-8} \left[ \frac{\sin \pi H'_{sat}/\hat{H}}{\pi H'_{sat}/\hat{H}} \right]$$

and when the bias field  $H$  is zero, these will be exactly 180 deg out of phase yielding a zero second-harmonic component.

Referring again to Fig. 1(b), the action of the positive bias field  $H$  is to advance the positive pulse train by the time  $H.T/4\hat{H}$ . Similarly, the negative pulse train is delayed by the same amount, i.e. the total change is  $H.T/2\hat{H}$ . The second-harmonic components will also be delayed relative to one another by a time  $H.T/2\hat{H}$ , and this is equivalent to a phase shift of the second-harmonic component of

$$\frac{H.T/2\hat{H}}{T/2} \cdot 2\pi = 2\pi \frac{H}{\hat{H}}$$

The resultant second-harmonic output is obtained by vectorial addition of the two components with the

above phase shift. Thus for small values of  $H$ , the phase shift is small and

$$\begin{aligned} V_{2f} &= 4NAB_{sat}f \times 10^{-8} \left[ \frac{\sin \pi H'_{sat}/\hat{H}}{\pi H'_{sat}/\hat{H}} \right] \cdot \frac{2\pi H}{\hat{H}} \\ &= 8NAB_{sat}f \times 10^{-8} \sin \frac{\pi H'_{sat}}{\hat{H}} \cdot \frac{H}{H'_{sat}} \end{aligned}$$

This has a maximum value of

$$8NAB_{sat}f \times 10^{-8} \cdot \frac{H}{H'_{sat}} \quad \dots\dots(21)$$

when

$$\frac{\hat{H}}{H'_{sat}} = 2 \quad \dots\dots(22)$$

In practice sine-wave modulation is usually used, as this is easier to generate and enables the bandwidth of the system and hence noise to be reduced. A corresponding analysis leads to the same maximum value of  $V_{2f}$ , but requires a field of amplitude  $\hat{H}$  such that

$$\frac{\hat{H}}{H'_{sat}} = \sqrt{2} \quad \dots\dots(23)$$

Equations (21) and (22) have been obtained in a manner which emphasizes those physical characteristics of the magnetic material which are important, i.e.  $B_{sat}$  and  $H'_{sat}$ .

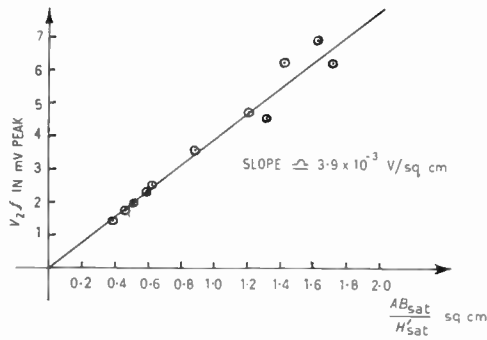
Now  $B_{sat}$  is mainly dependent on the constitution of the material, whilst  $H'_{sat}$  is in practice mainly determined by the term  $(L/4\pi)B_{sat}$ , and hence by the demagnetization coefficient and in turn the strip dimensions.

#### 6.1. Experimental Confirmation of Theoretical Expressions

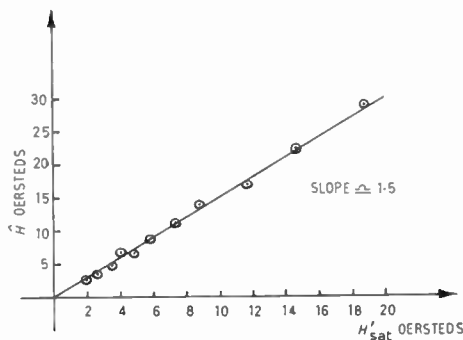
In order to test the validity of eqns. (21) and (23) the maximum second-harmonic output from strips of Permalloy C of rectangular cross-section and various dimensions was measured for a known value of  $H$  (0.028 oersteds). The amplitude of the sinusoidal modulation field (frequency 50 kc/s) necessary to achieve the maximum output was also measured. A separate experiment was performed which enabled the values of  $B_{sat}$  for the different strips to be ascertained.

Knowing the dimensions of each strip, it is possible to calculate<sup>1,2</sup> the value of  $L/4\pi$  if it is assumed that the strips are ellipsoids having axes whose lengths are equal to the strip dimensions. Values of  $B_{sat}$  are available from the second experiment and the value of  $H_{sat} = 0.8$  oersteds has been obtained from measurements on a hysteresis loop tester.

Results for twelve strips wound with a 50 turn 'read' winding and having dimensions ranging from



(a) Graph of  $V_{2f}$  vs.  $\frac{AB_{sat}}{H'_{sat}}$



(b) Graph of  $\hat{H}$  vs.  $H'_{sat}$

Fig. 22. Characteristics of experimental single-strip detectors.

1 cm  $\times$  2 mm  $\times$  0.015 mm to 2 cm  $\times$  4 mm  $\times$  0.044 mm have been obtained and graphs of

(a)  $V_{2f}$  vs  $\frac{AB_{sat}}{H'_{sat}} = \frac{AB_{sat}}{[H_{sat} + (L/4\pi)B_{sat}]}$

(b)  $\hat{H}$  vs  $H'_{sat} = [H_{sat} + (L/4\pi)B_{sat}]$

have been plotted in Figs. 22(a) and (b). Values of  $B_{sat}$  for the strips are tabulated in Table 1.

The graphs of Figs. 22(a) and (b) are both straight lines through the origin confirming the predicted variations of  $V_{2f}$  and  $\hat{H}$  with strip dimensions. Also in Fig. 22(a) the slope of the graph according to eqn. (21) should be

$$8NfH \times 10^{-8} = 5.6 \times 10^{-3}$$

In practice the slope is  $3.9 \times 10^{-3}$  so that only 0.7 of the expected second harmonic is obtained. This is presumably due to the non-zero slope of the saturation portion of the sheared  $B/H$  characteristic obtained in the practical head and consequent 'smoothing out' of the pulse train.

Similarly in Fig. 22(b) the slope of the graph according to eqn. (23) should be  $\sqrt{2}$ , the actual value of 1.48 being in reasonable agreement.

### 6.2. Detector Operation in a Field at 90 deg to the Principal Fields

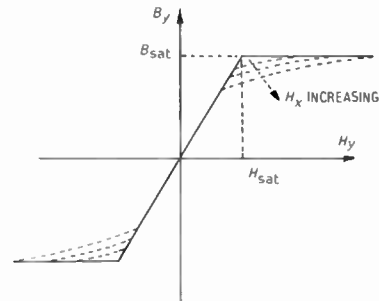
The effect on detector operation of a magnetic field at 90 deg to the direction of detection can be demonstrated by considering the effect of such a field on the  $B/H$  characteristic in the direction of interest.

Consider the idealized  $B/H$  characteristic shown in Fig. 23(a) with  $B = f(H)$  where:

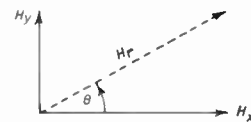
$$f(H) = \frac{B_{sat}}{H_{sat}} \quad \text{for } H < H_{sat}$$

and  $f(H) = B_{sat} \quad \text{for } H > H_{sat}$

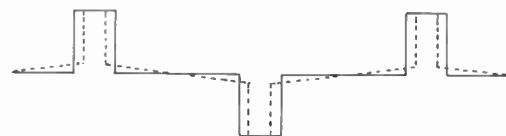
If an isotropic medium is assumed then the characteristic shown describes the relation between the net values of  $B$  and  $H$  in the medium, these being presumed to have the same directions. If  $B_y$  and  $H_y$  are the values of  $B$  and  $H$  in the direction of detection and  $B_x$  and  $H_x$  the corresponding values in a direction at 90 deg, then the resultant field  $H_r$  (see Fig. 23(b)) is



(a)  $B-H$  characteristics.  
(—  $H_x = 0$ ; - - -  $H_x \neq 0$ )



(b) Addition of field components.



(c) Effects on pulse shape.  
(—  $H_x = 0$ ; - - -  $H_x \neq 0$ )

Fig. 23. Operation in crossed fields.

given by

$$H_r = (H_x^2 + H_y^2)^{\frac{1}{2}}$$

and makes an angle  $\theta$  with  $H_x$  such that

$$\sin \theta = \frac{H_y}{H_r}$$

The resultant induction  $B_r$  is then

$$B_r = f(H_r)$$

and the component in the y direction is

$$B_y = B_r \sin \theta$$

or

$$B_y = \frac{f(H_r)}{H_r} \cdot H_y$$

Now for  $|H_r| \leq H_{sat}$ ,  $f(H_r) = B_{sat}/H_{sat}$ , so that

$$B_y = \frac{B_{sat}}{H_{sat}} H_y \quad \dots\dots(24)$$

This holds for values of  $H_y$  such that:

$$|H_y| < (H_{sat}^2 - H_x^2)^{\frac{1}{2}}$$

For values of  $|H_y|$  greater than this value,  $f(H_r) = B_{sat}$  and

$$B_y = \frac{B_{sat}}{[1 + H_x^2/H_y^2]^{\frac{1}{2}}}$$

Thus, the effect of the 90 deg field is to leave the original  $B/H$  characteristic unchanged up to the point where  $|H_y| = (H_{sat}^2 - H_x^2)^{\frac{1}{2}}$ . Then the induction approaches  $B_{sat}$  asymptotically. This is depicted in Fig. 23(a) by the family of dotted curves for increasing values of  $H_x$ . The resultant pulse train at the output of the detector read winding will now take the form shown in Fig. 23(c). The same general form as in Fig. 1(d) is still evident, but now not all the flux is switched at the high rate.

To obtain some idea of the magnitude of the effect, consider a value of  $H_x$  such that

$$H_x = 1/3 H_{sat}$$

The high rate of flux switching is then maintained up to the point where

$$\begin{aligned} |H_y| &= (H_{sat}^2 - 1/9 H_{sat}^2)^{\frac{1}{2}} \\ &\simeq 0.94 H_{sat} \quad \dots\dots(25) \end{aligned}$$

Combining eqns. (24) and (25)

$$B_y = 0.94 B_{sat}$$

Thus even with  $B_x = 1/3 B_{sat}$ , only 6% of the total possible flux is not switched at the high rate, so that the effect on the second-harmonic output of the head should be correspondingly small.

### 6.3. Conclusions to Appendix

In conclusion, eqns. (21) and (23) describe, adequately for design purposes, the performance of a second-harmonic detector head having an incomplete magnetic circuit. The general agreement with experiment also confirms the validity of assuming the strips are ellipsoids when calculating values of the demagnetization coefficient.

In addition, it has been demonstrated that the above expressions should hold adequately when the detector is operated with superimposed 90 deg fields producing flux densities in the material as high as one-third of the saturation value.

*Manuscript first received by the Institution on 17th July 1963 and in final form on 1st November 1963. (Paper No. 881/C66.)*

© The British Institution of Radio Engineers, 1964

**Brit.I.R.E. Symposium on**  
**“COLD CATHODE TUBES AND THEIR APPLICATIONS”**  
Cavendish Laboratory, University of Cambridge, 16th to 19th March, 1964

TIME-TABLE AND PROGRAMME

**Monday, 16th March** 6.30—7.30 p.m.  
Institution Reception for Delegates at Downing College.

**Tuesday, 17th March** 9.30 a.m.—12.30 p.m.

**Session I: ‘PHYSICS OF OPERATION AND TUBE DEVELOPMENT’**

*Chairman:* PROFESSOR SIR NEVILL MOTT, F.R.S.

- ‘Cold Electrode Emission from Metal Surfaces in Gases’—F. LLEWELLYN JONES.
- ‘Temporal Growth of Ionization Currents in Gases’—C. G. MORGAN and T. WILLIAMS.
- ‘Statistical and Formative Time Lags in Cold Cathode Tubes’—D. W. E. FULLER.
- ‘Some Theoretical Considerations of Breakdown and Transfer Mechanisms in Multi-electrode Cold Cathode Tubes’—J. M. GLACKIN.
- ‘Impedance Characteristics of Glow Discharge Tubes in the Frequency Range 200 c/s–70 Mc/s’—  
F. A. BENSON and M. W. BRADSHAW.

2.15—5.15 p.m.

*Chairman:* MR. A. G. WRAY, M.A. (*Member*)

- ‘Primed Cold Cathode Diodes’—D. H. WRIGHT.
- ‘The Design and Operation of Glow Modulator Tubes’—D. REES.
- ‘The Multiple Anode Dekatron’—D. REANEY.
- ‘A 1-Mc/s Bi-directional Counting Tube’—P. F. K. APEL.
- ‘Design Considerations in Cold Cathode Display Tubes’—A. TURNER.

**Wednesday, 18th March** 9.30 a.m.—12.30 p.m.

**Session II: ‘CIRCUIT DESIGN AND RELIABILITY’**

*Chairman:* MR. D. REANEY (*Associate Member*)

- ‘Cold Cathode Counting—Design Considerations’—W. A. FAVILL.
- ‘Component Tolerances as a Governing Factor in the Success of Cold Cathode Tube Circuit Design’—  
D. M. NEALE.
- ‘Counting Circuit Design using the Inherent Reliability of Counting Tubes’—C. S. BARKER and G. F. JEYNES.
- ‘The Trigger Tube—Reliability and Ratings’—M. E. BOND.
- ‘A New Glow Discharge Alpha-numeric Display and the Associated Character Storage Circuitry’—  
T. C. MALONEY and D. GLASER.

2.15—5.15 p.m.

*Chairman:* MR. J. L. THOMPSON, *President of the Institution*

- ‘A New Trigger Tube for Logical Functions’—G. KERR.
- ‘The Glow Thyatron’—M. VOLLENWEIDER.
- ‘Coding with Multiple-anode Glow Discharge Tubes’—H. E. SEIFERT.
- ‘A System of Digital Building Blocks using Cold Cathode Tubes’—J. WAGNER.
- ‘Influence of a Passive Network on the Glow Transfer Characteristics of a Cold Cathode Decade’—  
P. K. PATWARDHAN and M. G. PHADNIS.

**7 for 7.30 p.m.—Symposium Dinner in Downing College**

Thursday, 19th March

9.30 a.m.—12.30 p.m.

**Session III: 'APPLICATIONS OF COLD CATHODE TUBES'**

*Chairman:* MR. J. R. HUGHES (*Member*)

- 'A Batch Weight Ratemeter using Cold Cathode Triode Memories'—W. W. WOOD.
- 'An Inexpensive Digital Voltmeter using Multiple Anode Dekatrons'—P. GLEGHORN.
- 'A Telemetry System Employing Cold Cathode Tubes'—J. B. RICHARDSON.
- 'Applications of Cold Cathode Trigger Tubes in Telephone Exchange Equipment'—R. E. BAXTER.
- 'The Use of Cold Cathode Tubes in Supervision of Burners of High Power'—J. M. MEGNOUX.

2.15—5.15 p.m.

*Chairman:* MR. J. R. BRINKLEY (*Member*)

- 'Use of Cold Cathode Trigger Tubes in Explosion Detection and Suppression Circuits'—J. B. COLLINS.
- 'Cold Cathode Trigger and Counter Tubes for Computing Applications'—N. KITZ.
- 'Some Applications of Glow Transfer Tubes'—C. C. H. WASHTELL.
- 'The Application of Gas Diodes in Electronic Musical Instruments'—H.v.d. KERCKHOFF.

## *Synopses of Papers to be presented at the Symposium*

### **Tuesday, 17th March. Session I: 'PHYSICS OF OPERATION AND TUBE DEVELOPMENT'**

#### **Cold Electrode Emission from Metal Surfaces in Gases**

PROFESSOR F. LLEWELLYN JONES. (*University College of Swansea.*)

The fundamental processes underlying the role of the cathode in the cold cathode glow discharge are discussed. Quantitative investigations of the cold field induced emission have been made and the mechanism investigated. This is the process which underlies the statistical time-lag in a cold cathode tube.

#### **Temporal Growth of Ionization Currents in Gases**

C. G. MORGAN, M.SC., PH.D., AND W. TERRY WILLIAMS, B.SC. (*University College of Swansea.*)

This paper is an analysis of the collisional processes involving metastable atoms, positive ions and photons, as well as primary electron ionization, which are involved in the rapid growth of ionization. The paper is thus relevant to the action of trigger tubes, spark gaps, thyatron, etc.

#### **Statistical and Formative Time Lags in Cold Cathode Tubes**

D. W. E. FULLER. (*Hivac.*)

Time lag of breakdown is important where high speed of count, or a rapid reaction to an input is required. Many papers have been published discussing time lags in general gas discharges, but few deal with the case of practical cold cathode tubes. Statistical time lags are inherent in glow-discharge cold cathode tubes but they can be reduced by the introduction of radioactive materials, a priming discharge or illumination. The theoretical aspects of formative and statistical lags are discussed and related to the design and use of cold cathode tubes. The influence of pulse amplitude, pulse rise time and pulse repetition rate will be dealt with, as well as the tube geometry, cathode material, gas filling and method of priming.

#### **Design Considerations in Cold Cathode Display Tubes**

A. TURNER. (*Ericsson Telephones.*)

As display tubes appear in the final stage of a 'black box', it is essential that there can be no mistake in reading the value displayed, and as human operators are involved at this stage it is necessary that the appearance is aesthetically pleasing. In addition, the electrical characteristics must be compatible with the preceding counting or logic stage, and when considering both electrical and appearance requirements, certain compromises must be made. The relationship between these two considerations will be discussed, with reference to currently available tubes.

### Impedance Characteristics of Glow-Discharge Tubes in the Frequency Range 200 c/s–70 Mc/s

F. A. BENSON, D.ENG., PH.D., AND M. W. BRADSHAW, B.ENG. (*University of Sheffield.*)

The impedance presented to a small alternating signal, superimposed on the steady operating voltage of a glow-discharge tube, increases with frequency. To explain the origin of various observed effects van Geel derived a theory by considering perturbations about the steady-state maintenance condition and assuming that physical quantities in the discharge are functions of the instantaneous current and voltage alone. This predicts that the impedance loci (reactance-resistance curves) should be semicircles (neglecting displacement current). The impedance locus of a tube has the form predicted by this theory if it is extended to include several delayed effects. Secondary processes of electron production can be regarded as retarded functions of current and voltage since they are associated with a delay time.

To confirm the theory impedance measurements were first made over the frequency range 300 c/s to 5 Mc/s on tubes with pure-neon fillings at various pressures and several neon-argon mixtures. These have recently been extended up to a frequency of 70 Mc/s using pure-neon tubes having cathodes of various materials with several gas pressures and steady tube currents. The results of these measurements will be discussed and compared with theoretical predictions.

The equivalent circuit of a glow-discharge tube may be determined from the impedance investigations.

### Primed Cold Cathode Diodes

D. H. WRIGHT. (*Hivac.*)

The simplest form of cold cathode diode has two properties which are of value in electronic circuits; the firing voltage and the maintaining voltage. The firing voltage when measured infinitely slowly in ideal conditions is fixed by the materials and geometry of the electrodes and the gas filling. Unfortunately in practice external influences have profound effects on the firing voltage, particularly in fast operating conditions.

A diode can be made in which the external effects can be reduced and more control exercised over the firing voltage by supplying the required priming agents for firing internally in the tube which in the simple diode were randomly supplied. Initial electrons and ions required for striking can be obtained either photo-electrically or from an ion source. The ion source can either be radioactive or an additional low current glow discharge. A tube is described in which an increased level of control of firing voltage is obtained. Such tubes are employed where a stable value of firing voltage is required.

### The Design and Operation of Glow Modulator Tubes

D. REES, B.SC. (*English Electric Valve Company.*)

The glow modulator is a gas-filled cold cathode tube, which makes use of the special properties of a hollow cathode or crater type cathode. Selection of the gas mixture and choice of optimum pressure result in a light source which fulfils all the requirements of photo-facsimile equipment. The hollow cathode provides a ring of intense light of small area which can be projected through an optical system.

The construction of these tubes will be described together with the influence of geometry, gas pressure and composition on the light output. The effect on life of these same variables will also be discussed. Spectra of the visible radiation will be shown and discussed in relation to the photographic paper used in equipment.

### The Multiple Anode Dekatron

D. REANEY (*Associate Member.*) (*Ericsson Telephones.*)

The principles of the double-pulse dekatron will be briefly reviewed and some of the difficulties both of production and application will be outlined.

Two classes of tube are defined:

- (a) Having multiple anodes and multiple cathodes suitable for conventional counting and directly coupled read-out.
- (b) Having multiple anodes and a single cathode.

This latter group contains both two-guide tubes of a more or less conventional type and tubes having a single locking electrode with a magnetic bias to provide directional information.

The advantages of the latter tube include the fact that it is virtually independent of the form of the stepping pulse. Experimental tubes have been made but in the present form are rather slow.

The characteristics of these tubes and possible future developments and applications will be discussed.

### **A 1-Mc/s Bi-directional Counting Tube**

P. F. K. APEL. (*Elesta.*)

The ECT 100 is a gas-filled, bi-directional counting tube with twenty cold cathodes designed for high counting speeds and simple counting circuits. The mechanical construction was designed with the aim of high stability of the glow discharge in a wide current range, of optimal output conditions and counting reliability at high frequencies. Insulation resistance stability in spite of cathode sputtering is essential for long life.

The counting principle is described. Special problems arise when the counting frequency reaches the frequency limit, which is set by ionization and deionization processes. Periodical and statistically arriving input pulses result in different behaviours of the counting tube.

Simple counting decades for counting frequencies up to 1 Mc/s and bi-directional operation are possible. A combination of transistor circuits and the low drive pulse requirements give very uncritical and reliable operating conditions.

A standard driver stage for frequencies up to 100 kc/s is described.

## **Wednesday, 18th March. Session II: 'CIRCUIT DESIGN AND RELIABILITY'**

### **Cold Cathode Counting—Design Considerations**

W. A. FAVILL. (*Integral.*)

Counting techniques are considered from the point of view of equipment design, where the method of counting can be selected from a wide range of circuits based on a variety of devices, e.g. valves, transistors, ferromagnetic components, dekatrons, etc.

The reasons and considerations in the adoption of cold cathode devices for counting and display purposes, are discussed.

The design of counting circuits is then considered, the subjects being divided into:

- (a) Choice of display tubes.
- (b) Choice of display drives.
- (c) Design requirements of cold-cathode drive stages and practical circuits.

Reliability and life questions are considered.

### **Counting Circuit Design using the Inherent Reliability of Counting Tubes**

C. S. BARKER, B.SC., AND G. F. JEYNES. (*Mullard Radio Valve Company.*)

The paper outlines the results of a series of experiments aimed at establishing the inherent reliability of the conventional double-pulse, thirty-cathode stepping tube. The approach has been to investigate the effect of variations in the applied voltages, the duration of the discharge on each main and guide cathode, and the total current. From the results of this work which are based on life tests under a large number of conditions the areas of operation for optimum reliability for a particular tube type are now precisely defined.

In addition, the interpretation of these results into concepts which can be used by a circuit designer together with practical waveforms from economically designed circuits are given. Finally, three proven circuit designs with hard valves, trigger tubes, and transistors and their very low failure rates are presented.

### **The Trigger Tube—Reliability and Ratings**

M. E. BOND (*Associate Member.*) (*Mullard Radio Valve Company.*)

The paper will first discuss the meaning of reliability in relation to trigger tubes which are essentially bi-stable devices. It will study the effect of changes in the various characteristics on the reliability and give results showing what changes do occur.

Previous experiments have shown that in many cases trigger-tube behaviour can be related by precise laws to the conditions of use. The latest results from these and further experiments which have given a fuller knowledge of the physical limits of operation for trigger tubes will be presented.

The way in which a circuit designer can use the work described will be discussed and examples given of the reliability obtained in specific instances.

### Component Tolerances as a Governing Factor in the Success of Cold Cathode Tube Circuit Design

D. M. NEALE. (*Ilford.*)

It is shown that, whereas the rather large spreads in characteristics of thermionic valves are reduced by the circuits in which they are commonly used, cold cathode tubes tend to exaggerate the effects of circuit tolerances. Most cold cathode tube circuits require tube currents to be held within a range of less than 2 to 1 in all circumstances. Even with modern close-tolerance tubes, the tolerance on h.t. and resistor values must be less than  $\pm 10\%$ .

Ring and chain counters using the pulse-plus-bias technique call for much closer tolerances. Reliable operation can be assured only as the result of very careful design, catering for the 'worst  $\times$  worst' extremes. Generally this requires  $\pm 5\%$  resistors with arbitrary supply voltages or  $\pm 2\%$  resistors if rationalized voltages are needed. Often it will be found simpler and cheaper to use alternative circuits based on stepping tubes and transistors.

### A System of Digital Building Blocks using Cold Cathode Tubes

J. WAGNER. (*Osram.*)

For electronic control systems, a system of digital building blocks with cold cathode tubes has been developed. It contains monostable and bistable multivibrators, triggers, pulse-shaping units, and gates. The system lends itself also for counting problems in interworking with preset-count decodes using the same tube. The maximum operating frequency is about 1 kc/s. The building blocks comprise printed circuitry on plug-in conductor cards.

### A New Trigger Tube for Logical Functions

G. KERR, B.SC. (*Philips.*)

Development work has been completed on a new trigger tube for application in logical functions such as calculating and machine control. The tube has been designed with a view to large scale mechanized production with the least possible handling and this has affected the mechanical form and electrical characteristics.

A study of the basic operation of the tube has led to a new way of presenting its characteristics, enabling the equipment designer to calculate more exactly the requirements for ignition and extinction. In particular, the build-up of current between trigger and cathode after the application of an over-voltage has been studied, and from the results are derived the requirements for pulse ignition of the tube and the effect of different pulse shapes.

The requirements for extinction of the anode-cathode discharge either by an externally produced pulse or in a self-extinguishing circuit are also discussed.

### The Glow Thyatron

M. VOLLENWEIDER. (*Cerberus.*)

The glow-thyatron type GT 21 has been developed from the well-known cold cathode relay tubes. The most significant difference between these tubes is the low control voltage required to operate the glow-thyatron (approx. 5 V).

First, the paper will explain the principle of operation followed by a brief description of the tube characteristics. Afterwards emphasis is given to the application side, where circuits with 'low-power' and 'low-voltage' control elements are shown. The two most important circuits are: a temperature controlled relay with thermistor and an inductive limit sensor with transistor oscillator.

### Coding with Multiple-anode Glow-discharge Tubes

H. E. SEIFERT, DIPL.-PHYS. (*Cerberus.*)

For optical indication of numerals or symbols glow-discharge tubes or fluorescence devices are often utilized. These have a multitude of luminous elements and the symbol is obtained by paralleling some of these elements. A new tube having several equal anodes has been developed to switch such indicators in a simple way. The number of the anodes is the same as the number of the lighting elements in the optical device. Utilizing the GT-mechanism, it is possible to operate the tube with a signal-voltage of about 5 V only. Circuits for controlling both a glow-discharge-indicator tube or a fluorescence plate, are shown.

### **A New Glow Discharge Alpha-numeric Display and the Associated Character Storage Circuitry**

THOMAS C. MALONEY AND D. GLASER. (*Burroughs Corporation.*)

A display providing a  $2\frac{1}{4}$ -in high character is presented. Design details are correlated with product objectives, human engineering aspects and the physics of gaseous discharge. The technique employed to obtain ultra-long life is described and explained. Problems encountered during development which effected the design are discussed. Other sizes in a family of alpha-numeric displays are shown.

Two basic methods of display logic, random access and serial shift, together with a brief discussion of coding and decoding requirements for the respective character generation and display are given.

Several basic types of circuits are examined in terms of twelve operational and economic criteria. Among the circuits are: gas trigger tubes (GTR-120W) solid-state pnp-npn latch, flip flop, three and four-terminal pnpn devices and relays.

A table is presented which summarizes the discussion. An interesting circuit which prevents information loss in the event of transient failure is also shown.

### **Influence of a Passive Network on the Glow Transfer Characteristics of a Cold Cathode Decade**

P. K. PATWARDHAN, M.S.C. (*Associate Member*) AND M. G. PHADNIS. (*Atomic Energy Establishment, Bombay, India.*)

The conventional drive circuits for dekatrons employ vacuum tubes, cold cathode trigger tubes, transistors, or a combination of an active device linked with a pulse transformer. This paper describes a novel method of inter-coupling and independently driving GC10D fast dekatrons. The drive mechanism employs a positive input pulse applied to the commoned cathodes, instead of guides. Inter-stage coupling is purely with a passive network.

Special features include neon stabilization for guides, elimination of d.c. stabilized line, and extreme economy in terms of components and power. Practical application has been as a display element of a 10-channel pulse analyser. The glow transfer mechanism in the new design has been successfully explained by defining two new types of transfers 'alpha-transfer and beta-transfer'.

## **Thursday, 19th March. Session III: 'APPLICATIONS OF COLD CATHODE TUBES'**

### **A Batch Weight Ratemeter using Cold Cathode Triode Memories**

W. W. WOOD. (*Imperial Chemical Industries.*)

An equipment was required to monitor the operation of seven batch weighing machines. This has been built using 400 trigger tubes, and is now used in a process control loop. The equipment has one channel for each weighing machine, each channel using an input store trigger tube followed by 60 tubes in a step-on memory, which are mounted for visual display.

When a tip occurs, the input store trigger tube is ignited. Every 20 seconds the pattern in the memory moves on one place and the state of the input store is transferred to the first memory tube. The memories are divided into two 10-minute groups (tubes 1-30 and 31-60) and the cathode currents of tubes 31-60, in all seven channels, are summed to give a signal representing the number of tips which took place in the penultimate 10-minute period. This signal is revised every 20 seconds. The 10-minute delay provided in tubes 1-30 simulates a plant transport lag. Excepting the trigger tubes, solid-state circuitry is used throughout and details will be given of the timing, pulsing and anti-coincidence circuits. The development of circuits giving reliable operation of the trigger tubes will be described.

### **An Inexpensive Digital Voltmeter using Multiple Anode Dekatrons**

P. GLEGHORN. (*Gloster Equipment.*)

A design was required for a medium accuracy digital voltmeter which would be robust and reliable whilst selling at an attractive price. The introduction illustrates how the use of cold cathode counters was found to be essential in these interests.

A general description of the digital voltmeter follows, with particular reference to the requirement for decade counters which need only be capable of counting at moderate speeds.

Various types of counters are then discussed, and comparison made of their costs. The conclusion is reached that the use of a dekatron counting tube in conjunction with a cold cathode indicator tube provide the most economic method of counting.

A detailed description is given of the counters used in the digital voltmeter, covering the type of dekatron tube, its coupling to the indicator tube, the drive circuits and the reset and carry arrangements.

### Applications of Cold Cathode Trigger Tubes in Telephone Exchange Equipment

R. E. BAXTER. (*Pye Telecommunications.*)

A simple crossbar switching matrix is described in which twin-trigger cold cathode tubes are employed as speech passing elements. The use of each trigger electrode as an AND gate, requiring a coincidence of voltage bias and pulse for operation, is explained together with circuit details of the register and link allotter which provide the logical gating signals.

The line circuit and link control equipment are discussed on a functional basis without reference to circuit details and logical analysis of the complete system is performed to illustrate exchange operations.

### The Use of Cold Cathode Tubes in Supervision of Burners of High Power

J. M. MEGNOUX. (*Electricité de France.*)

The cold cathode tubes used in this equipment are in effect photo-sensitive cells which detect ultra-violet radiation. Fail-safe circuit arrangements are presented for detecting whether a burner is lit or not.

### Use of Cold Cathode Trigger Tubes in Explosion Detection and Suppression Circuits

J. B. COLLINS. (*Wilkinson Sword (International).*)

This application is an abnormal use of a cold cathode trigger tube in which the manufacturer's nominal current rating is grossly exceeded for short periods. No other device giving a comparable performance was available when the system was developed. The basic requirements for an explosion protection system are firstly, extreme sensitivity to detect the initiation of an explosion, and secondly, a rapid reaction to suppress the explosion before the pressure has built up to the danger level.

One method of detection is by means of a photo-multiplier, the signal from which fires a cold cathode trigger tube which discharges a large capacitor through detonators. These in turn propagate the extinguishant from special containers in the protected space, thus suppressing the incipient explosion. In this application the cold cathode tube is only required to operate in an emergency and during its short period of operation a tube nominally rated at 1.5 milliamps is required to conduct a current exceeding 5 amperes.

The ability of a small cold cathode trigger tube to meet this requirement depends on the surface conditions of its cathode and special non-destructive tests were devised to ensure satisfactory operation.

### Cold Cathode Trigger and Counter Tubes for Computing Applications

N. KITZ. (*Bell Punch Company.*)

The paper deals with the uses of cold cathode trigger and counter tubes in the design of electronic desk calculating machines. The advantages and disadvantages of the techniques are discussed from both the design and production viewpoints.

An outline is given of the logical design problems which arise from using electronic circuitry basically limited in speed and the conclusion is drawn that provided great care is taken in the logical design, trigger tubes can be used to make a successful machine.

Two typical counters of the decimal ring configuration are described. One counter used as a register stage is capable of responding to pulses at a speed of 4000 counts per second. The other counter is of a more conventional nature and can work at 400 cycles.

### Some Applications of Glow Transfer Tubes

C. C. H. WASHTELL (*Member*). (*Labgear.*)

The paper will cover various sequential radiation measurements associated with nuclear power instrumentation utilizing digital ratio counting. These techniques are particularly suited to burst fuel element detection and effluent monitoring incorporating warning systems and, in a modified sense, to some aspects of uranium mining assay procedure.

Three cold-cathode digital counters are employed: (i) a ratio counter; (ii) a slave counter with print-out facilities; and (iii) a pre-set time counter. The third unit in conjunction with a step-by-step scanner and channel selector forms the programme memory. This arrangement permits the individual examination of the fuel channels on either a conventional 'time' or 'count' basis immediately following start-up, but is also capable of completely automatic operation on either a ratio or percentage basis for routine monitoring.

### A Telemetry System Employing Cold Cathode Tubes

J. B. RICHARDSON, M.A. (*Pye Telecommunications.*)

An industrial telemetering and telecontrol system has been developed which is suitable for use over radio links where many outstations share the same frequency allocation. The system is a digital one, and a design utilizing cold cathode tubes, semiconductors and reed relays gives reliability and ease of servicing, using a minimum of test equipment.

A description of the operation of the system is followed by a more detailed examination of some of the cold cathode circuitry.

### The Application of Gas Diodes in Electronic Musical Instruments

H.v.d. KERCKHOFF. (*Philips.*)

The recent development of a gas diode, ZA1001, with very small dimensions and reproducible characteristics, which remain extremely constant over life, has made possible the application of this element in the tone generator part of electronic musical instruments. After dealing with the possibilities of tone generating and tone forming, a short survey will be given of the important characteristics of the gas diode, followed by the design considerations of synchronized saw-tooth generators. A short description will be given of an electronic musical instrument (the 'Philicorda').

---

The following paper will not be read at the Symposium but will be included with the preprints:

### A Glow Discharge Indicator for Small Signals

Y. FUKUKAWA. (*Fujitsu Laboratory.*)

A new type of the glow-discharge indicator for small signals is described. The principle of operation is based on the fact that the current transfer between two cathodes can be controlled by a small potential difference between them when the two cathodes are close together. The arrangement and the shape of these electrodes is entirely different from the original type of this tube, thus giving a better visibility and brightness of indication. The transfer voltage is less than 6 V at the operating current of 800  $\mu$ A. Several electrical characteristics and application problems of this indicator tube including pulse operation, i.e. self-sustained indication and a.c. operation, are also described. A simple method of indicating very small signals of the order of 0.5 V is also detailed.

---

## Residential Accommodation at Downing College



DOWNING COLLEGE

Many of those attending the Symposium will be able to stay at Downing College. Founded in 1800 by Sir George Downing, Bart., it is unique among Cambridge colleges in its open plan, the buildings being ranged round a quadrangle which calls to mind the campus of an American university.

The Hall is on the extreme left of the photograph and rooms allotted to the Institution for the Symposium are along the north side on either side of the Chapel which is seen in the centre of the facing range of buildings. These were completed in 1953.

The College was the headquarters of the 1959 Brit.I.R.E. Television Engineering Convention. It is only a few minutes walk from the Cavendish Laboratory where the Symposium sessions are to be held.

# An Equalizer for an Electro-magnetic Vibrator System Employing Analogue Computing Techniques

By

E. J. ELLIS (*Associate Member*)<sup>†</sup>

*Presented at a meeting of the Electro-Acoustics Group in London on 19th December 1962.*

**Summary:** The response characteristics of a typical vibration system are considered and the transfer functions of the various resonances are given. It is shown that by employing analogue computing techniques it is possible to construct an equalizer for the system by simulating the reciprocal of its characteristic. The design for such an equalizer is described and details are given of equipment, which enables satisfactory equalization to be carried out in the frequency range 10–4000 c/s. The setting-up procedure is explained and details are given of the results obtained.

## List of Symbols

$M_c$	mass of driving coil.
$M_t$	mass of table.
$M_s$	effective mass of specimen.
$K_f$	spring rate of flexures.
$K_t$	spring rate of coil to table coupling.
$K_s$	spring rate of table to specimen coupling.
$D_f$	damping of flexures.
$D_t$	damping of coil to table coupling.
$D_s$	damping of table to specimen coupling.
$\omega_e$	frequency of electrical resonance (rad/s).
$\omega_a$	frequency of axial resonance.
$\omega_p$	frequency of peak resonance.
$\omega_n$	frequency of notch resonance.
$Q_e$	$Q$ of electrical resonance.
$Q_a$	$Q$ of axial resonance.
$Q_p$	$Q$ of peak resonance.
$Q_n$	$Q$ of notch resonance.
$T$	force factor of vibrator (lb/amp).
$L_c$	vibrator coil inductance.
$R_c$	vibrator coil resistance.
$p$	Laplace variable.

## 1. Introduction

When vibration testing over a wide frequency spectrum it is often desirable that the system used should provide a direct correspondence between the input signal and the acceleration produced at the specimen. Such occasions may arise either when sweep-frequency testing or when carrying out random-motion tests. When sweep-frequency testing, servo control can be used to obtain a level acceleration and, by programming the feedback network against frequency, a specified response envelope may be obtained. This technique is possible because at any instant the input signal is at a single frequency only. Such servo-control systems, however, are not entirely satisfactory because it is often the case that the feedback signal

<sup>†</sup> U.K. Atomic Energy Authority, Atomic Weapons Research Establishment, Aldermaston, Berkshire.

from the specimen is not pure but has a considerable harmonic content. When carrying out tests with random motion the simple servo technique is not possible. Multi-band servo systems have been designed and are available, but although these have considerable advantages in some respects, it is felt that the equalization system described in this paper has advantages of a more general character.

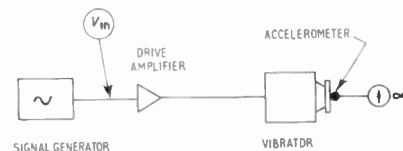


Fig. 1. Simple vibration system.

If one considers a typical vibration system as shown in Fig. 1 the over-all response characteristic may be obtained by plotting the log. reciprocal of input voltage required to raise constant acceleration at the vibrator against log. frequency. In the case of an unloaded vibrator, this would be generally of the form shown in Fig. 2. It is seen that two major

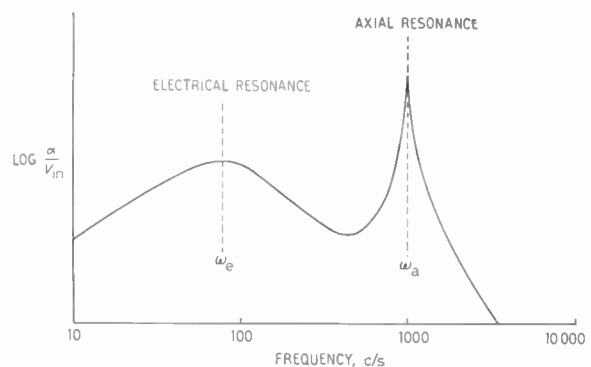


Fig. 2. Typical acceleration characteristic of the vibrator.

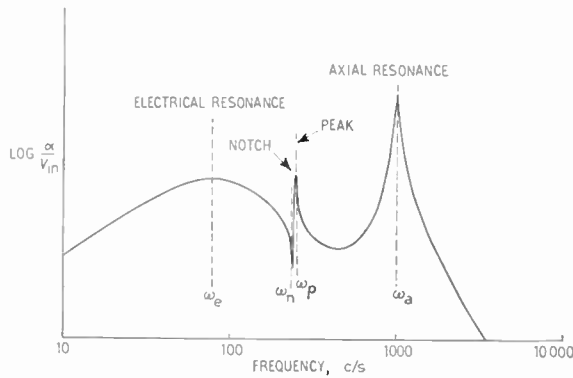


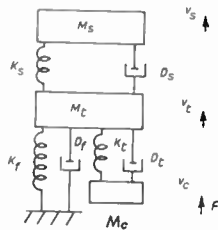
Fig. 3. Typical acceleration characteristic of vibrator with a simple specimen.

resonances occur, one in the lower mid-band region and the other at the top end of the frequency range. A further complication in the characteristic occurs when a resonant specimen is mounted on the vibrator as in Fig. 3.

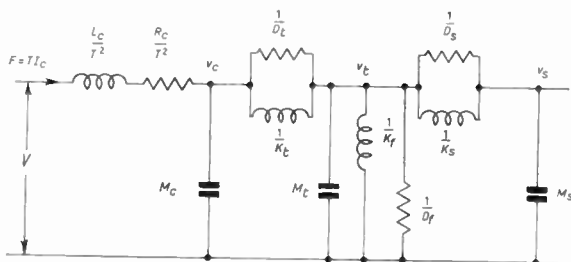
The amplifier normally has a level response extending beyond the range of the vibrator and contributes little to the characteristic. The resonances may be accounted for entirely by considering the electrical and mechanical features of the vibrator and specimen.

2. System Characteristics

Electrical engineers will find it convenient to consider the response in terms of equivalent electrical parameters and the mobility analogue<sup>1,6</sup> is used throughout this paper. Lumped parameters are assumed and the analogous terms used are given in Table 1.



(a) Simplified mechanical circuit.



(b) Equivalent electrical circuit.

Fig. 4. Vibrator with resonant specimen mounted.

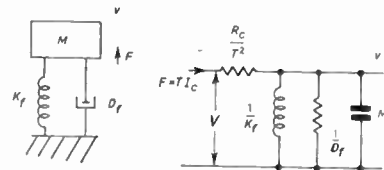
Table 1  
Analogous Terms

MECHANICAL		ELECTRICAL
Force	(F)	Current (I)
Velocity	(v)	Voltage (V)
Spring compliance	(1/K)	Inductance (L)
Damping	(D)	Conductance (1/R)
Mass	(M)	Capacitance (C)

The vibrator, when loaded with a simple specimen having one degree of freedom, may be represented by the mechanical system shown in Fig. 4(a). By applying the mobility analogue, we obtain the electrical equivalent given in Fig. 4(b). The electrical parameters of the vibrator are included to complete the analogy and have been suitably modified by a factor  $1/T^2$  which allows for their reference to the secondary of an ideal transformer having turns ratio  $T$ , transforming the vibrator coil current to mechanical force.

2.1. Unloaded Vibrator

Let us consider the characteristics of the vibrator without the specimen. At the very lowest frequencies the parameters  $L_c$  and  $1/K_f$  may be ignored and consequently the circuit simplifies to that in Fig. 5, where the coupled masses have been lumped to give  $M$ .



(a) Mechanical circuit. (b) Equivalent electrical circuit.

Fig. 5. Vibrator without the specimen at very-low frequency.

The spring  $K_f$  is very compliant and resonates at a low frequency with the mass  $M$  affecting the current characteristic of the vibrator considerably, but not the voltage.

At a higher frequency  $1/K_f$  may be ignored, but the reactance of  $L_c$  is now significant and a series resonance occurs with  $M$ . This is commonly called the 'electrical resonance' since it is produced by the electrical parameters of the coil  $L_c$  reacting with the mass  $M$ , of the moving parts. Figure 6 gives the

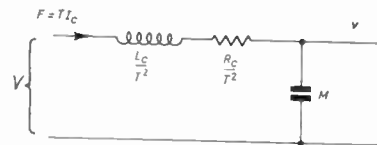
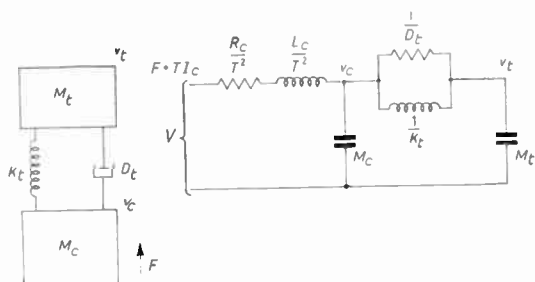


Fig. 6. Equivalent circuit at electrical resonance.

mechanical system that applies at this frequency, together with the electrical equivalent. The transfer function for the velocity/voltage characteristic is modified at this frequency by

$$\frac{1}{\frac{p^2}{\omega_e^2} + \frac{p}{\omega_e Q_e} + 1} \dots\dots(1)$$



(a) Mechanical circuit. (b) Equivalent electrical circuit.

Fig. 7. Axial resonance.

At a higher frequency still the circuit in Fig. 7 applies.  $1/K_t$  is now significant and series resonance occurs between the parameters  $1/K_t$ ,  $M_c$  and  $M_t$ . This is known as the 'axial resonance' and the velocity/voltage transfer function is further modified by

$$\frac{1}{\frac{p^2}{\omega_a^2} + \frac{p}{\omega_a Q_a} + 1} \dots\dots(2)$$

The transfer function of the unloaded vibrator is modified overall by

$$\frac{1}{\left(\frac{p^2}{\omega_e^2} + \frac{p}{\omega_e Q_e} + 1\right) \left(\frac{p^2}{\omega_a^2} + \frac{p}{\omega_a Q_a} + 1\right)} \dots\dots(3)$$

due to the electrical and axial resonances.

2.2. Loaded Vibrator

Loading the vibrator with a rigid mass simply serves to increase the table weight and reduce the frequencies of the characteristic resonances.

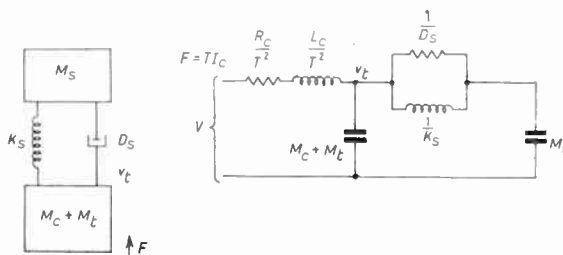
If the specimen is not rigid and consists of a mass having a single degree of movement, the parameters  $M_s$ ,  $1/K_s$  and  $1/D_s$  in Fig. 4(b) apply.

So far the transfer functions have been referred to the table of the vibrator, but now that a specimen is mounted, a decision is necessary on the point at which equalization is to be carried out. The specimen should be allowed to respond naturally, but imposing equalization or control at any point on it would prevent this and could possibly result in exceeding the

test specification in some parts. Quite obviously then, equalization should be done at the point at which vibration is applied, i.e. the vibrator table.

Another point to be considered is that for most sweep or random-motion testing the vibrator is of limited use at frequencies above the axial resonance. The characteristic here is very complex so that equalization becomes virtually impossible. Consequently, equalization for specimen resonances may only be carried out satisfactorily for those below this frequency.

As a result of the above considerations, the equivalent electrical circuit in Fig. 8 now applies. Series resonance occurs between  $1/K_s$  and  $M_s$ , producing a notch in the velocity/voltage characteristic at a particular frequency. At a higher frequency parallel resonance occurs between  $M_c + M_t$  and  $1/K_s$ , the reactance of  $M_s$  now being negligible.



(a) Mechanical circuit. (b) Equivalent electrical circuit.

Fig. 8. Peak-notch resonance.

The transfer function for the velocity/voltage characteristic is then modified by

$$\frac{\frac{p^2}{\omega_n^2} + \frac{p}{\omega_n Q_n} + 1}{\frac{p^2}{\omega_p^2} + \frac{p}{\omega_p Q_p} + 1} \dots\dots(4)$$

In practice, simple specimens are rarely encountered and a typical velocity/voltage characteristic contains many peak-notch pairs, each of the general form given in eqn. (4).

2.3. Overall Characteristic

The characteristics of the main resonances of a vibration system have now been considered and for convenience this has been done in terms of velocity. It is acceleration with which we are concerned, however, and all that is required is the multiplication of the transfer function by the Laplace variable  $p$  to give this. The overall transfer function modifying the acceleration/voltage characteristic then has the general form

$$p \left[ \frac{1}{\left( \frac{p^2}{\omega_e^2} + \frac{p}{\omega_e Q_e} + 1 \right) \left( \frac{p^2}{\omega_a^2} + \frac{p}{\omega_a Q_a} + 1 \right)} \cdot \frac{p^2}{\omega_{n'}^2} + \frac{p}{\omega_{n'} Q_{n'}} + 1 \cdot \frac{p^2}{\omega_{n''}^2} + \frac{p}{\omega_{n''} Q_{n''}} + 1 \cdot \dots \right] \dots\dots(5)$$

electrical resonance
axial resonance
notch resonances
peak resonances

**3. Equalization**

Equalization is accomplished by introducing a network at the input of the driving amplifier having a transfer function corresponding to the reciprocal of the system characteristic. This is illustrated in Fig. 9. The system to be described employs well-known analogue computing techniques to produce the transfer functions required.

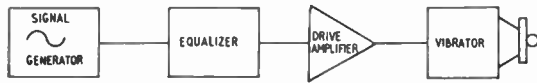


Fig. 9. Block diagram of the vibrator system showing the position of the equalizer.

Since we are concerned with frequency responses only, we may replace  $p$  by  $j\omega$  in the functions already given and accordingly we will treat the computing operations to be described in terms of  $j\omega$  also.

A computing amplifier is necessary which has high gain and low phase shift over the required frequency range, in addition to the essential requirement of very high input impedance and low output impedance.<sup>2</sup>

By means of suitable combinations of input and feedback elements, all the necessary operations of integration, differentiation, summing and sign inversion are obtained<sup>2</sup> (Fig. 10).

The overall transfer function may be factorized giving the individual second order polynomials in the numerator and denominator. Each of these describes a particular resonance and we can now see that the

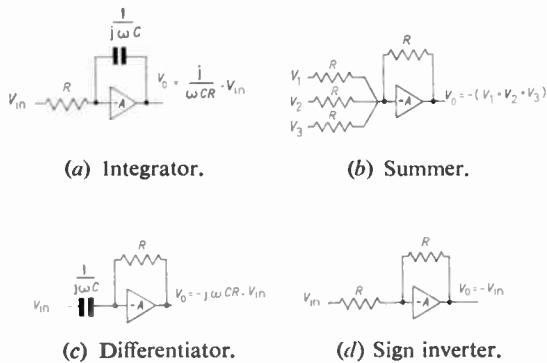


Fig. 10. Generation of transfer functions using operational amplifiers.

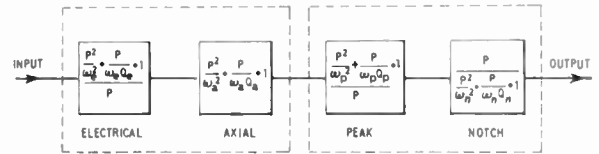


Fig. 11. Equalizer with one peak and notch section only.

overall equalizer may comprise sections arranged in series, each concerned with a single resonance only. This is illustrated in Fig. 11.

**3.1. Electrical Resonance Equalizer**

Writing  $j\omega$  for  $p$  in the transfer function eqn. (1) and taking the reciprocal, we obtain the transfer function

$$\frac{(j\omega)^2}{\omega_e^2} + \frac{j\omega}{\omega_e Q_e} + 1 \dots\dots(6)$$

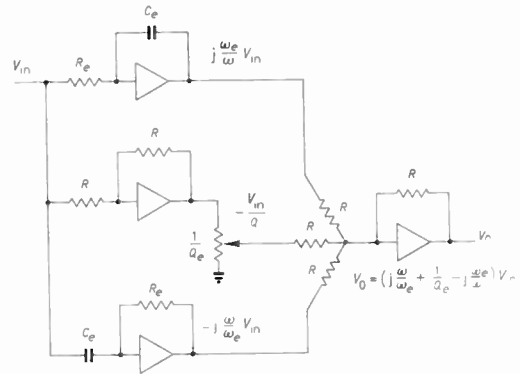


Fig. 12. Simplified electrical resonance equalizer.

It is at this stage that the equalization for the  $p$  introduced into the general expression (5) is made (see Section 2.3). This is done by multiplying eqn. (6) by  $1/p$  (or  $1/j\omega$ ), and rearranging to give

$$\frac{1}{\omega_e} \left[ j \frac{\omega}{\omega_e} + \frac{1}{Q_e} - j \frac{\omega_e}{\omega} \right] \dots\dots(7)$$

Since only the terms within the brackets contribute to the shape of the response, the constant outside the brackets may be ignored and the analogue circuit of Fig. 12 may be cast, where

$$V_o = \left( j \frac{\omega}{\omega_e} + \frac{1}{Q_e} - j \frac{\omega_e}{\omega} \right) V_{in}$$

and

$$\omega_e = \frac{1}{R_e C_e}$$

3.2. Axial Resonance Equalizer

The transfer function required is the reciprocal of eqn. (2),

$$\frac{(j\omega)^2}{\omega_a^2} + \frac{j\omega}{\omega_a Q_a} + 1 \quad \dots\dots(8)$$

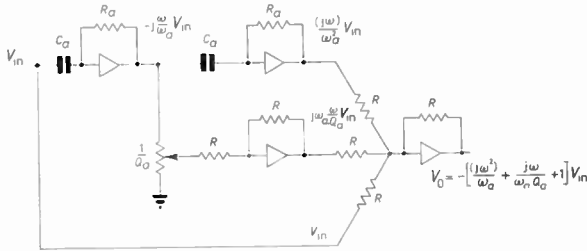


Fig. 13. Simplified axial resonance equalizer.

The analogue circuit for this is given in Fig. 13, where

$$V_0 = -\left(\frac{(j\omega)^2}{\omega_a^2} + \frac{j\omega}{\omega_a Q_a} + 1\right) V_{in} \quad \dots\dots(9)$$

and

$$\omega_a = \frac{1}{R_a C_a}$$

3.3. Peak-Notch Equalizer

The peak-notch equalizer transfer function is the reciprocal of eqn. (4),

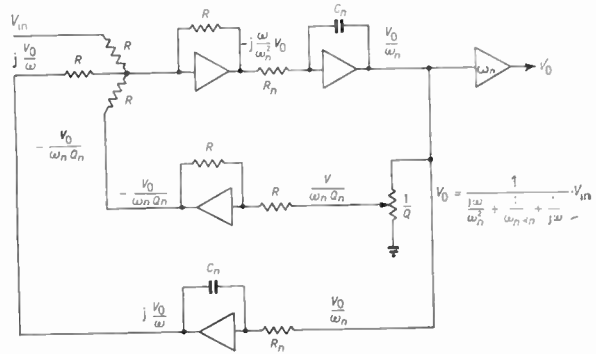


Fig. 14. Simplified notch equalizer.

$$\frac{(j\omega)^2}{\omega_p^2} + \frac{j\omega}{\omega_p Q_p} + 1 \quad \text{where } \omega_p = \frac{1}{R_p C_p} \quad \dots\dots(10)$$

$$\frac{(j\omega)^2}{\omega_n^2} + \frac{j\omega}{\omega_n Q_n} + 1 \quad \text{and } \omega_n = \frac{1}{R_n C_n}$$

The peak equalizer section has the form

$$j\frac{\omega}{\omega_p} + \frac{1}{Q_p} - j\frac{\omega_p}{\omega} \quad \dots\dots(11)$$

which is the same as that for the electrical resonance equalizer (Fig. 12). The notch equalizer section has the form

$$\frac{j\omega}{\omega_n^2 + \frac{j\omega}{\omega_n Q_n} + 1} \quad \dots\dots(12)$$

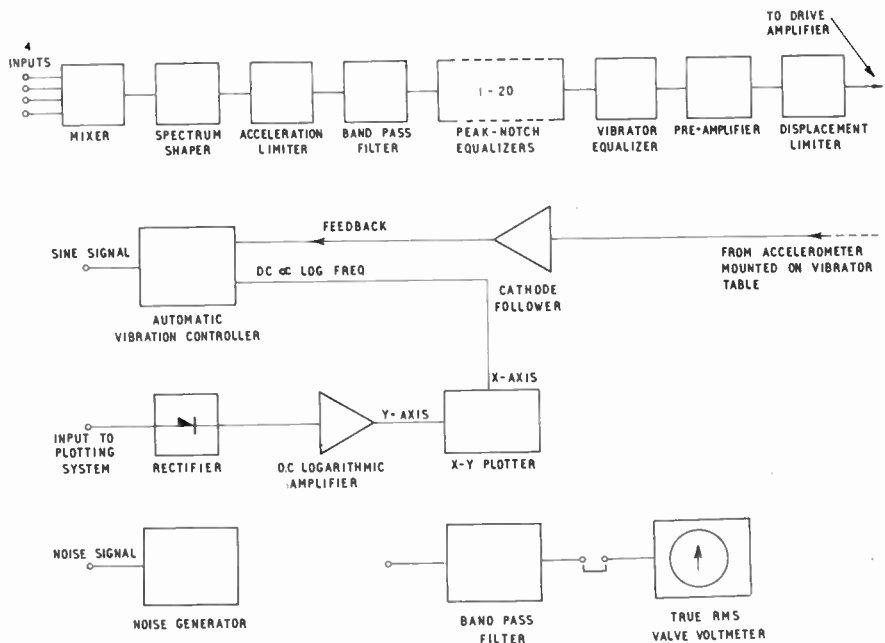


Fig. 15. Simplified block diagram of the equalizer and auxiliary equipment.

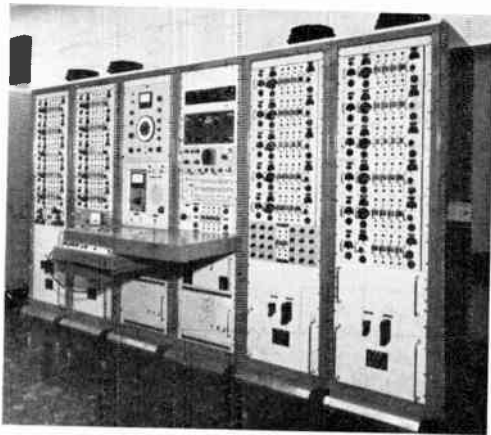


Fig. 16. Complete equalization equipment.

The analogue circuit for this is given in Fig. 14 where

$$V_0 = \frac{1}{\frac{j\omega}{\omega_n^2} + \frac{1}{\omega_n Q_n} + \frac{1}{j\omega}} \cdot V_{in} \quad \dots\dots(13)$$

4. Complete System

4.1. Auxiliary Units

The main part of the system has now been considered and the remainder is largely composed of units providing facilities for setting up or giving some degree of protection to the specimen against operational error. An idea of the overall system may be obtained from the block diagram of Fig. 15 and the photograph in Fig. 16.

*Mixer unit.* This unit allows up to a maximum of four different input signals to be mixed before feeding into the system. For example, a specification may demand random noise with three sine waves superimposed, each having different amplitude and frequency.

*Band-pass filter.* A variable band-pass filter is included for the purpose of defining the frequency range of the input signal, especially when random noise is used. It is also available to facilitate setting-up of random noise levels.

*True r.m.s. voltmeter.* For making measurements of random noise, a true r.m.s. voltmeter must be used.

*Spectrum shaper.* This unit is used for shaping the input signals to meet a specified acceleration/frequency or spectral-density envelope.

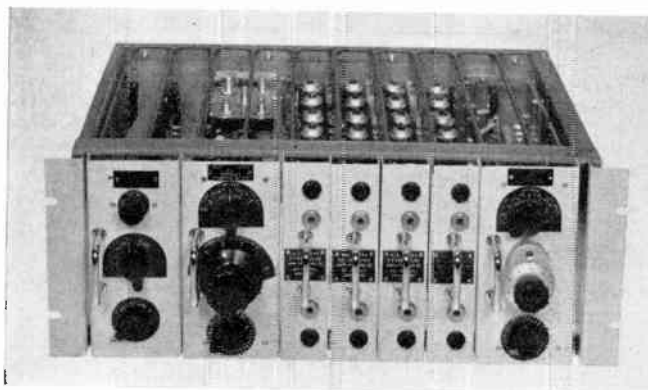
*Acceleration limiter.* This provides a facility for limiting the level of acceleration raised to a preset value and thus minimizes the possibility of accidentally exceeding the specification.

*Displacement limiter.* Instrumentation at the input to the drive amplifier is very susceptible to operator errors, mains transients, etc., which might result in excessive displacements occurring at the vibrator. This unit, situated at the drive-amplifier input, senses the excessive displacement content of the signal and limits it at a preset level.

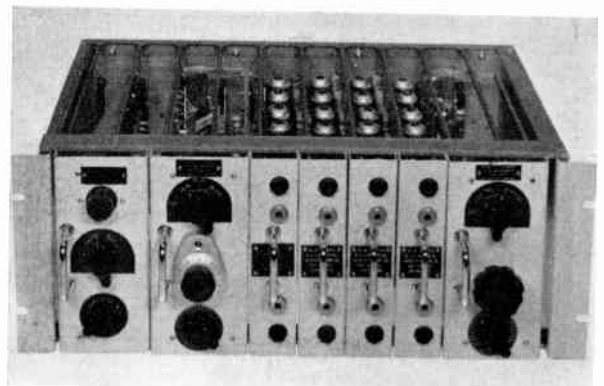
4.2. Construction

The equipment is accommodated in a bay of 6-ft standard racks, the centre two of which have an operator's desk position. All the auxiliary units are situated here, while the equalizers are mounted in the racks on either side. The d.c. heater supplies for the computing amplifiers are situated in the base of these racks. The stabilized h.t. supplies are beneath the central desk position.

Wherever possible the construction is to a modular system, facilitating easy maintenance and flexibility. This is illustrated in Fig. 17 which shows the construction of the vibrator and peak-notch equalizers.



(a) Peak-notch equalizer.



(b) Vibrator equalizer.

Fig. 17. Equalizer modules.

### 4.3. Equalization Capacity

Sufficient units are provided in the system to allow the equalization of a vibrator characteristic and up to a maximum of twenty peak-notch resonances.

The individual ranges of the equalizers are as follows:

Electrical resonance—frequency ranges  
 10–40 c/s    30–120 c/s    100–400 c/s  
*Q* range adjustable to a maximum of 2.

Axial resonance—frequency ranges  
 300–1200 c/s    1000–4000 c/s  
*Q* range adjustable to a maximum of 100.

Peak-notch resonance—frequency ranges  
 10–40 c/s    30–120 c/s    100–400 c/s  
 300–1200 c/s    1000–4000 c/s  
*Q* range adjustable to a maximum of 100.

## 5. Setting-up Procedure

### 5.1. Plotting System Characteristic

Before any attempt at equalization is made, it is necessary to plot the characteristic of the system. The method by which this is done can be seen in Fig. 18. Having allowed time from switching on for all the equipment in the system to reach a stable operating condition, standard *g*-controlling equipment is used to hold the acceleration at the monitoring point constant. To avoid exceeding the test specification, a low level of acceleration is agreed and a sweep is carried out over the specified frequency range. The varying input voltage to the drive amplifier is rectified and its logarithm is plotted against log. frequency on the X-Y plotter, giving the inverted acceleration characteristic in Fig. 19.

### 5.2. Adjusting the Equalizers

The process of equalization is carried out by inserting the equalizer by means of the switch in Fig. 18. The X-Y plot of the characteristic is left on the plotter and the individual equalizers are switched in one by one and adjusted for frequency and *Q*. This is done by sweeping the oscillator frequency back and forth by hand while making adjustments so that the motion of the plotter pen in the Y direction is reduced to a minimum over the whole range. The electrical resonance equalizer is the first adjusted, followed by the axial and then the peak-notches. Good equalization will result in a level response being plotted and adjustments are carried out until an acceptable result is achieved.

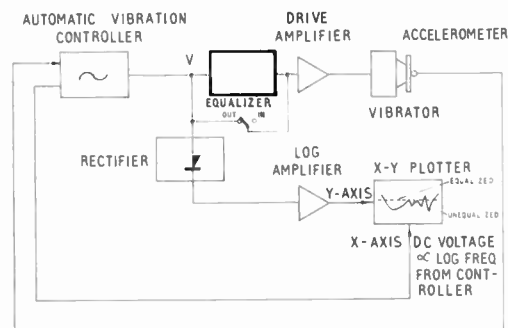


Fig. 18. Block diagram of the method used to plot the system characteristic.

### 5.3. Degree of Equalization

The individual equalizer sections may be adjusted to equalize the resonances described in Section 2 to within  $\pm 0.2$  dB. This does not mean, however, that an actual specimen can be equalized to this same degree of accuracy. Theoretically, this would be possible provided the response of the specimen was absolutely linear but in practice this is usually not the case and since setting-up is carried out at a low level of acceleration the equalization will not necessarily hold to the same degree at the specified level.

A change in temperature of the vibrator or specimens could also impair the equalization and it may be necessary to allow the rig to warm up before commencing to equalize. Even if these two effects are not troublesome it will be found that the main resonances of the specimen are attended by numerous smaller ones and these are usually the limiting factors contributing to the ultimate degree of equalization.

Tolerances of  $\pm 1$  dB have been achieved but usually the tolerance allowed in the test specification

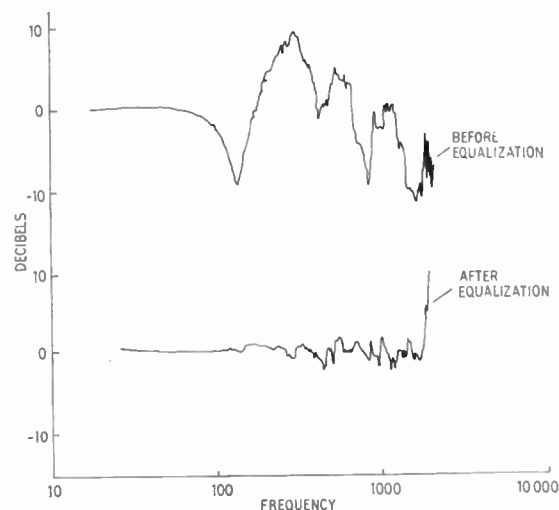


Fig. 19. Inverted system response before and after equalization.

is very much wider than this, making the process of equalization very much easier.

Figure 19 gives examples of an actual system characteristic before and after equalization.

## 6. Conclusions

The equipment described has been in use for over a year and for the most part has been employed on random-motion testing. Experience with it is not yet very great, but the main observation is that an excessive number of peak-notch equalizers has been provided. Experience has shown that four peak-notch equalizers to a single vibrator equalizer would have been a satisfactory ratio. Fortunately, due to the modular construction of the equipment, this is easy to rectify, making it possible for four separate vibration systems to be equalized. Such an arrangement, however, may be a disadvantage because it would, to a certain extent, result in remote working, but it does have the advantage that the auxiliary equipment, which is only used periodically (except for the limiters), is available to serve the four systems.

Setting-up is apt to be a laborious process, but in time operators become quite skilful and can quickly equalize for normal resonances. Experience has shown that equalization can be very unsatisfactory above the axial resonance of the vibrator and wherever possible a vibrator should be selected with an axial resonance above the range of the specification.

It is believed that equalization, with input-signal shaping, may be used to an advantage in some cases where sweep testing to a specified response envelope is required. The *g*-controlling equipment normally employed is occasionally unsatisfactory due to insufficient speed of response, a deficiency not encountered in this equipment.

Simple equalization, perhaps employing a single vibrator or peak-notch equalizer, and used in conjunction with *g*-controlling equipment, would seem to be a possible method of dealing with specimens having a very wide dynamic response.

Because of the modular construction, the equalizer may be employed as an analogue simulator by the introduction of different computer element panels. By this means electrical models of simple mechanical systems may be set up to evaluate the performance of control instrumentation.

The main rival to this system of equalization is the parallel filter<sup>3, 5</sup> method which lends itself to automatic servo control.<sup>4</sup> This method is, however, at best merely a compromise, whereas the analogue method is theoretically capable of perfect equalization provided that there are no non-linearities in the specimen.<sup>8</sup> The main advantage of the parallel filter

technique is of course the shorter setting-up time, especially if automatic servo control is employed.

Obviously then there are advantages and disadvantages in each method and the one employed depends on the nature of the requirement.

The author feels that this method of equalization is satisfactory for most equalization requirements and that the equipment can be usefully employed for a variety of other purposes in the laboratory. Simple equalization is generally all that is required in most cases, perhaps only for the main vibrator resonances, and this method is probably the most satisfactory way of providing it.

## 7. Acknowledgments

The permission of the Director of A.W.R.E. to publish this paper is gratefully acknowledged. The author wishes to acknowledge the assistance given by his colleagues of the Electronic Engineering Department, A.W.R.E., and also the helpful discussions with Mr. A. M. P. Brookes and members of the Engineering Department, Cambridge University.

## 8. References and Bibliography

1. F. A. Firestone, "The mobility method of computing the vibration of linear mechanical and acoustical systems", *J. Appl. Phys.*, **9**, p. 373, June 1938.
2. A. S. Jackson, "Analogue Computation", (McGraw-Hill, New York, 1960).
3. J. A. Ross, "A New Method of Equalization in Random-vibration Testing", Ling-Altec Electronics Inc.
4. C. E. Maki, "Automatic spectrum equalization for random-motion testing", *MB Electronics Vibration Notebook*, **5**, No. 4.
5. D. E. Mullinger, "The application of statistical techniques to vibration analysis and testing", *The Radio and Electronic Engineer (J. Brit.I.R.E.)*, **25**, No. 6, p. 525, June 1963.
6. D. Burger, "Mechanical impedance and mobility—useful but unused". Symposium of the Wright Engineering Co., 1957.
7. "Vibration exciter characteristics", *Brüel and Kjer Technical Review*, No. 3, 1960.
8. C. E. Maki, "Mobility analogue technique in complex-wave system equalization", *MB Electronics Vibration Notebook*, **4**, Nos. 2, 3 and 4.
9. G. B. Booth, "Random Vibration Test Techniques", *Proceedings of the National Meeting of the Institution of Environmental Engineers*, 1959.
10. Wilbur Du Bois, "Random-noise vibration test procedure", Environmental Test Group, Boeing Airplane Co., Seattle.
11. C. E. Maki, "Frequency response characteristics of random-noise systems", 55th Meeting of the Acoustical Society of America, 1958.
12. G. G. Gouriet, "A new approach to control system analysis", Wayne-Kerr Laboratories, 1962.

*Manuscript first received by the Institution on 13th February 1963 and in final form on 13th November 1963. (Paper No. 882/EA13.)*

© The British Institution of Radio Engineers, 1964

# Sensitivity of an Oscillator to Periodic Conductance Changes

By

A. G. J. HOLT, Ph.D., Dip.El.  
(Associate Member)†

**Summary:** The oscillator is considered as a means whereby changes in the conductance of its grid tuned circuit may be detected. A brief treatment of variable circuits is given, together with a physical interpretation of the results. Expressions are derived for the output voltage obtained from the oscillator when its grid tuned circuit conductance is varied in a periodic manner, and the results of experimental work confirming the theory are given. Expressions for the noise output are also given.

## 1. Introduction

By the application of the techniques of radio-frequency spectroscopy it is possible to detect the resonant absorption of energy by certain substances. Such a substance is the free radical diphenyl trinitrophenyl hydrazyl. Absorption occurs when the substance is placed in correctly orientated steady and r.f. magnetic fields and the relationships shown below are satisfied:

$$\gamma = \frac{21.4184}{g\lambda} \dots\dots(1)$$

$$= \frac{3 \times 10^{10}}{\lambda} \dots\dots(2)$$

Here  $\gamma$  is the steady field value in kilogauss,  
 $\lambda$  is the wavelength of the radio frequency in centimetres,  
 $f$  is the radio frequency in c/s,  
 and  $g = 2.0036$ .

These equations are quoted from Ingram<sup>1</sup> in which many aspects of radio-frequency spectroscopy are discussed. When absorption occurs energy is extracted from the r.f. field and the apparent admittance of the coil supplying the field is changed. Usually a small amplitude alternating field of low frequency is superimposed upon the steady field  $\gamma$ , so that the absorption occurs periodically and the apparent admittance of the coil also varies periodically. Thus the study of methods for detecting absorptions becomes a problem concerning circuits having time varying components, the object being to detect small changes in coil conductance.

The detection of absorptions is complicated by such phenomena as saturation broadening<sup>1</sup> which depend upon the characteristics of the substance under test, not upon the detecting system. In order to make the system independent of such effects the changes in coil admittance can be simulated by a variable conductance circuit. It is also possible to simulate the susceptance

variations but this was not done because it is usually the conductance change that is detected with an oscillator. Other applications of the oscillator include the detection of the presence of resonant circuits and quartz crystals coupled to the oscillator tank circuit. Since the problem is that of detecting small variations in circuit conductance a brief exposition of circuits with variable elements follows.

## 2. Variable Circuits

The theory of linear circuits having constant components is now well understood. Circuits in which the component values vary with time have received less attention and the general theory is not yet such that it may easily be used for engineering work.<sup>2, 3</sup> If the variation is of a simple form and of amplitude much less than that of the constant components in the circuit, the method developed by Carson<sup>2</sup> may be applied.

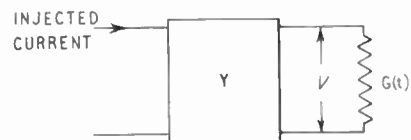


Fig. 1. Simple variable circuit.

When a current is injected into such a circuit the voltage  $V$  developed across it is of the form

$$V = V_0 + V_1 + V_2 + V_3 \dots \dots\dots(3)$$

where the terms  $V_m$  are given by integral equations. Carson's method shows that the steady state voltage  $V$  across a network constructed from invariable components and having a variable conductance  $G(t)$  with mean value equal to zero in parallel, as shown in Fig. 1, is

$$V = V_0 - \frac{V \cdot G(t)}{Y} \dots\dots(4)$$

Here  $V_0$  is the voltage that would be produced in the absence of conductance variation and  $Y$  is the

† Department of Electrical Engineering, University of Newcastle upon Tyne.

generalized admittance of the invariant network as seen from the variable arm.

The admittance  $Y$  will depend upon frequency, let its value at angular frequency  $\omega$  be

$$Y(\omega) = Y_0 \quad \dots\dots(5)$$

while at angular frequency  $(\omega + mp)$  its value may be written as

$$Y(\omega + mp) = Y_m \quad \dots\dots(6)$$

The terms in the series for  $V$  in eqn. (3) are

$$V_1 = - \frac{V_0 \cdot G(t)}{Y} \quad \dots\dots(7)$$

$$V_{m+1} = - \frac{V_m \cdot G(t)}{Y} \quad \dots\dots(8)$$

If  $V_0$  is of the form  $E_0 \cos \omega t$  and  $G(t)$  is of the form  $\delta G \cos pt$

$$V_1 = - \frac{\delta G \cdot E_0}{2} \left[ \frac{\cos(\omega + p)t}{Y_{+1}} + \frac{\cos(\omega - p)t}{Y_{-1}} \right] \quad \dots\dots(9)$$

Note that the sidebands are produced about  $\omega$  the frequency of the applied current.

$$V_2 = \left(\frac{\delta G}{2}\right)^2 E_0 \left[ \frac{\cos(\omega + 2p)t}{Y_1 \cdot Y_2} + \frac{\cos(\omega - 2p)t}{Y_{-1} \cdot Y_{-2}} + \left(\frac{1}{Y_1} + \frac{1}{Y_{-1}}\right) \frac{\cos \omega t}{Y_0} \right] \quad \dots\dots(10)$$

and so on for the other terms in eqn. (3).

2.1. Physical Interpretation

It is characteristic of variable circuits that if a current of frequency  $\omega$  flows in an element varying at a frequency  $p$ , a beat phenomena occurs producing frequency components at  $\omega \pm p$ . When current is injected into the combination of the variable and invariant networks in parallel, a voltage  $V_0$  is produced across the invariant arm, and beats occur in the variable arm to generate currents at frequencies  $\omega \pm p$ . These currents flow into the invariant network, which offers admittances  $Y_1$  and  $Y_{-1}$ , producing the two sideband voltages which together make up  $V_1$ . The sideband voltages cause currents to flow in the variable arm and these also beat with the frequency of the conductance variation to generate other currents at frequencies  $\omega$  and  $\omega \pm 2p$ . These flow into the invariant network and produce voltage  $V_2$  across it. Other terms in the series are built up in a similar manner, the frequency components in each term are shown below.

$V_0$	contains the frequency $\omega$	}	.....(11)
$V_1$	„ „ „ $\omega \pm p$		
$V_2$	„ „ „ $\omega, \omega \pm 2p$		
$V_3$	„ „ „ $\omega \pm p, \omega \pm 3p$		
$V_4$	„ „ „ $\omega, \omega \pm 2p, \omega \pm 4p$		

and so on.

The amplitude of any component  $V_m$  is proportional to  $(\delta G)^m$ , so that if  $\delta G$  is small only the first few terms of the series in eqn. (1) need be considered.

It was found experimentally that the first two terms gave sufficient accuracy and the total voltage could be written as

$$V \simeq V_0 + V_1 \quad \dots\dots(12)$$

2.2. Variations Applied to a Parallel Resonant Circuit

If the invariant circuit consists of a parallel tuned circuit, as shown in Fig. 2 and the frequency of the injected current  $I_{in}$  is the resonant frequency of this circuit  $\omega_0$ , then the term  $V_0$  in eqn. (12) becomes:

$$V_0 = \frac{I_{in}}{Y_0} = \frac{I_{in}}{G} \quad \dots\dots(13)$$

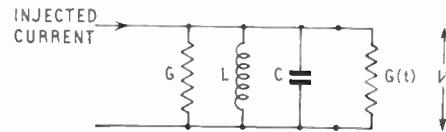


Fig. 2. Parallel resonant circuit having variable conductance connected in parallel.

When the conductance is varied cosinusoidally at frequency  $p$ , the voltages  $V_1, V_2$  etc. are produced. From eqn. (7) the value of  $V_1$  is:

$$V_1 = - \frac{V_0 \cdot \delta G \cos pt}{G(1 + jyQ)} \quad \dots\dots(14)$$

Here

$$V_0 = E_0 \cos \omega_0 t$$

$G(1 + jyQ)$  = admittance of the tuned circuit

$$y = \left( \frac{\omega}{\omega_0} - \frac{\omega_0}{\omega} \right)$$

$$\omega_0^2 = \frac{1}{LC}$$

$$Q = \text{coil quality factor} = \frac{1}{\omega_0 LG}$$

For the tuned circuit  $Y_m$  in eqn. (6) becomes

$$Y_m = G(1 + jy_m Q) \quad \dots\dots(15)$$

where

$$y_m = \left( \frac{\omega_0 + mp}{\omega_0} - \frac{\omega_0}{\omega_0 + mp} \right) \quad \dots\dots(16)$$

The amplitudes of the first pair of sidebands about  $\omega_0$  are obtained from  $V_1$ :

$$V_1 = - \frac{E_0 (\delta G)}{2 \left( \frac{\delta G}{G} \right)} \left[ \frac{\cos(\omega_0 + p)t}{1 + jy_1 Q} + \frac{\cos(\omega_0 - p)t}{1 + jy_{-1} Q} \right] \quad \dots\dots(17)$$

Using the two term approximation for  $V$  given by equation (12), the voltage across the tuned circuit is

given by the expression

$$V = E_0 \left[ 1 - \left( \frac{\delta G}{G} \right) \frac{\cos pt}{(1 + jyQ)} \right] \cos \omega_0 t \dots\dots(18)$$

Equation (18) shows the signal produced across a passive tuned circuit when the circuit conductance is varied cosinusoidally by a small amount  $\delta G$ . We shall now consider the effect of varying the conductance of the tuned circuit in an oscillator.

### 3. Sensitivity of the Oscillator

The analysis of the LC oscillator was first carried out by van der Pol<sup>4</sup> who obtained an expression showing the dependance of the oscillator voltage upon the non-linearity which occurs in the valve characteristic. van der Pol did not consider the effect upon the oscillator voltages of varying the tuned circuit conductance, but his paper is the basis of later work on the analysis of oscillator circuits.

The sensitivity of the oscillator to conductance changes has been studied by Bruin and Schimmel<sup>5</sup> who divided oscillators into two groups, one open circuit stable and the other short circuit stable; they apply Nyquist diagrams to the problem. Bruin has also published an excellent review of the oscillator applied to paramagnetic resonance.<sup>6</sup> The method has been used by Pound and Knight to detect nuclear resonances.<sup>7</sup> Watkins<sup>8</sup> has modified the Pound oscillator and obtained a noise figure for the resulting circuit. The cathode-coupled circuit has been widely used and will be considered here, although other circuits have been employed successfully.<sup>9</sup>

The amplitude of oscillation is determined by the valve characteristics and the losses in the tuned circuit. If these losses are increased the amplitude will be decreased, while a reduction of the loss produces a rise in amplitude. When the tuned circuit conductance is varied periodically the oscillator voltage is amplitude modulated and can be demodulated and displayed.

### 4. Static Characteristics of the Oscillator

As a first step it is interesting to consider the effect of connecting resistors in parallel with the grid tuned circuit of the cathode-coupled oscillator shown in Fig. 3, the feedback resistor R1 being made zero. It was found that when the tuned circuit conductance was raised the measured level of oscillation fell: this was the result to be expected.

It is desirable to identify the conductances which make up the total grid tuned circuit damping; these are as follows:

- $G_0$  equivalent conductance of the coil at the frequency of oscillation.
- $G_1$  conductance due to the output admittance of the amplifier section of the oscillator.

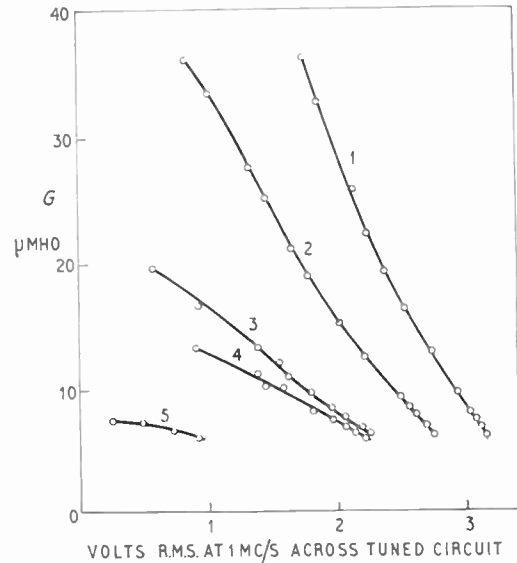
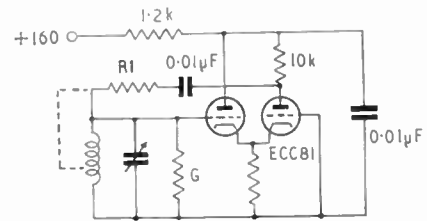


Fig. 3. Sensitivity of oscillator to static damping.

$G_2$  input conductance of circuits coupled to the oscillator grid tuned circuit.

$G_3$  conductance due to the input admittance of the amplifier section.

Frequently  $G_2$  and  $G_3$  are small enough to neglect, for zero grid current, but  $G_0$  and  $G_1$  must be considered.

The value of  $G_0$  varies with frequency and with the  $Q$  factor of the coil: a typical value at 1 Mc/s is  $G_0 = 2.5 \times 10^{-5} \text{ ohm}^{-1}$ . The output admittance  $Y_{out}$  of the cathode-coupled amplifier operated linearly is:

$$Y_{out} = \frac{Z_L + r_{a2} + Z_k(\mu_2 + 1) \left[ 1 - \frac{Z_k(\mu_1 + 1)}{r_{a1} + Z_k(\mu_1 + 1)} \right]}{Z_L \left\{ r_{a2} + Z_k(\mu_2 + 1) \left[ 1 - \frac{Z_k(\mu_1 + 1)}{r_{a1} + Z_k(\mu_1 + 1)} \right] \right\}} \dots\dots(19)$$

where  $Z_k$  = impedance of the cathode load

$Z_L$  = impedance of the anode load of the second triode stage.

$\mu$  and  $r_a$  are the valve parameters; the subscripts 1 and 2 refer to the cathode follower and grounded-grid stages respectively.

Inserting typical values gives  $G_1 = 1.4 \times 10^{-4}$  ohm<sup>-1</sup>. Thus most of the damping is due to the output impedance of the amplifier section. The value of  $G_1$  can be reduced by operating the valves with low anode currents to give larger  $r_a$  and by using a tuned circuit as the anode load, thus increasing  $Z_L$ . Another method, adopted by Watkins,<sup>8</sup> is to insert a resistor  $R_1$  in the feedback loop, reducing the feedback factor  $\beta$  from unity to

$$\beta = \frac{1}{1 + R_1 G_0 (1 + jyQ)} \quad \dots\dots(20)$$

The equivalent conductance due to the output impedance is then

$$\frac{G_1}{1 + G_1 \cdot R_1} \text{ at } \omega = \omega_0 \quad \dots\dots(9)$$

4.1. Experimental Check on the Effect of Reducing the Feedback Factor

Figure 3 shows the change in the level of oscillation when damping resistors were connected in parallel with the tuned circuit; the sensitivities  $\delta V/\delta G$  are listed in Table 1.

Table 1

Curve No.	$R_k$ in kilohms	$R_1$ in kilohms	$\frac{\delta V}{\delta G} \times 10^6$
1	1.5	22	0.08
2	1.5	47	0.15
3	1.5	100	0.17
4	1.1	200	0.29
5	1.5	100	0.46

As  $R_1$  is increased, i.e.  $\beta$  is reduced, the sensitivity to static damping is increased. A further increase in sensitivity is obtained by connecting the feedback resistor to a tapping on the coil, reducing the feedback factor  $\beta$  to

$$\beta = \frac{T}{1 + R_1 \cdot G_0 T^2} \quad \dots\dots(21)$$

where  $T$  is the transformation ratio, assuming a coupling coefficient of unity. The effect of the amplifier section output admittance and feedback resistor on the grid tuned circuit is then given by the conductance

$$\frac{G_1}{T^2(1 + R_1 \cdot G_1)}$$

Curve 5 on Fig. 3 shows the effect of the modification on the sensitivity. Since three connections to the tapped coil are required, instead of the two needed without the tapping, the method was not proceeded with. It may be concluded that the result of reducing  $\beta$  is to increase the sensitivity of the oscillator to static damping.

4.2. Effect of Non-linearity in the Amplifier Section

When the oscillator voltage rises from the initiating noise pulse the non-linear gain  $A'$  of the amplifier section is reduced and the voltage gain settles to the value  $A$  for which  $A \cdot \beta$  is equal to unity.

Thus 
$$\frac{dA}{d\beta} = -\frac{1}{\beta^2} \quad \dots\dots(22)$$

if 
$$A = A_0 + A_1 \cdot V + A_2 \cdot V^2 + \dots$$

where  $V$  is the voltage across the tuned circuit in Fig. 4.

$$\frac{dV}{d\beta} = -\frac{1}{\beta^2(A_1 + 2A_2 V + 3A_3 V^2 + \dots)} \quad \dots\dots(23)$$

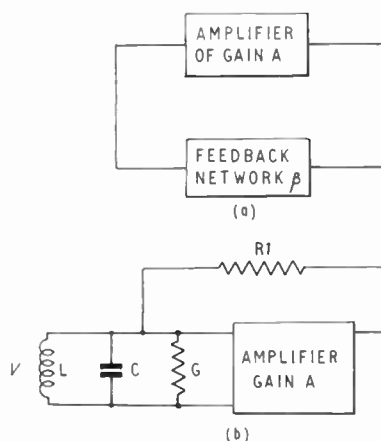


Fig. 4. Basic oscillator circuit.

For high sensitivity  $dV/d\beta$  must be large, i.e.  $\beta$  and the non-linear terms  $A_1, A_2$  etc. must be small.

The causes of non-linearity are as follows:

- (a) Grid current in either of the triodes.
- (b) Curvature of the valve characteristics.

The grid current is usually of the order of a few microamperes; its effect is to introduce clipping of the amplified signal, to bias the valve and to damp the grid tuned circuit. It may be reduced by raising the cathode voltage of the first triode so that the grid to cathode voltage is never positive for the levels of oscillation in use.

Non-linearity of the valve characteristics causes changes of the average anode current when a signal is being amplified. This produces a bias change which alters the amplifier gain. This may be minimized in a cathode-coupled circuit by connecting a capacitor between the two valve cathodes in order to prevent the bias on one affecting the gain of the other stage.

A circuit was built having a bias on the cathode of the first stage large enough to prevent grid current, a

capacitor between the cathode of the two triodes, a feedback resistor R1 in the feedback loop, and a tuned load in the second stage. Tests showed that when this circuit was operated at a frequency of 1 Mc/s, the non-linear terms in the characteristic of the amplifier section of the oscillator and grid current in the first stage were considerably reduced.

**5. Analysis of the Oscillator Circuit**

The differential equation for the circuit shown in Fig. 4 may be written:

$$C \frac{dV}{dt} + G.V + \frac{1}{L} \int V dt = \frac{(A_0 - 1)V}{R_1} + \frac{A_1 V^2}{R_1} + \frac{A_2 V^3}{R_1} \dots\dots(24)$$

In the steady state  $V = E_0 \cdot \cos \omega_0 t$  where  $\omega_0^2 \simeq 1/LC$  for a circuit having a high  $Q$  factor. By rearranging eqn. (56) in Section 10, it may be shown that when a disturbing current at frequency  $\omega_1$  is injected into the tuned circuit the response is

$$E_1 = \frac{I}{G'(1 + jy_1 Q')} \dots\dots(25)$$

where  $G' = G - \frac{A_0 - 1}{R_1}$

$$y_1 = \left( \frac{\omega_1}{\omega_0} - \frac{\omega_0}{\omega_1} \right)$$

and  $Q' = \frac{\omega_0 \cdot C}{G'}$

The effect of a small conductance variation of the form  $\delta G \cos pt$ , using the method of Section 2 and assuming that  $\delta G$  is small enough not to change  $E_0$ , is such as to produce a voltage  $V_1$ :

$$V_1 \simeq \frac{E_0 (\delta G)}{2 (G')} \left[ \frac{\cos(\omega_0 + p)t}{(1 + jy_1 Q')} + \frac{\cos(\omega_0 - p)t}{(1 + jy_{-1} Q')} \right] \dots\dots(26)$$

and similarly

$$V_2 \simeq \frac{E_0 (\delta G)^2}{4 (G')^2} \left[ \frac{\cos(\omega_0 + 2p)t}{(1 + jy_1 Q')(1 + jy_2 Q')} + \frac{\cos(\omega_0 - 2p)t}{(1 + jy_{-1} Q')(1 + jy_{-2} Q')} \right] \dots\dots(27)$$

The small term in  $\cos \omega_0 t$  is neglected.

For  $\delta G \ll G$  the approximate tuned circuit voltage is given by

$$V \simeq E_0 \left[ 1 - \frac{\delta G \cos pt}{G'(1 + jy Q')} \right] \cos \omega_0 t \dots\dots(28)$$

In the steady state, when only the frequencies  $\omega_0$  and  $\omega_0 \pm p$  are considered, an expression may be obtained which shows the dependence of the frequency response upon the value of  $E_0$ . Equating the steady state currents in the tuned circuit and the feedback resistor R1, and assuming that both sidebands are of equal

amplitude and are much smaller than the carrier amplitude  $E_0$ , gives the tuned circuit voltage as

$$V \simeq E_0 \left[ 1 - \frac{\delta G \cdot \cos pt}{G''(1 + jy Q'')} \right] \cos \omega_0 t \dots\dots(29)$$

where  $G'' = G - \frac{A_0 - 1}{R_1} - \frac{9A_2 E_0^2}{4R_1}$

and  $Q'' = \frac{\omega_0 C}{G''}$

**5.1. Optimum Operating Voltage**

It is to be expected from the form of eqn. (29) that an optimum value of  $E_0$  should exist giving maximum value of sideband amplitude for a given frequency of conductance variation  $p$ .

Let equation (29) be written as

$$V = V_0 + V'_1 \dots\dots(30)$$

where  $V'_1 \simeq - \frac{E_0 \cdot \delta G \cdot \cos pt}{G''(1 + jy Q'')} \dots\dots(31)$

Differentiating the magnitude of  $V'_1$  (eqn. 31) with respect to  $E_0$  and equating the result to zero, gives the optimum  $E_0$  as follows

$$E_{0opt}^2 = \frac{2y\omega_0 CR_1}{3A_2} \dots\dots(32)$$

Substitution gives

$$V'_{1max} = \frac{\delta G \cdot \cos pt}{\sqrt{\frac{3 \cdot A_2 \cdot y \cdot \omega_0 \cdot C}{R_1}}} \dots\dots(33)$$

For  $p \ll \omega_0$  eqn. (33) simplifies to

$$V'_{1max} \simeq \frac{\delta G \cdot \cos pt}{\sqrt{\frac{6 \cdot A_2 \cdot p \cdot C}{R_1}}} \dots\dots(34)$$

Thus for large sideband amplitude at optimum  $E_0$ ,  $\delta G$  and  $R_1$  must be made large and  $A_2$ ,  $p$  and  $C$  small. In practice  $p$  and  $R_1$  are the terms most easily controlled.

**5.2. Effect of Injecting an Audio-frequency Current into the Oscillator**

It frequently happens that some audio-frequency current due to pick-up is injected into the oscillator circuit. This frequency will be outside the oscillator pass band but will modulate the voltage at the carrier frequency  $\omega_0$ , producing sidebands evenly spaced about it at  $\omega_0 \pm p$ . In addition to the possibility of modulating the oscillator for test purposes it is desirable to have an analysis to show the effects of pick-up signals from the mains.

Let a current  $I \cos pt$  be injected into the oscillator tuned circuit in Fig. 4 and assume the oscillator to be

operating at frequency  $\omega_0$ . Voltages at both frequencies will be amplified and will beat together to produce voltages at frequencies of  $\omega_0 \pm p$ .

Equating the steady current through the feedback resistor to that in the tuned circuit gives

$$I \cos pt + \frac{(A_0 - 1)V}{R_1} + \frac{A_1 \cdot V^2}{R_1} + \frac{A_2 \cdot V^3}{R_1} = G(1 + jyQ)V \dots\dots(35)$$

where

$$V = E_0 \cos \omega_0 t + E_1 \cos pt + E_2 \cos(\omega_0 + p)t + E_3 \cos(\omega_0 - p)t \dots\dots(36)$$

Expanding and retaining the terms at the frequencies  $\omega_0, p, (\omega_0 \pm p)$ , then equating coefficients of these terms assuming  $E_0 \gg E_1 \gg E_2$  and that  $|E_2| = |E_3|$  gives, after some manipulation,

$$E_1 \simeq \frac{I}{G' \left[ 1 + j \left( \frac{p}{\omega_0} - \frac{\omega_0}{p} \right) Q' \right] - \frac{3 \cdot A_2 \cdot E_0^2}{2R_1}} \dots\dots(37)$$

$$E_2 \simeq - \frac{A_1 \cdot E_1 \cdot E_0}{R_1 \cdot G'' \cdot (1 + jy_1 Q'')} \dots\dots(38)$$

$$E_3 \simeq - \frac{A_1 \cdot E_1 \cdot E_0}{R_1 \cdot G''(1 + jy_{-1} Q'')} \dots\dots(39)$$

When interpreting these equations it must be remembered that  $G_0$  and the amplifier gain are not constant over the whole frequency range.

The voltage  $E_1$  at the frequency  $p$  can be excluded from the demodulated output of the oscillator by means of filter circuits between the oscillator grid tuned circuit and the radio-frequency amplifier. The frequencies  $\omega_0 \pm p$  will pass through any such filter, be demodulated, and may interfere with the required signal output due to conductance variations. Even when the interfering and required signals are at the same frequency they may not be in phase. The analysis has shown that the amplitudes of the sidebands due to the interfering signal is proportional to  $A_1$  while the amplitude of the required signal is not. This appears to offer a means for reducing the amplitude of the interference by reducing  $A_1$ , but unfortunately it is difficult to control this term independently in any of the conventional oscillator circuits. When all the non-linear terms were reduced both the required and interfering signal amplitudes were increased because  $A_2$  was reduced as well as  $A_1$ .

**6. Experimental Work to Check Theory**

In the preceding sections equations have been obtained which describe the operation of the oscillator as a detector of periodic conductance changes. Because the derivation differs from that usually employed in circuit theory, in that the operation of the oscillator is non-linear, it was decided to confirm the equation

experimentally.

To this end an oscillator was constructed to operate at 1 Mc/s; this frequency was chosen in order to avoid difficulties at higher frequencies due to the effects of stray capacitances.

The conclusions which may be drawn from eqn. (29) are as follows:

- (1) The sideband amplitude is proportional to  $\delta G$ , the amplitude of the conductance variation, provided that  $\delta G$  is small.
- (2) The sideband amplitude should vary with the frequency of the conductance change in a manner similar to the frequency response of a parallel tuned circuit.
- (3) The frequency response should vary with  $A_2, R_1,$  and  $E_0$ .
- (4) For small values of  $E_0$  and  $p$  the bandwidth between the 70% response frequency is proportional to

$$\frac{A_2 \cdot E_0^2}{2\pi \cdot R_1 \cdot C}$$

That is, the effective  $Q$  factor of the oscillator varies where

$$Q \simeq \frac{f_0}{\Delta f} \dots\dots(40)$$

and

$$f_0 \simeq \frac{1}{2\pi\sqrt{LC}}$$

- (5) When the oscillator is operated in its steady state and the conductance is varied periodically at frequency  $p$  an optimum value of grid tuned circuit voltage  $E_0$  should exist giving maximum signal power.

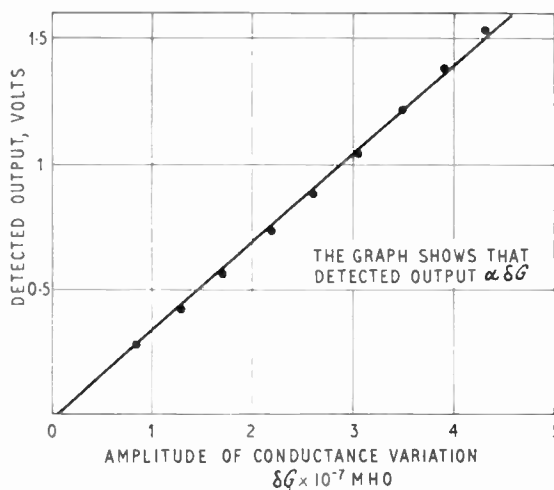


Fig. 5. Plot showing amplitude of conductance variations against output signal.

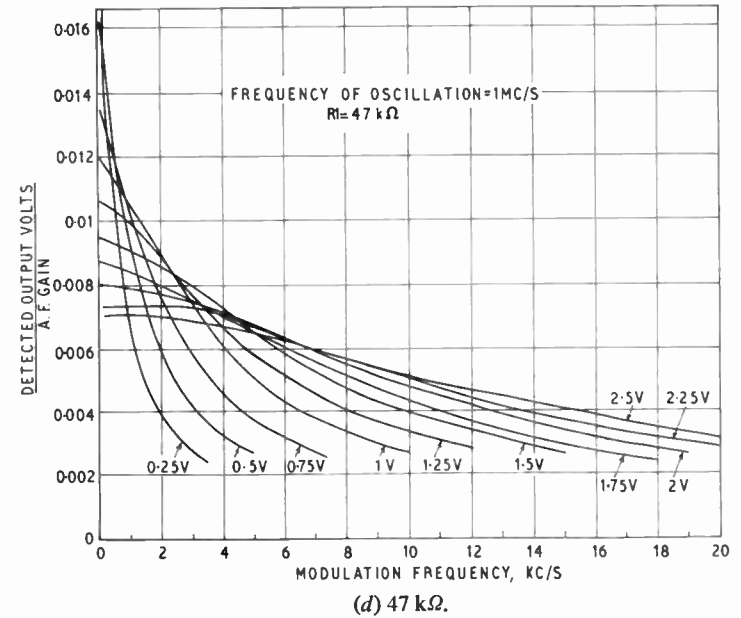
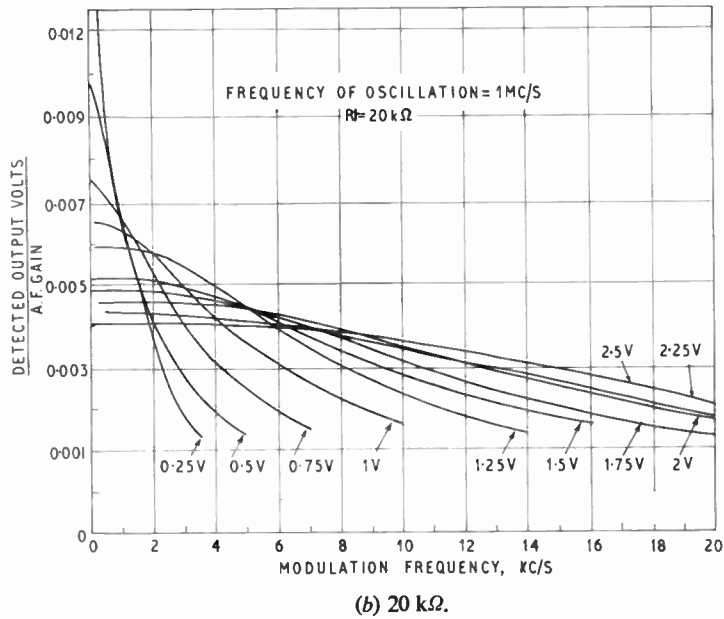
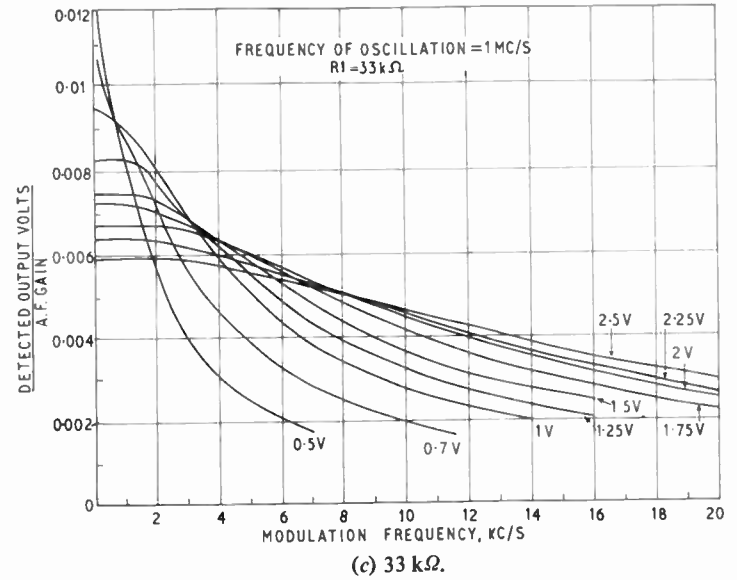
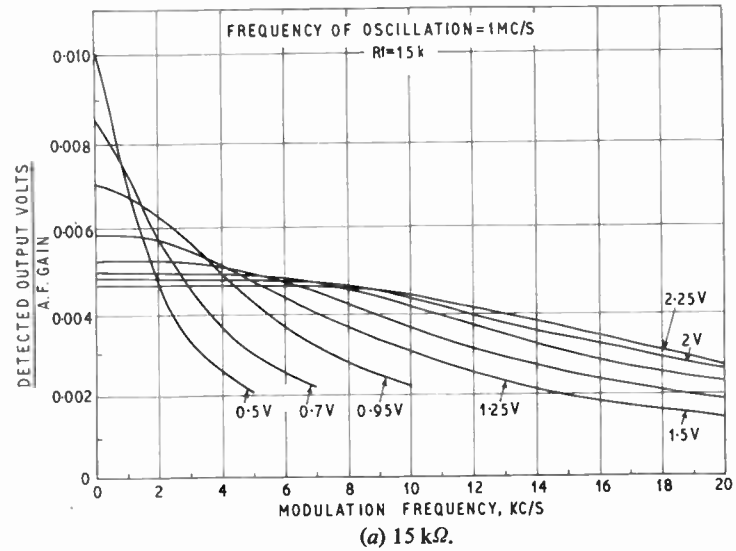
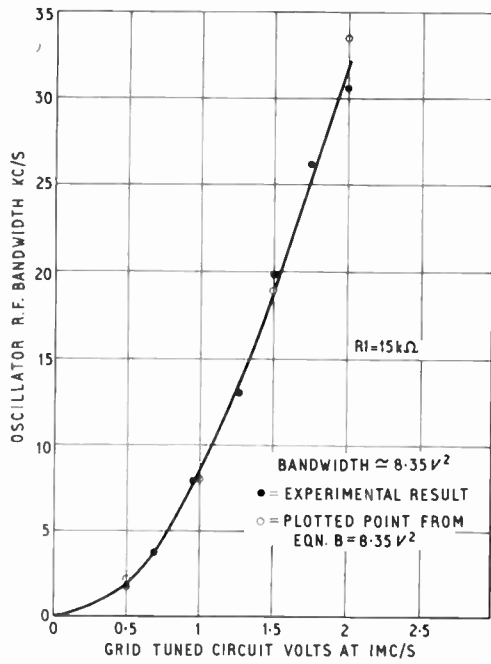
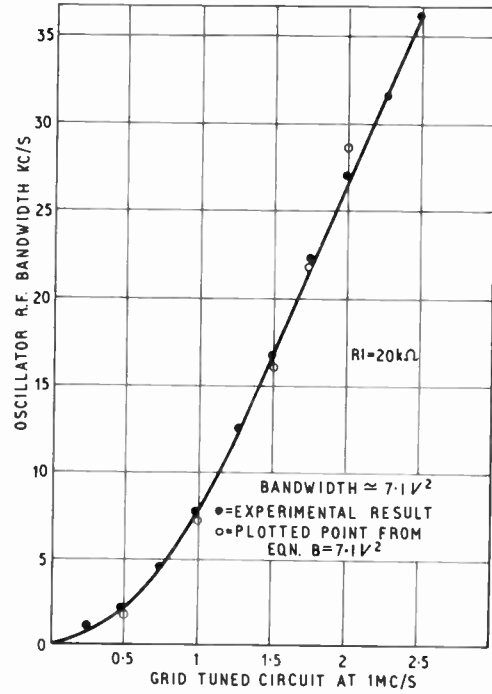


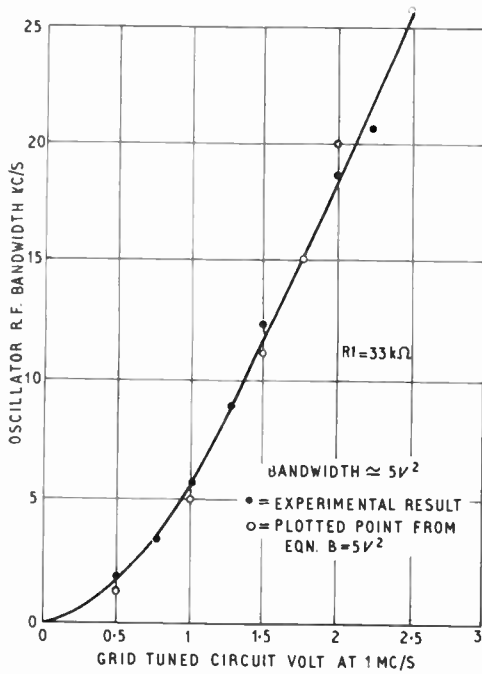
Fig. 6. Plots of signal output against the frequency of the conductance variations for different values of feedback resistor.



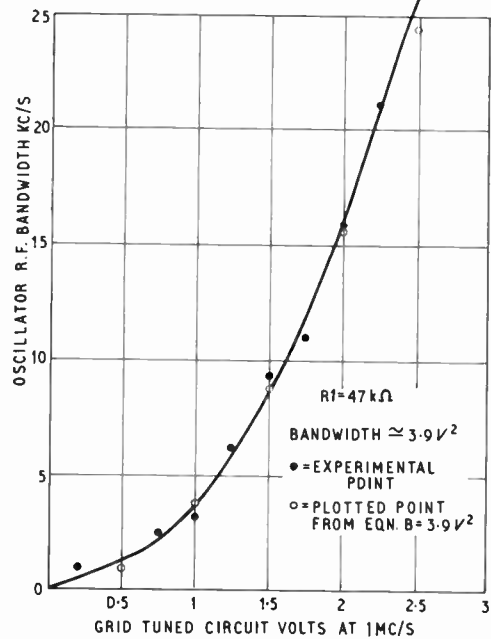
(a) 15 kΩ.



(b) 20 kΩ.



(c) 33 kΩ.



(d) 47 kΩ.

Fig. 7. Plots of oscillator bandwidth against grid tuned circuit voltage for different values of feedback resistor.

(6) When  $p$  is varied the value of tuned circuit voltage giving maximum signal power is changed.

It was not possible to observe the modulation of the 1-Mc/s waveform directly on an oscilloscope, because the percentage of modulation was usually too small. The radio-frequency wave was amplified, demodulated, and the amplitude of the low-frequency signal measured after further amplification. A block diagram of the apparatus is given in the Appendix.

Using the oscillator and amplifiers described, with a valve voltmeter and oscillograph connected to the low-frequency amplifier output, tests were carried out to find if the conclusions drawn from the theory were confirmed by experiment.

6.1. Signal Amplitude Proportional to Conductance Variation

A variable conductance circuit was connected to the oscillator grid tuned circuit and the amplitude of the conductance variation was increased in steps. The demodulated waveform was observed to be sinusoidal and its amplitude was plotted against the amplitude of conductance variation. The straight line graph of Fig. 5 shows that the sideband amplitude is proportional to the amplitude of conductance variation, confirming conclusion (1).

6.2. Effect of the Frequency of Conductance Variation

A voltage of constant amplitude but variable frequency was applied to the grid of the variable conductance valve and the oscillator grid tuned circuit voltage was measured. This voltage was maintained constant while the frequency, but not the amplitude, of the conductance swing was varied. The amplitude of the demodulated sideband was measured and is plotted in Fig. 6. Experimental points are omitted from the curves in the interests of clarity. It is evident from the shape of, for example, the 1.25-V curve that the sideband amplitude falls as the frequency of the conductance variation is increased and that the oscillator frequency response is similar to that of a parallel resonant circuit. Thus conclusion (2) is confirmed. This method of determining the frequency response of an oscillator by varying a conductance, instead of injecting a radio frequency voltage into the grid tuned circuit, has the advantage that no pulling of the oscillator frequency is introduced.

6.3. Effect of  $E_0$ ,  $R_1$  and  $A_2$  on the Frequency Response

It has been predicted that the frequency response would depend upon  $E_0$ . This was confirmed by adjusting the oscillator grid tuned circuit voltage by increments of about 0.25 V r.m.s. and repeating the measurements of the previous section for the same range of frequencies. The demodulated signal voltage amplitudes are plotted in Fig. 6. The curves show that

as the tuned circuit voltage is reduced there is a considerable change in the frequency response of the oscillator.

The effect of the feedback resistor on the frequency was checked by connecting four different values of  $R_1$  and measuring the frequency response for a range of oscillator tuned circuit voltages. The demodulated signal voltages are plotted in Figs. 6, (a) to (d) for  $R_1 = 15, 20, 33$  and  $47 \text{ k}\Omega$  respectively. These curves show that frequency response changes when different values of resistance are inserted in the feedback lead.

It was not possible to vary  $A_2$  in a sufficiently controlled manner for measurement purposes, but it was found that decreasing the non-linear term in the amplifier section of the oscillator increased the sensitivity to conductance changes.

6.4. Bandwidth between 70% Response Frequencies

The half-bandwidth  $B$  between the 70% response frequencies may be measured from the curves on Figs. 6, (a) to (d). The values so obtained are plotted in Figs. 7 (a) to (d) for feedback resistance values of 15, 20, 33 and 47 kΩ respectively. The curves have the form  $B = K \cdot V^2$ , and this is of the same form as the expression

$$\frac{A_2 \cdot E_0^2}{2\pi \cdot R_1 \cdot C} \dots\dots(41)$$

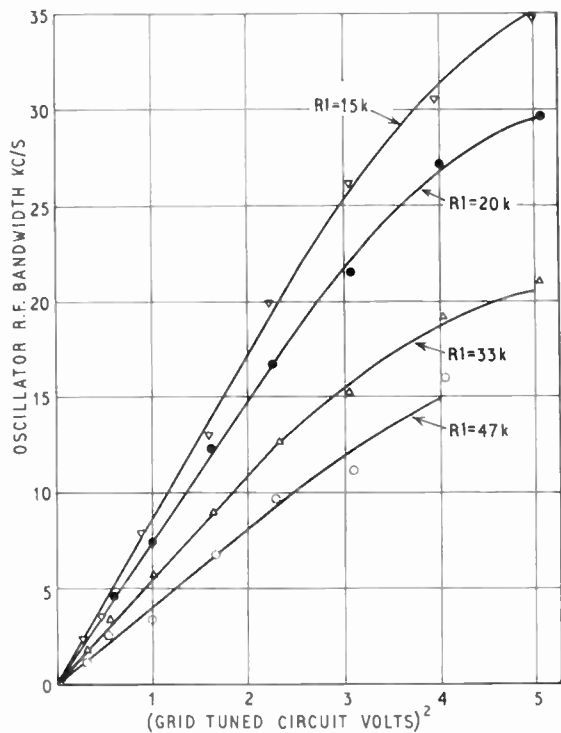


Fig. 8. Plot of oscillator bandwidth against the square of the grid tuned circuit voltage.

from eqn. (29) which gives the 3dB bandwidth.

Here  $B = \Delta f/2 =$  half the oscillator bandwidth in cycles per second;  $K$  is a constant.

In Fig. 8 the bandwidth is plotted against the square of the oscillator voltage, a straight line relationship holds for values of  $V^2$  up to 2.5. It may be seen from these curves that a larger  $Q$  factor is obtained when  $R_1$  is large.

It is to be expected that a plot of  $B$  against  $1/R_1$  with  $V^2$  as the parameter should be a straight line through the origin. In fact the experimental points are scattered and this is thought to be due to the variations in  $A_2$  which occur when the oscillator controls are adjusted to change  $V$ . In order to check this  $B$  was plotted against  $K' \cdot A_2/R_1$ , where  $K'$  is a constant, with  $V^2$  as the parameter. Figure 9 shows graphs for two values of  $V$ , both are straight lines through the origin. Thus conclusion (4) is confirmed.

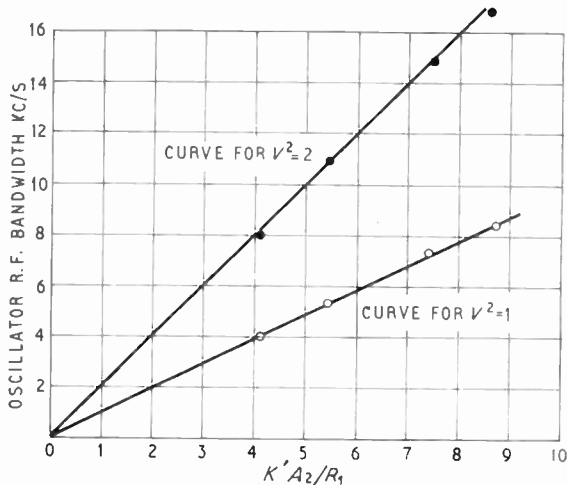


Fig. 9. Plot of oscillator bandwidth against  $K'A_2/R_1$

6.5. Optimum Oscillator Voltage

The detected signal voltage produced by a conductance variation at 1 kc/s for a range of oscillator grid tuned circuit voltages is shown in Fig. 10(a). Four curves are shown, one for each value of the feedback resistor  $R_1$ . These curves show clearly the existence of the optimum level of oscillation predicted in conclusion (5).

In Fig. 10(b) similar curves are shown for a conductance variation frequency of 2 kc/s; it is evident from these curves that the maximum values of output signal occur at different voltages from those which give the maxima in Fig. 10(a). This confirms that the optimum value of oscillator voltage depends upon  $p$ , as predicted in conclusion (6). The maxima of the curves in Fig. 10 are rather flat, but if the voltages for which the maxima occur are compared between the

two graphs for the same value of feedback resistor the results are as follows:

For feedback resistors of 15 kΩ and 20 kΩ the voltage at which the maximum output occurs with a conductance variation frequency of 1000 c/s is about 0.7 V r.m.s. When this frequency is increased to 2000 c/s the maximum output occurs at 0.95 V r.m.s. for 15 kΩ and 1.05 V r.m.s. for 20 kΩ.

Theory predicts that when the frequency of conductance variation is doubled the voltages for which the maximum signal output occurs should be increased by a factor  $\sqrt{2}$ ; it is evident that close agreement exists between theory and experiment for feedback resistors of 15 kΩ and 20 kΩ.

The results for feedback resistors of 33 kΩ and 47 kΩ do not show such close agreement with the theory. When the frequency of conductance variation is doubled the voltages at which the maximum signal appears are related by a factor of about 1.17 for the 33 kΩ and 1.22 for the 47 kΩ feedback resistors. This error may be due to changes in the term  $A_2$ .

7. Operation of the Oscillator as a Square Law Demodulator

When detecting periodic conductance changes, the resulting amplitude-modulated wave may be demodulated by an auxiliary diode circuit, or demodulation may be carried out by the oscillator.

At the anode of the second triode stage in Fig. 4 the alternating voltage is as follows:

Alternating voltage  

$$= (A_0 \cdot V + A_1 \cdot V^2 + A_2 \cdot V^3 + \dots) \dots\dots(42)$$

where  $V$  is the voltage across the grid tuned circuit.

Let the anode load be purely resistive for simplicity, and equal to  $R_L$ . The alternating current  $i_L$  through  $R_L$  is given by:

$$i_L = \frac{1}{R_L} (A_0 \cdot V + A_1 \cdot V^2 + A_2 \cdot V^3 + \dots) \dots\dots(43)$$

Inserting the value of  $V$  from eqn. (29), expanding and selecting  $i'_L$ , the component of  $i_L$  at the modulation frequency  $p$  gives:

$$i'_L = \frac{E_0^2 \cdot \delta G \cdot A_1 \cdot \cos(pt + \phi)}{R_L \cdot G'' \sqrt{[1 + (y \cdot Q'')^2]}} \dots\dots(44)$$

Here

$$\phi = \tan^{-1} yQ''$$

The demodulated voltage at frequency  $p$  appearing across the resistor  $R_L$  is  $R_L \cdot i'_L$ . Thus for a large demodulated signal  $A_1$  should be made large.

8. Frequency Modulation of the Oscillator

When detecting quadripole resonances it is convenient to modulate the frequency of the oscillator.

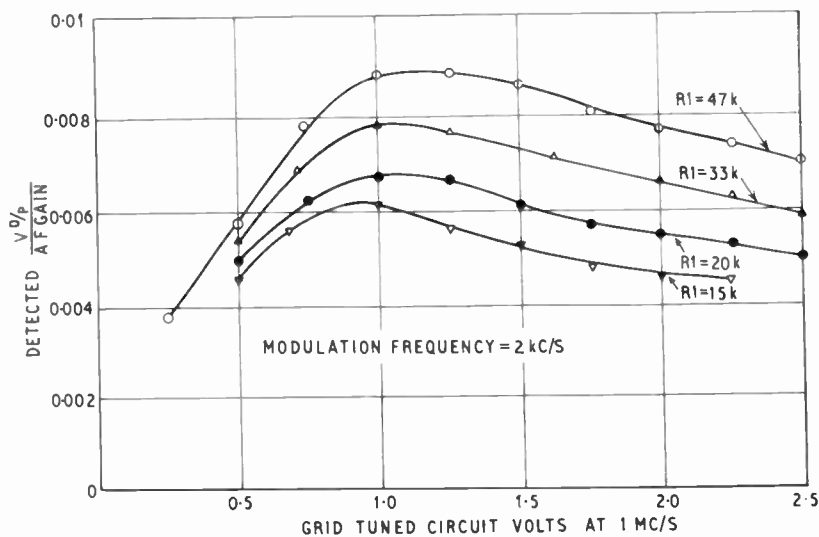
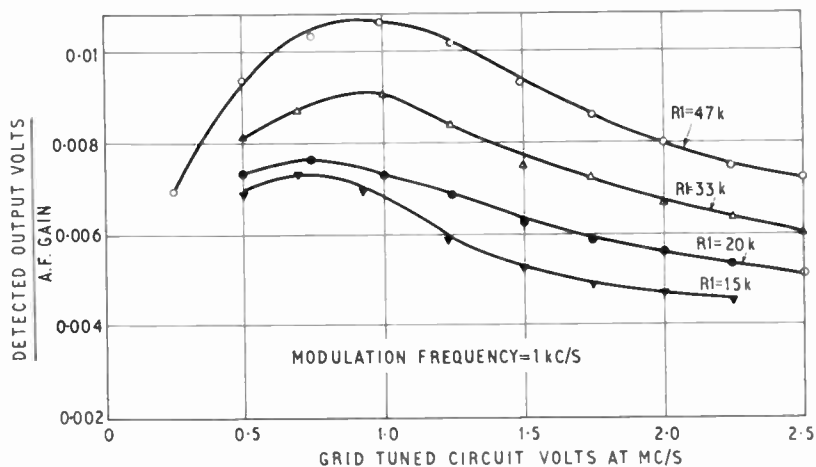


Fig. 10. Plot of output signal against grid tuned circuit voltage for a conductance variation (a) at 1 kc/s, (b) at 2 kc/s.

This is simply done by connecting, in parallel with the main tuning capacitor, a small variable capacitor driven by a suitable motor device. It is found that, when the oscillator output voltage is frequency modulated, an amplitude modulation which may obscure the required signal, is also produced.

It is desirable to know the factors which determine the depth of amplitude modulation produced by a given degree of frequency modulation. For large percentages of frequency modulation this is not a simple problem, but it is found experimentally that small amplitudes of capacitance variation of cosinusoidal form produce a cosinusoidal amplitude modulation. This problem has been previously considered by Cunningham<sup>10</sup> using a method different from that employed here. The simplicity of the present method is such that it is thought to be worthy of inclusion.

Let the circuit be oscillating with voltage  $V$  across the grid tuned circuit.

Let the capacitor variation be  $\delta C \cos pt$ , the grid tuned circuit capacitance be  $C_0$ , and the grid tuned circuit inductance be  $L$ . The approximate frequency of oscillation is

$$f = \frac{1}{2\pi\sqrt{LC}} \quad \dots\dots(45)$$

For  $\frac{\delta C}{C_0} \ll 1$

$$f \simeq f_0 \left( 1 - \frac{\delta C}{2C_0} \cos pt \right) \quad \dots\dots(46)$$

where  $\omega \simeq \frac{1}{2\pi\sqrt{LC_0}}$

Considering only the fundamental angular frequency  $\omega_0$  and the two sidebands generated at  $\omega_0 \pm p$  or amplitude modulation, the application of

Carson's method gives:

$$V \approx V_0 + V_1 \dots\dots(47)$$

where  $V_0 = E_0 \cos \omega_0 t$

$$V = - \frac{j\omega \cdot \delta C \cdot V_0 \cdot \cos pt}{Y} \dots\dots(48)$$

and for  $\omega \approx \omega_0$

$$V \approx V_0 \left[ 1 - \frac{j \cdot \delta C \cdot Q'' \cdot \cos pt}{C_0(1 + jyQ'')} \right] \dots\dots(49)$$

8.1. Conclusions on Frequency Sweep

Both frequency and amplitude variations are proportional to  $\delta C/C_0$ , so that large frequency modulation will produce large amplitude modulation. The phase relationship between the capacitance variation and the amplitude modulation it produces depends upon  $Q''$ , that is, upon the oscillator voltage  $E_0$ . The degree of amplitude modulation is greater for large values of  $Q''$ . Thus the condition giving high sensitivity to conductance changes also makes the oscillator liable to undesired amplitude modulation when its frequency is swept. This undesired modulation may mask the required signal.

9. Sensitivity to Changes in Reactance of the Oscillator Coil

When a nuclear resonance is detected one effect is to change the reactance of the oscillator coil and so produce frequency modulation of the oscillator output voltage. This may be demodulated by a discriminator and displayed in the same way as the signal produced by a conductance change.<sup>11</sup> Usually the signal due to the conductance change is used because the apparatus required is simpler.

Assuming that the reactance change can be treated as an inductance change of the form  $\delta L \cdot \cos pt$ , where  $\delta L \ll L_0$ , the frequency deviation  $\Delta f'$  produced is as follows.

The instantaneous frequency of the oscillator is

$$f \approx \frac{1}{2\pi\sqrt{LC}} \dots\dots(45)$$

$$f = f_0 \left( 1 - \frac{\delta L}{2L_0} \cos pt \right) \dots\dots(46a)$$

where  $f_0 \approx \frac{1}{2\pi\sqrt{L_0 C}}$

and  $L_0$  is the inductance of the oscillator grid tuned circuit coil.

Therefore  $\Delta f' = \frac{f_0 \cdot \delta L}{2L_0} \dots\dots(50)$

The similarity to frequency modulation by varying the capacitance is obvious.

10. Noise Produced in the Oscillator

The treatment given here extends that given by van der Ziel.<sup>12</sup> Consider the oscillator to be made up from an amplifier of gain  $A$  and a feedback network.

Here  $A = (A_0 + A_1 V + A_2 V^2 + \dots)$

and the feedback factor  $\beta$ , from Fig. 4 is

$$\beta = \frac{Z}{R_1 + Z}$$

where  $Z$  is the impedance of the oscillator tuned circuit  $L, C, G$ .

$$Z = \frac{1}{G(1 + jyQ)}$$

It is known that a sustained oscillation  $V$  will exist across the tuned circuit such that

$$V \approx E_0 \cdot \cos \omega t \dots\dots(51)$$

where

$$\omega \approx \omega_0$$

and

$$\omega_0^2 = \frac{1}{L \cdot C}$$

Let a disturbing current  $I \cdot \sin(\omega_1 t + \theta)$  be injected into the oscillator loop as shown in Fig. 11(a). From the voltage drop across the feedback resistor  $R_1$  the feedback current to the tuned circuit is:

$$\frac{(A_0 - 1)V}{R_1} + \frac{A_1 \cdot V^2}{R_1} + \frac{A_2 \cdot V^3}{R_1} \dots\dots(52)$$

This is shown in Fig. 11(b).

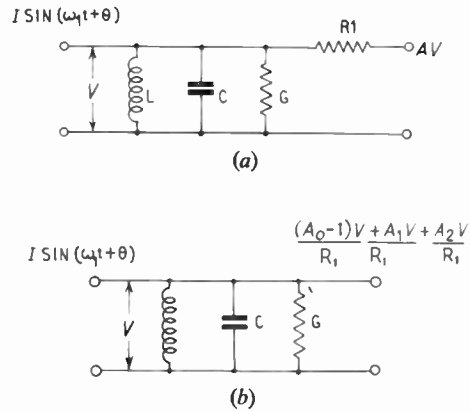


Fig. 11. Oscillator with disturbing current.

The differential equation is:

$$C \frac{dV}{dt} + G \cdot V + \frac{1}{L} \int V dt = \frac{(A_0 - 1)V}{R_1} + \frac{A_1 \cdot V^2}{R_1} + \frac{A_2 \cdot V^3}{R_1} + I \sin(\omega_1 t + \theta) \dots\dots(53)$$

Experiment shows that if the pulling effects are neglected the solution is of the form

$$V \simeq E_0 \cos \omega_0 t + E_1 \cos \omega_1 t \quad \dots\dots(54)$$

Differentiation of eqn. (53) with respect to time, and substitution for  $V$  gives the relationships:

$$E_{0\max}^2 - 2E_1^2 = E_0^2 \quad \dots\dots(55)$$

$$E_1^2 \left\{ \frac{(\omega_0^2 - \omega_1^2)^2}{\omega_1^2} + \frac{\left(G - \frac{A_0 - 1}{R_1}\right)^2}{C^2} \times \left[ 1 - \frac{3E_1^2}{E_{0\max}^2} \right]^2 \right\} = \frac{I^2}{C^2} \quad \dots\dots(56)$$

where  $E_{0\max}$  is the value of  $E_0$  when no disturbing current is injected, i.e. when  $I = 0$ . Equations (55) and (56) are of the same form as those derived by van der Pol<sup>4</sup> for an oscillator having an external voltage applied.

The results obtained when the disturbing force is a sinusoidal current may be applied to show the effects of random noise. Let the thermal noise arising in the circuit have a mean square value  $\bar{i}_1^2$ . In an infinitesimal frequency interval  $df$ :

$$i^2 = 4k \cdot TG \cdot df \quad \dots\dots(57)$$

where  $k$  is Boltzmann's constant and  $T$  is temperature in deg K.

Let the noise arising in the amplifier section of the oscillator be  $\bar{i}_2^2$  (for the same frequency interval  $df$ ).

$$\bar{i}_2^2 = D \cdot df \quad \dots\dots(58)$$

The term  $D$  gives the noise due to thermal agitation and shot effect in the amplifier section. It depends upon the valves used and the circuitry of the amplifier; a value of  $D$  must be worked out for each different oscillator circuit.

Let 
$$\bar{i}^2 = \bar{i}_1^2 + \bar{i}_2^2 \quad \dots\dots(59)$$

This current is injected into the tuned circuit of the oscillator and if the interval  $df$  is about the frequency  $f_1 = \omega_1/2\pi$  the result of eqn. (56) may be used. Writing  $I^2$  in eqn. (53) as  $2(D+4kTG)df$  and using the solution of eqn. (56) gives

$$\bar{V}_n^2 \left\{ \frac{(\omega_0^2 - \omega_1^2)^2}{\omega_1^2} + \frac{1}{C^2} \left[ G - \frac{(A_0 - 1)}{R_1} \right]^2 \times \left[ 1 - \frac{6 \cdot \bar{V}_n^2}{E_{0\max}^2} \right]^2 \right\} = \frac{(D+4kTG)df}{C^2} \quad \dots\dots(60)$$

where  $\bar{V}_n^2$  is the mean square noise voltage across the tuned circuit. In the frequency interval  $df$ , the noise voltage produced must be much smaller than  $E_{0\max}$ . Thus eqn. (60) above may be simplified by neglecting the term  $6\bar{V}_n^2/E_{0\max}^2$  which is much less than unity.

$$\bar{V}_n^2 = \frac{(D+4kTG)df}{C^2 \left\{ \frac{(\omega_0^2 - \omega_1^2)^2}{\omega_1^2} + \frac{1}{C^2} \left[ G - \frac{(A_0 - 1)}{R_1} \right]^2 \right\}} \quad \dots\dots(61)$$

The noise voltage  $\bar{V}_n^2$  is that produced by a small disturbance about the angular frequency  $\omega_1$  and in order to find the total noise across the tuned circuit it is necessary to sum (i.e. integrate) the effects of disturbances at all frequencies. To add these noise voltages it is necessary to add mean square voltages. Let the total noise be  $\bar{V}_{in}^2$ .

$$\bar{V}_{in}^2 = \int_0^\infty \frac{(D+4kTG) \cdot df}{\left[ G - \frac{(A_0 - 1)}{R_1} \right]^2 \cdot \left\{ \frac{C^2 \omega_0^2}{\left[ G - \frac{(A_0 - 1)}{R_1} \right]^2} \left( \frac{\omega_0}{\omega} - \frac{\omega}{\omega_0} \right)^2 + 1 \right\}} \quad \dots\dots(62)$$

Using the standard form

$$\int_0^\infty \frac{x}{(x-1/x)^2 a^2 + 1} = \frac{\pi}{2a}$$

where  $a$  is a constant, yields

$$\bar{V}_{in}^2 = \frac{(D+4kTG)}{4C \left[ G - \frac{(A_0 - 1)}{R_1} \right]} \quad \dots\dots(63)$$

The total noise output power  $P_{in}$  is proportional to  $\bar{V}_{in}^2$ , thus:

$$P_{in} = M \bar{V}_{in}^2 \quad \dots\dots(64)$$

This expression for noise holds if the detecting system used is of large bandwidth, so that almost all the noise is displayed at the output. If a narrow band detecting system is used the following simplification can be made. Let the detector bandwidth be  $H$  c/s, then the maximum value of  $\omega_1$  that need be considered is  $\omega_0 - 2\pi H$ , which is approximately equal to  $\omega_0$ . The following approximation may be made to eqn. (61):

$$\frac{(\omega_0^2 - \omega_1^2)^2}{\omega_1^2} \ll \frac{1}{C^2} \left[ G - \frac{(A_0 - 1)}{R_1} \right]^2 \quad \dots\dots(65)$$

This will be true over the comparatively flat portion at the top of the oscillator response curve. Thus  $\bar{V}_n^2$  becomes

$$\bar{V}_n^2 = \frac{(D+4kTG)df}{\left[ G - \frac{(A_0 - 1)}{R_1} \right]^2} \quad \dots\dots(66)$$

The noise power  $P_n$  obtained from a narrow frequency band close to the resonant frequency of the oscillator is given by

$$P_n = \frac{2MH(D+4kTG)}{\left[ G - \frac{(A_0 - 1)}{R_1} \right]^2} \quad \dots\dots(67)$$

The factor 2 appears in the numerator of eqn. (67) because the total oscillator bandwidth contributing to the noise output to the detector output is  $2H$ . Equation (67) holds when the frequency of conductance variation  $p$  is low and the detector bandwidth is narrow.

In order to derive the noise power for bandwidths not restricted to the top of the oscillator response curve, nor so large that all frequencies may be assumed to contribute to the output, it is necessary to integrate eqn. (61) between the limits  $f_0 - H$  and  $f_0 + H$ . Thus

$$P_n = \frac{M(D + 4kTG)}{2\pi C \left[ G - \frac{A_0 - 1}{R_1} \right]} \tan^{-1} \frac{4HC\pi}{\left[ G - \frac{A_0 - 1}{R_1} \right]} \dots\dots(68)$$

using the integral

$$\int_{x_1}^{x_2} \frac{dx}{x^2 + a^2} = \left[ \frac{1}{a} \tan^{-1} \frac{x}{a} \right]_{x_1}^{x_2}$$

This expression gives the noise power for any bandwidth likely to be used.

10.1 Factors which Determine the Noise Output

From a consideration of the expressions for noise power it is evident that the noise output will be reduced if the following conditions are observed:

- (1) Low valve currents and 'low-noise' components should be used in the amplifier section of the oscillator in order to reduce the term  $D$ .

- (2) The  $Q$  factor of the grid tuned circuit should be high so that less thermal-agitation noise is present.
- (3) The term  $[G - (A_0 - 1)/R_1]$  should be made large to reduce the sensitivity of the oscillator to disturbing forces. This condition is not simple to satisfy, because if  $G$  is to be small  $R_1$  must be large or it will introduce damping of the tuned circuit and increase  $G$ . Raising  $A_0$  will probably increase the noise generated in the amplifier section. Another important point is that increasing the term  $[G - A_0 - 1/R_1]$  has the effect of reducing the sensitivity of the oscillator to conductance changes.

10.2. Effect of the Non-linear Terms on the Noise

Because of the approximation made in eqn. (61) the non-linear terms  $A_1$  and  $A_2$  do not appear in the expressions for noise power. This means that the contributions to the noise output from noise voltages beating with one another and with the main output voltage are neglected. Without analysis of the beating effects it is obvious that they will be greater if the non-linear terms are large, thus the total noise output is reduced if the terms  $A_1$  and  $A_2$  are made small.

11. Measurement of Noise

Measurements were made of the detected demodulated noise output from the oscillator using the experimental set-up shown in block form in Fig. 12. Here v.v.m. indicates the valve voltmeters measuring the oscillator grid tuned circuit voltage  $V$  and the demodu-

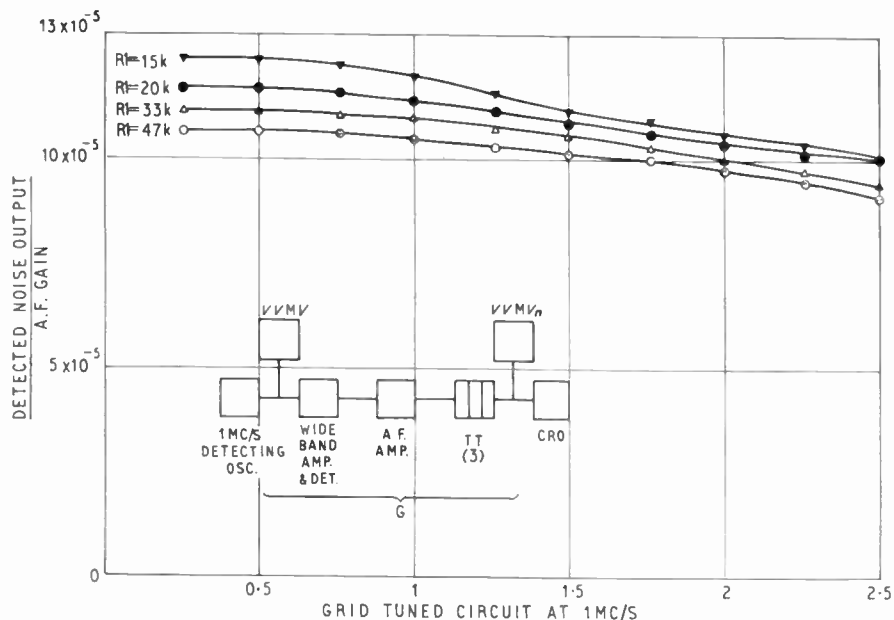


Fig. 12. Plot of oscillator noise output against grid. Tuned circuit voltage.

lated noise voltage  $V_n$ . Twin-T networks were used to attenuate the mains pick-up voltages in the demodulated noise.

The experimental results in Fig. 12 show that when  $V$  is raised the noise output is reduced because the value of  $Q$ , and hence the amplification of the noise generated in the oscillator, is lowered. The curves also show that, as predicted in eqn. (61), the noise is reduced if the value of the feedback resistor  $R_1$  is increased. This is because  $\beta$  is reduced, so reducing the noise currents fed back from the amplifier section of the oscillator to the grid tuned circuit.

### 12. Signal/Noise Ratio

Although the sensitivity of the oscillator to conductance changes may be increased, it is the signal/noise ratio which is important and must be made large in order to enable small conductance changes to be detected. The signal power  $P_s$  is proportional to the power in the sidebands and from eqn. (29) is given by

$$P_s = \frac{ME_0^2}{1+(yQ'')^2} \left( \frac{\delta G}{G''} \right)^2 \quad \dots\dots(69)$$

where  $M$  is a constant.

Thus the signal/noise power ratio becomes

$$\frac{S}{N} = \frac{P_s}{P_n} \quad \dots\dots(70)$$

$$\frac{S}{N} = \frac{M \cdot E_0^2}{P_n [1+(yQ'')^2]} \left( \frac{\delta G}{G''} \right)^2 \quad \dots\dots(71)$$

The value of  $P_n$  (or  $P_{in}$ ) is obtained from eqns. (64), (67) or (68) and depends upon the bandwidth of the detecting system employed. If a phase-sensitive detector and a low-frequency of conductance variation are employed, eqn. (67) gives the value of  $P_n$  required. For intermediate cases eqn. (68) is used.

### 13. Conclusions

The experimental results given in Section 6 show that the  $LC$  oscillator may profitably be treated as a special case of a variable circuit which can be analysed using the method developed by Carson.<sup>2</sup> Variations in conductance, inductance and capacitance may be treated in this way, which yields simple results capable of physical explanation, when the amplitude of the component variations is small.

Noise may also be accounted for in a fairly straightforward manner, provided that the beating effects which arise due to the presence of non-linear terms are neglected. Expressions for the signal/noise ratio appearing at the output from the detector can be obtained by combining the equations for sideband power and noise power over various bandwidths.

### 14. Acknowledgments

Thanks are due to Professor E. E. Zepler and Mr. S. W. Punnett of the University of Southampton, and Professor D. J. E. Ingram of the University of Keele for their valuable advice. Thanks are also due to Professor R. L. Russell of the University of Newcastle upon Tyne, for his interest.

### 15. References

1. D. J. E. Ingram, "Spectroscopy at Radio and Microwave Frequencies", p. 304 (Butterworth, London, 1955).
2. J. R. Carson, "Theory and calculations of variable electrical systems", *Physical Review*, 17, p. 116, 1921.
3. L. A. Pipes, "Four methods for the analysis of time-variable circuits", *Trans. Inst. Radio Engrs (Circuit Theory)*, CT-2, No. 1, p. 4, March 1955.
4. B. van der Pol, "The non-linear theory of electric oscillations", *Proc. Inst. Radio Engrs*, 22, p. 1051, 1934.
5. F. Bruin and J. M. Schimmel, "Theory of the autodyne detector for paramagnetic resonance", *Physica*, 21, No. 11, p. 867, 1955.
6. F. Bruin, "The autodyne as applied to paramagnetic resonance", *Advances in Electronics and Electron Physics*, 15, p. 327, 1961.
7. R. V. Pound and W. D. Knight, "A radio-frequency spectrograph and simple magnetic-field meter", *Rev. Sci. Instrum.*, 21, p. 219, March 1950.
8. G. D. Watkins, Ph.D. Thesis, Harvard University, 1952.
9. N. J. Hopkins, "A magnetic field-strength meter using the proton magnetic moment", *Rev. Sci. Instrum.*, 20, p. 401, June 1949.
10. W. J. Cunningham, "Amplitude variations in a frequency-modulated oscillator", *J. Franklin Inst.*, 256, No. 4, p. 311, 1953.
11. A. Roberts, "Two new methods for detecting nuclear radio-frequency resonance absorption", *Rev. Sci. Instrum.*, 18, p. 845, November 1947.
12. A. van der Ziel, "Noise", p. 283 (Chapman and Hall, London, 1955).
13. S. W. Punnett, "Audio-frequency selective amplifiers", *J. Brit.I.R.E.*, 10, p. 39, February 1950.
14. G. Valley and H. Wallman, "Vacuum Tube Amplifiers", p. 384 (McGraw-Hill, New York, 1948).
15. I. A. Greenwood, "Electronic Instruments", ed. J. Holdam and D. Macrae, p. 383 (McGraw-Hill, New York, 1948).
16. "Royal Signals Handbook of Line Communication", p. 520 (H.M.S.O. 1947).
17. F. E. Terman, "Radio Engineers' Handbook", p. 918 (McGraw-Hill, New York, 1943).
18. A. G. J. Holt, "An investigation of methods for the detection of small periodic changes in circuit conductance", Ph.D. Thesis, University of Southampton, 1959.

### 16. Appendix 1

#### The Test Apparatus

The general testing apparatus is shown in block form in Fig. 13. It consists of the following items:

- (1) Amplifiers (wideband and selective),

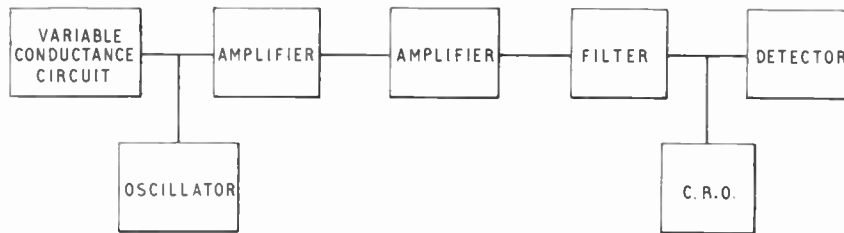


Fig. 13. Block diagram of test apparatus.

- (2) Display system (cathode-ray oscillograph and phase-sensitive detector),
- (3) Variable conductance circuit,
- (4) Filters,
- (5) Power supplies.

The amplifiers and phase-sensitive detector are of conventional design and will not be discussed here. Helpful references to the design of low-frequency selective amplifiers are Punnett<sup>13</sup> and Valley and Wallman.<sup>14</sup> Phase-sensitive detectors are discussed by Greenwood.<sup>15</sup> Reference 16 is also helpful on this subject.

The variable conductance used was very similar to that employed by Watkins.<sup>8</sup> A curve showing the variation of conductance with applied voltage for the circuit is given in Fig. 14.

Twin-T filters, designed from equations given by Terman,<sup>17</sup> were used in order to attenuate the pick-up from the mains frequency and its harmonics which appeared at the amplifier outputs. In service the filter was the last stage before the oscillograph and attenuated the 50 c/s pick-up by 30 dB.

The stabilized power supply was capable of delivering 100 mA at 300 V to the load. Stabilization

was carried out by a series-valve regulator using a 12E1 beam-tetrode as the series valve. Further details of the apparatus are given in Reference 18.

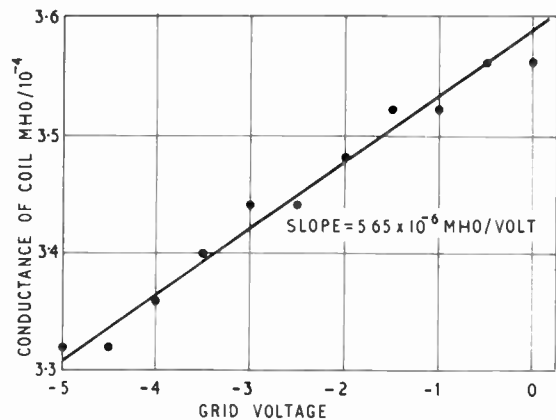


Fig. 14. Variation of conductance with applied voltage.

Manuscript first received by the Institution on 6th March 1963 and in final form on 11th July 1963. (Paper No. 883.)

© The British Institution of Radio Engineers 1964

# The Prediction of the Optimum Noise Performance of a Reflection Cavity Maser

By

C. R. DITCHFIELD†

Presented at the Symposium on "Masers and Lasers" in London on 2nd January 1963.

**Summary:** Maser performance depends on the microwave circuit, on the total concentration of paramagnetic centres in the energy states used in the crystal and on the degree of inversion of population differences which can be obtained by pumping. At any temperature there will be an optimum concentration for maximum performance and to determine this optimum a knowledge is needed of certain parameters. Although some of these are difficult to measure directly a method is suggested which enables an adequate determination to be made.

## List of Symbols

$B$	Amplifying bandwidth of the maser.
$\beta_a$	Ratio $Q_u/Q_a$
$\beta_m$	Ratio $Q_u/Q_m$
$\beta_1$	Ratio $Q_u/Q_1$
$G$	Power gain of the maser.
$I$	Inversion ratio of the maser crystal.
$N_0$	Concentration of paramagnetic centres in the maser crystal.
$\nu_s$	Signal frequency.
$\Delta\nu$	Absorption line-width of the maser crystal.
$Q_a$	Absorptive $Q$ factor of the maser crystal.
$Q_m$	Emissive $Q$ factor of the maser crystal.
$Q_u$	Unloaded $Q$ factor of the cavity.
$Q_1$	Input coupling $Q$ factor of the cavity.
$\rho$	Voltage reflection coefficient of the cavity off magnetic resonance.
$\rho'$	Voltage reflection coefficient of the cavity on magnetic resonance (absorptive).
$T_e$	Ambient cavity temperature.
$T_e$	Input noise temperature of the maser at the low temperature terminals.
$T_m$	Spin temperature of the maser crystal.
$x$	Power transmission coefficient of the input guides.

## 1. Introduction

The input noise temperature of a maser  $T_e$  at its low-temperature terminals, consists of two components, one due to the spin temperature of the paramagnetic crystal and one due to thermal emission from the cavity walls or travelling wave structure. In a maser at helium temperature these contributions tend to be masked by a larger amount of noise from the input line between the room-temperature and the low-temperature terminals. This has made it difficult to confirm precisely by experiment the predictions of

theory, but the possibility of maser amplification at higher temperatures<sup>1</sup> such as 77°K (liquid nitrogen) decreases these difficulties because of the larger noise contribution of the maser at its low-temperature terminals.

Nevertheless the usual expression for  $T_e$  involves parameters which are not easily measurable separately, so that it is difficult to be certain of the value of input noise temperature to be expected at the low-temperature terminals. Any direct measurement of noise performance gives only the value at the room-temperature input. In the following sections  $T_e$ , for a reflection cavity maser, is expressed in an alternative fashion involving more easily measurable parameters. A series of experiments, illustrated by a hypothetical example, is suggested to give information regarding the inversion ratio, spin temperature and magnetic  $Q$  for any degree of pumping. This is of particular importance in deciding the optimum concentration of paramagnetic ions to use in the maser.

## 2. The Noise Temperature of a Reflection Cavity Maser

After allowance has been made for the noise contributions of the following stage and the input loss, the input noise temperature  $T_e$  of a reflection cavity maser is usually expressed in terms of the power gain,  $G$ , the cavity temperature,  $T_c$ , the spin temperature,  $T_m$  and the emissive  $Q$  factor,  $Q_m$ , of the crystal as<sup>2-4</sup>

$$T_e = \left[ 1 - \frac{1}{G} \right] \left[ \frac{T_c}{|\beta_m| - 1} + \frac{|T_m|}{1 - |\beta_m|} \right] \dots\dots(1)$$

For a high temperature maser, in which the magnetic  $Q$  of the crystal is high compared with the  $Q$  of the paramagnetic absorption line,  $|\beta_m| = \frac{Q_u}{|Q_m|}$  where  $Q_u$  is the unloaded  $Q$  of the cavity. Unfortunately  $|T_m|$

† Royal Radar Establishment, Great Malvern, Worcestershire.

and  $|\beta_m|$  cannot be measured directly and consequently eqn. (1) cannot be checked easily against a measured value of maser noise temperature.

However eqn. (1) may be rewritten using the following relationships:

$$\text{Inversion ratio } I = \frac{Q_a}{|Q_m|} = \frac{|\beta_m|}{\beta_a} = \frac{T_c}{|T_m|} \dots\dots(2)$$

$$\text{and } |\beta_m| - 1 = \beta_1 \frac{\sqrt{G-1}}{\sqrt{G+1}} \dots\dots(3)$$

where  $\beta_1 = \frac{Q_u}{Q_1}$  and  $Q_1$  is the input coupling  $Q$  factor.

$Q_a$  and  $\beta_a$  refer to the crystal in the absorptive state under conditions of thermal equilibrium. We now obtain

$$T_e = \left[ 1 + \frac{1}{\sqrt{G}} \right]^2 \left[ \frac{1 + \beta_a}{\beta_1} \right] T_c \dots\dots(4)$$

This equation has the advantage that it is expressed in terms of  $T_c$  and  $G$ , which are easily measurable, and  $\beta_a$  and  $\beta_1$  which can be expressed in terms of the reflection coefficients of the cavity-crystal combination in thermal equilibrium. Indeed the middle term simplifies still further because the voltage reflection coefficient of the cavity,  $\rho'$ , with the crystal on magnetic resonance in its absorptive state is given by

$$\rho' = \frac{\beta_1 - (\beta_a + 1)}{\beta_1 + (\beta_a + 1)}$$

$$\text{or } \frac{\beta_a + 1}{\beta_1} = \frac{1 - \rho'}{1 + \rho'} \dots\dots(5)$$

It should be noted that if the cavity is under-coupled  $\beta_1 < (\beta_a + 1)$  and  $\rho'$  is negative, whereas  $\rho'$  is positive for an over-coupled cavity. The algebraic sign of  $\rho'$  must be maintained, therefore, in the following expression. Combining eqns. (4) and (5) we obtain:

$$T_e = \left[ 1 + \frac{1}{\sqrt{G}} \right]^2 \left[ \frac{1 - \rho'}{1 + \rho'} \right] T_c \dots\dots(6)$$

The quantities  $G$ ,  $\rho'$  and  $T_c$  are very easily measurable and thus the original difficulty of comparing theoretically predicted and experimentally obtained values of input noise temperature has been removed.

Moreover if the pump power is decreased until the transition is no longer saturated this will change the inversion ratio and consequently the gain and input noise temperature. A linear graph may be plotted of

$T_e$  against  $\left[ 1 + \frac{1}{\sqrt{G}} \right]^2$  to give an intersection on the

ordinate of  $\left[ \frac{1 - \rho'}{1 + \rho'} \right] T_c$  when  $G$  is infinite (Fig. 1). Any

difference between the measured noise temperature extrapolated to infinite gain and the value of

$\left[ \frac{1 - \rho'}{1 + \rho'} \right] T_c$  gives a measure of the degradation of performance due to input loss. Furthermore having measured the reflection coefficient  $\rho$ , of the cavity off magnetic resonance and the amplifying bandwidth  $B$  of the maser one can deduce from the graph the values of  $Q_u$ ,  $Q_1$ ,  $Q_a$ ,  $I$ ,  $Q_m$  and  $T_m$  for any degree of pumping, whereas these quantities are usually very difficult to measure directly. The method may be clarified by consideration of a hypothetical example.

### 3. Hypothetical Experimental Data

Consider a cavity maser operating at  $T_c = 77^\circ\text{K}$ , which, at a signal frequency of 9 Gc/s, gives a gain of 24.6dB ( $\sqrt{G} = 17$ ) and a bandwidth of 1 Mc/s. In the absorptive state reflection coefficients are measured to be  $\rho' = \frac{1}{3}$  and  $\rho = \frac{2}{3}$ . A noise measurement at the high temperature terminals gives a value of  $96^\circ\text{K}$ .

To obtain the input noise temperature and an estimate of input loss we proceed as follows: From eqn. (6) we obtain

$$T_e = \left[ 1 + \frac{1}{17} \right]^2 \times \frac{7}{9} \times 77 = 67^\circ\text{K}$$

If the noise temperature of the following stage is  $2890^\circ\text{K}$ , this is reduced by the gain of the maser to a contribution of  $10^\circ\text{K}$  at the input terminals of the

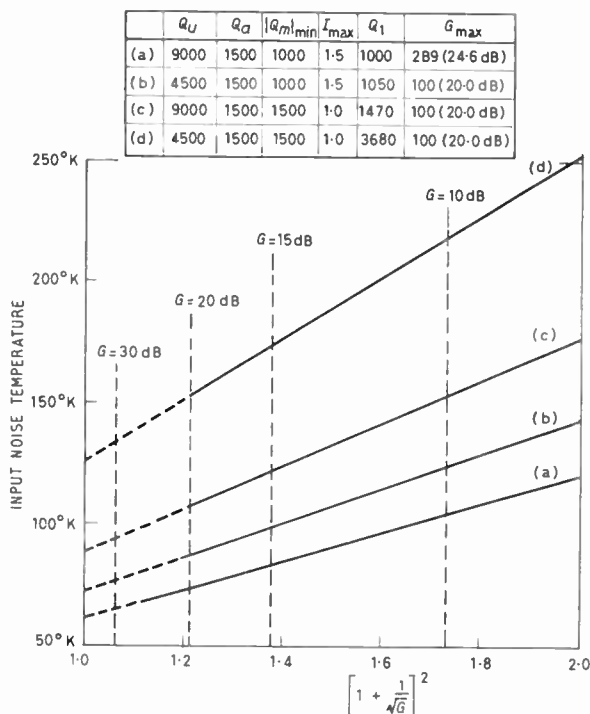


Fig. 1. Variation of maser noise temperature with gain for four hypothetical masers.

maser, giving a total of 77° K. The further degradation, 96–77 = 19° K may be ascribed to the input loss and its noise contribution. Writing  $x$  for the power transmission coefficient of the input loss and assuming it to be at room temperature (which is a fair approximation as most of the loss will be in the circulator) we have

$$96 = \left(\frac{1-x}{x}\right) 290 + \frac{77}{x}$$

Hence  $x = 0.95$  or a 0.22dB loss. This value can be checked against a direct measurement of circulator insertion loss.

To obtain the value of the unloaded cavity  $Q$ , the input coupling  $Q$  and the absorptive  $Q$  of the sample we have

$$\beta_1 = \frac{1+\rho}{1-\rho} = 9$$

Therefore

$$Q_u = \frac{2\beta_1 v_s}{(\sqrt{G+1})B} = \frac{2 \times 9 \times 9000}{18 \times 1} = 9000$$

$$Q_1 = \frac{Q_u}{\beta_1} = 1000$$

$$\beta_a + 1 = \beta_1 \frac{1-\rho'}{1+\rho'} = 9 \times \frac{7}{9} = 7$$

Therefore

$$Q_a = \frac{Q_u}{\beta_a} = 1500$$

Finally we derive the magnetic  $Q$  in the emissive state and the spin temperature of the crystal.

$$|\beta_m| - 1 = \left[ \frac{\sqrt{G-1}}{\sqrt{G+1}} \right] \beta_1 = \frac{16}{18} \times 9 = 8$$

$$|\beta_m| = 9$$

$$|Q_m| = \frac{Q_u}{|\beta_m|} = 1000$$

Therefore  $I = \frac{1500}{1000} = 1.5$

$$|T_m| = \frac{T_c}{I} = \frac{77}{1.5} = 51^\circ \text{ K}$$

It is instructive to refer these values of  $|\beta_m|$  and  $|T_m|$  to eqn. (1) in order to demonstrate the relative contributions to the input noise temperature which arise from the cavity walls and the sample respectively.

$$\begin{aligned} T_e &= \left[ 1 - \frac{1}{289} \right] \left[ \frac{77}{8} + \frac{51}{9} \right] \\ &= \frac{288}{289} [9.6 + 5.7] \\ &= 67^\circ \text{ K} \end{aligned}$$

#### 4. The Significance of the Derived Results

##### 4.1. Input Insertion Loss

The insertion loss of the input circulator may be measured directly and the loss of the input guide between the circulator and the cavity may be computed from a measurement of v.s.w.r. just off cavity resonance. The loss itself will degrade the receiver performance but, in addition, there will be a thermal noise contribution dependent on the loss and its temperature. The temperature will vary along the input guide but a fair correlation may be expected between an estimated noise contribution calculated from the insertion loss data and the value obtained as in Section 2.

##### 4.2. Unloaded Cavity $Q$

Using a swept oscillator and frequency markers the unloaded cavity  $Q$  may be measured when the cavity is very undercoupled but this  $Q$  value is not necessarily the one relevant to the maser cavity in the amplifying condition, when it is heavily overcoupled. The large coupling slots may affect the current flow in the cavity walls to an extent sufficient to change the  $Q$  appreciably. In this event  $Q_u$  can be obtained only by the method of Section 2 and comparison of this value with the value obtained with light coupling enables the coupling design to be optimized. The value of  $Q_a$  depends on an accurate value of  $Q_u$ .

##### 4.3. The Absorptive and Emissive $Q$ Factors of the Crystal

If  $Q_u$  is known  $Q_a$  can be calculated as in Section 2. It should be compared with the value predicted from the paramagnetic properties of the crystal. Under conditions of thermal equilibrium the absorptive  $Q$  factor of the ruby depends on the temperature, the concentration of paramagnetic ions and the line width as follows:

$$Q_a = K T_c \left[ \frac{\Delta\nu}{N_0} \right]$$

where  $K$  has a value of about  $9 \times 10^{18}$  for ruby at a signal frequency of 9 Gc/s. Thus if  $T_c = 77^\circ$ ,

$$Q_a = 7 \times 10^{20} \left[ \frac{\Delta\nu}{N_0} \right]$$

with  $\Delta\nu$  expressed in Mc/s and  $N_0$  as the concentration of chromium ions per cubic centimetre.

$\left( \frac{\Delta\nu}{N_0} \right)$  decreases to an asymptotic minimum as the concentration is increased but the minimum value of  $Q_a$  does not necessarily give the minimum value of  $|Q_m|$ , which is the important parameter for maser action. This is because cross-relaxation effects between various transition frequencies of the crystal can

decrease the inversion ratio, the effect becoming more pronounced at higher concentrations.

$Q_a$ ,  $Q_m$  and  $I$  are not obtainable easily for the maser crystal except by the method outlined in Section 2. They could be measured on a small spectrometer sample, but there may be some difficulty in correlation with the maser crystal due to a lack of homogeneity in the larger ruby crystal used in the maser.

#### 4.4. Crystal Spin Temperature

To measure the input noise temperature demands experimental techniques of a high order using preferably thermal sources at known temperatures rather than indirectly calibrated noise lamps. Particular care must be given to minimizing insertion losses in the maser system and calibration apparatus and to obtain precise values of any losses present. Thus it is somewhat difficult to obtain the spin temperature with precision from the measured input noise temperature whereas it may be calculated directly from the ratio of cavity temperature divided by inversion ratio.

#### 4.5. Overall Performance

It is worth pointing out that the gain bandwidth product of the maser

$$B(\sqrt{G}-1) = 2\nu_s \left[ \frac{1}{Q_m} - \frac{1}{Q_u} \right]$$

is not a good guide to optimum performance because a lower value of inversion ratio, as cross relaxation sets in, is offset to some extent by a lower value of  $Q_a$  so that  $|Q_m|$  does not increase too rapidly at

concentrations above the optimum. Therefore a knowledge of  $|T_m|$ , which is dependent directly on  $I$ , enables one to arrive at the optimum concentration more readily. The inversion ratio may also suffer as a result of too low a pump power and similar considerations obviously apply.

### 5. Conclusions

The experimental procedure outlined enables values to be obtained for the parameters of the cavity maser system which are difficult or even impossible to obtain otherwise. A knowledge of these parameters is particularly valuable in the design stage of the maser to enable correct decisions to be made on cavity design, optimum chromium concentration and pump power requirements. Similar considerations would apply to a travelling wave maser system but at present such an amplifier has not been constructed at these relatively high temperatures.

### 6. References

1. C. R. Ditchfield and P. A. Forrester, "Maser action in the region of 60°K", *Phys. Rev. Letters*, 1, p. 12, 1958.
2. C. R. Ditchfield, "Noise in quantum mechanical amplifiers", "Low Noise Receiver Symposium". Lincoln Laboratories, M.I.T., 1960.
3. A. E. Siegman, "Thermal noise in microwave systems", *Microwave Journal*, 4, No. 4, p. 66, April 1961.
4. T. H. Maiman, "Temperature and concentration effects in a ruby maser", "Quantum Electronics", p. 324, (Columbia University Press 1960).

*Manuscript first received by the Institution on 12th December 1962 and in final form on 16th October 1963 (Paper No. 884).*

© The British Institution of Radio Engineers, 1964

## DISCUSSION

**Mr. W. D. Worthy:** Would Mr. Ditchfield amplify his remarks on the factors influencing line-width and  $Q$  factors. Could he give some explanation of the various mechanisms involved and their relative importance?

**The Author (in reply):** Cross-relaxation is a process whereby spin energy may be interchanged between the ions of the crystal even though the transitions involved in the spin flips are not exactly equal nor exactly related by a simple ratio. The effect is appreciable even if the transitions differ in frequency by more than ten line-widths and thus the possibility of cross-relaxation limits the concentration of paramagnetic ions which can be used. If the concentration (and hence line-width) is too great the energy is exchanged so rapidly that the signal transition is not inverted, the net result being simply an equalizing of population in all levels. Thus at 4°K the upper concentra-

tion useful in ruby is about 0.05% chromium whereas at 77°K about 0.2% may be used. Dr. Maiman discusses the effect in more detail<sup>4</sup>, but the main point is that an increase of concentration and line-width may lead to a lower value of absorptive  $Q$  but, if the inversion ratio suffers, the emissive  $Q$  may be high or even infinite. In a practical crystal there are many causes of line-width due to both homogeneous and inhomogeneous broadening. In the theory of paramagnetic resonance homogeneous broadening is associated with coupling between nearby spins, somewhat analogous to light coupling between adjacent tuned circuits. This process is characterized by a spin-spin relaxation time  $T_2$  and a line-width of  $1/\pi T_2$ . Any defects in the crystal lattice, e.g. wander of the crystallographic axes, strain etc., can lead to further broadening. A full answer to this aspect of the question is not possible in a short space.

# The Performance and the Flux Patterns of a Special Shape Multi-aperture Device

By

D. J. MORRIS, Dip. Eng., M.Sc.,  
(Associate Member)†

**Summary:** This paper describes a special-shaped multi-aperture device which can perform the operation of a circuit element equivalent to a two-input AND gate. One interesting feature of this device is that it may be interrogated non-destructively. Although this shape basically performs the AND function, it is possible for it to perform a wider range of logical operations, such as OR-AND, negation, exclusive-OR, etc. Furthermore, by combining different switching paths within the component, a single device may perform the operation of a half-adder. This multi-aperture device may be used in all-magnetic logical systems, where the connection between this device and others can be of wire only. However, this feature applies only when it functions as an AND gate. Various flux switching paths within the device are described and it is demonstrated that the guidance of the switching flux into particular paths leads to a variety of logical operations.

## List of Principal Symbols

$A, B$	input signals
$F$	magnetomotive force
$F_c$	threshold m.m.f.
$H$	magnetic field intensity
$H_c$	coercive force
$l$	increment of the switching path length
$L$	length of a switching path
$N$	number of turns
$r$	radius of an aperture

## 1. Introduction

Multi-aperture devices have many attractive features as switching elements for digital computers. They combine the performance of a circuit element which is equivalent to a switch with the storage function. The same attractive features of the multi-aperture devices for logical operations were found also with ferrite toroidal cores. However, ferrite cores are limited in the number of logical operations which may be performed by a single core and, furthermore, they require driving currents of very close tolerances. The multi-aperture device can provide isolation of the output load from the input circuit and thus broaden the logical application of each device. The tolerances of the driving currents applied to the multi-aperture devices are much wider, compared with ferrite cores, due to the isolation of the output from the input. This latter feature allows non-destructive reading of the information stored in the devices.

In multi-aperture devices the flux may switch round

† English Electric-Leo Computers Limited, Kidsgrove, Staffordshire.

a number of switching paths, whereas in ferrite toroidal cores the flux can switch along only one path which is round its single aperture. This feature enables the employment of multi-aperture devices in circuits having more flexibility in performing a wider range of logical operations which are too complex for ferrite cores.

The multi-aperture devices are made of the same material as the ferrite toroidal cores, which is characterized by the approximate rectangular hysteresis loops and its two well-defined remanent states of magnetization. A core may be brought to a state of positive or negative magnetic remanence by feeding a current pulse in a winding round the core. The two states of magnetization found in ferrite toroidal cores are used for storing the binary information '1' and '0'. This principle is also observed in multi-aperture devices, but here, however, the realization of the binary '1' or '0' is dependent on only part of the device being in the positive or the negative state of magnetization.

The description given in this paper of the logical magnetic element is the outcome of an investigation into the performance and operation of the special-shaped multi-aperture device. In this paper a theory is developed of the flux patterns in the device which is based on the observed behaviour of the device.

In analysing the performance of this device a theory of the flux switching patterns was propounded which was then correlated by the initial investigation. However, a more refined analysis revealed that the initial predicted behaviour of the device was false. This led to a further investigation into the switching mechanism of this device and a new theory of the flux switching patterns was formed. This new

approach enables the broadening of the application of the device from its basic AND function to perform more complex logic, for example exclusive-OR function and furthermore a half-adder function.

It is intended first to describe the initial theory of the flux patterns in the device and then develop the new theory which is based on experimental verifications.

Experience with these multi-aperture magnetic circuits is still limited, and many results may be misleading, thus it is too early to permit detailed statements. The switching phenomena of the multi-aperture devices are more complex than anticipated and a lot of their behaviour is not yet completely understood. More questions can be posed than can be fully answered.

The purpose of this paper is to attempt to bring new light on the switching properties of a complex-shaped multi-aperture device. The interesting aspect of the selection of one flux switching path rather than another may assist in understanding the switching behaviour of multi-aperture devices. Some features of the special-shaped device given in the paper are considered by two different hypotheses in anticipation of future criticism and to stimulate a discussion on flux patterns and switching.

There are two methods of approach when writing a paper on these flux patterns; the first of these is to describe only the final flux patterns with conclusions. The second method, which was the one chosen, is to describe the initial flux patterns, and with the aid of the initial conclusions build up a more refined analysis. Although the method chosen is somewhat unconventional, it was felt that this approach was more likely to stimulate interest and discussion on the subject.

In order to simplify the flux patterns in the multi-aperture device, an arrow model is used, where the arrowhead represents the direction of magnetization. The actual flux patterns are considerably more complicated but nevertheless the arrow model is convenient in explaining the switching properties of the multi-aperture device.

## 2. General Description of the Device

The special configuration of the multi-aperture device has three large apertures (which will be designated a, b and c) evenly spaced round a central minor aperture (designated d). The wiring diagram used for the initial investigation, is illustrated in Fig. 1. In order to demonstrate the shape and size of this multi-aperture device, it is pictured in Fig. 2.†

† The device was manufactured by Siemens & Halske and is type 9ZL entw1088 T8.

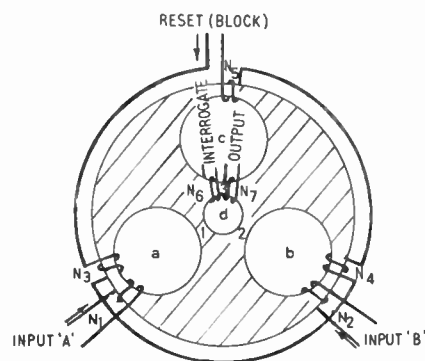


Fig. 1. Wiring diagram of the multi-aperture device.

The geometrical structure is important and must be borne in mind when considering the device. The material between the centre minor aperture and each of the three large apertures forms three distinct legs 1, 2 and 3. The minimum cross-sectional area of each of these three legs must be equal. Also, the minimum cross-sectional area of the legs must be equal to the minimum cross-sectional area of the outer leg of each of the larger apertures. Another structural requirement is that the minimum cross-sectional area of the material between two large apertures must be equal to, or greater than, twice the minimum cross-sectional area of each of legs 1, 2 and 3. Also, the diameter ratio of the large and small apertures should be as large as practicable. The bulk geometry of the rest of the device may vary between wide limits.

With this geometry of the device it is possible to control the amount of material switched along each path. The total cross-sectional area of a switching path is constant and equal to the minimum cross-sectional area of the material which can be switched, which is perpendicular to the applied m.m.f. As the flux distribution must be continuous within the

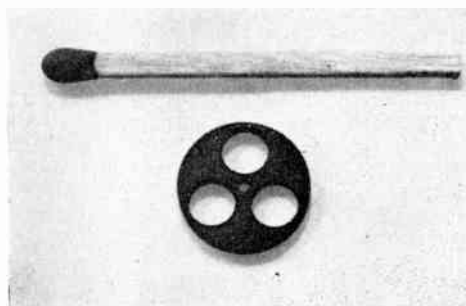


Fig. 2. Photograph of the multi-aperture device.

material and since the cross-sectional area of the material is not constant round the apertures, there will be regions in the device of local flux closures. These local flux closures will have little effect on the operation of the device, since the function of the device is dependent mainly on the flux patterns of the three legs round the centre minor aperture.

A reset winding is threaded through all the three large apertures a, b and c, thus passing round the outer legs of these apertures, while the input windings are only threaded through two of the large apertures a and b. The 'interrogate' and the output windings are threaded round leg 3 of the centre minor aperture d.

### 3. Basic Operation

The operation is best described with the aid of the flux patterns of the device in different modes as shown in Fig. 3. A 0 is said to be stored in the device

direction of the induced field. In this condition of the device, the flux in legs 1 and 2 is saturated in an opposite direction to that of leg 3 in relation to a path round the minor aperture and thus no switching can take place. A positive 'interrogate' pulse will only tend to drive legs 1 and 2 further into saturation and a negative 'interrogate' pulse will drive leg 3 further into saturation. The device in this condition is said to be 'blocked' as no flux changes may occur round the minor aperture and thus no output voltage will be induced in the output winding ( $N_7$ ).

An input m.m.f. caused by a current pulse applied to winding  $N_1$  of large aperture a, when the device is in its blocked condition, will switch the flux round this aperture in a clockwise direction, as shown in Fig. 3(b). The interrogate field, induced by the alternating-current pulses applied to winding  $N_6$ , will still be unable to switch the flux round the minor aperture, as now the flux directions in legs 1 and 3

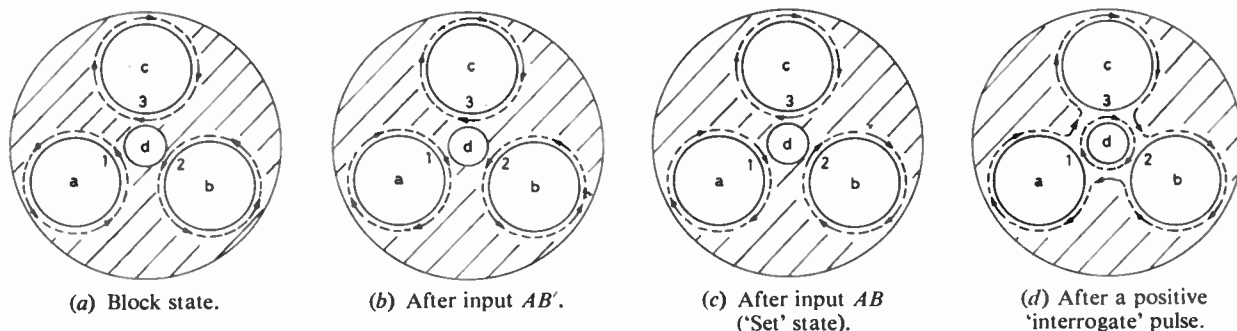


Fig. 3. Flux patterns in different modes of operation.

when it is in its 'blocked' state and a 1 is said to be stored when it is in the 'set' state. The 1 state represents an input logic combination of AB. Two clock pulses must be used for each cycle of logic operation, the reset clock pulse which switches the device into its 'blocked' state and an input clock pulse which may switch it into its 'set' state.

The reset field, which is induced by an m.m.f. caused by a current pulse in the reset windings  $N_3$ ,  $N_4$  and  $N_5$ , will switch the flux round the three large apertures to an initial flux pattern. When the reset field is removed, the flux pattern will be in a clockwise direction round aperture c and in a counter-clockwise direction around the input apertures a and b, as shown in Fig. 3(a). In this initial flux pattern of the device, the interrogating-alternating current pulses applied in winding  $N_6$  (which is on leg 3 of the minor centre aperture d), will not be able to switch any flux round the minor aperture. In any closed path, it is impossible to reverse the direction of the flux around the path, if any part of the path is already saturated in the

will be saturated in an opposite direction to that of leg 2. An input pulse applied in winding  $N_2$  of the large aperture b (provided no current pulse is applied to winding  $N_1$  of the large aperture a) will produce similar results. The 'interrogate' field will still be unable to switch the flux round the minor aperture, as in this case the flux in legs 2 and 3 will be saturated in an opposite direction to that of leg 1.

Only when current pulses are applied both to winding  $N_1$  of the large aperture a and to winding  $N_2$  of the large aperture b, will the interrogate field be able to switch the flux round the minor aperture. The two induced input fields will reverse the flux round both large apertures a and b, and switch them in a clockwise direction, as shown in Fig. 3(c). Since the flux in legs 1, 2 and 3 is all saturated in the same direction (in a counter-clockwise direction round the minor aperture), the interrogate field will be able to switch the flux round the minor aperture. The first positive 'interrogate' pulse will switch the flux in a clockwise direction and the first negative 'interro-

gate' pulse will switch it back again, and so on indefinitely. Each time the flux is reversed round the minor aperture, an output-voltage pulse will be induced in the output winding  $N_7$ . The device in this condition is called 'set' or unblocked.

Flux continuity must be preserved, and thus the flux lines must be closed on themselves. After the two input fields are removed, the interrogate field switches the flux round the minor aperture which will break the continuity of the flux round the larger apertures. Hence, extra reorientations of the domains must take place round the boundary of the three large apertures, as shown in Fig. 3(d).

This device may be regarded as a two-input AND gate having the two input signals  $A$  and  $B$  as the fields induced in windings  $N_1$  and  $N_2$ . This gate can store indefinitely this input information ( $AB$ ) and then allow it to be read out non-destructively.

#### 4. Non-Destructive Read-out

The non-destructive read-out is achieved by switching the flux round the minor aperture  $d$  by the 'interrogate' field which is generated by alternating positive and negative m.m.f. pulses. The minor aperture is continuously interrogated, thus giving output voltage pulses only after both inputs  $A$  and  $B$  have been applied, and no output if one or no input had been applied.

Similar to the ferrite cores, the signal/noise ratio of the output pulses will depend on the squareness of the hysteresis loop. However, as will be seen later, there are other factors appertaining to this device, the effect of which could reduce the signal/noise ratio. In multi-aperture devices the signal output occurs when the device is in its 'set' state and the noise output occurs when it is in its 'block' state.

It has been explained before that the interrogate field, when the device is in its 'block' state (Fig. 3(a)), cannot switch the flux round the minor aperture, since all the flux round the minor aperture is not saturated in the same direction. However, the flux round large aperture  $c$  is saturated in the same direction. Thus a large 'interrogate' field, induced in leg 3 which is also round the large aperture  $c$ , may tend to switch the flux round the large aperture when the device is in its block state. In other words, the 'interrogate' m.m.f. must be restricted to be larger than the threshold field required to switch the flux round the centre aperture but smaller than the threshold field required round the larger aperture. The threshold field ( $F_c$ ) is the line integral of the coercive force of the material ( $H_c$ ) along its shortest available switching path,  $F_c = \oint H_c dl$ . The shortest available switching path, in both cases, is a function of the diameters of the apertures,  $L_{min} = 2\pi r$ . Thus,

the range of the interrogate field will depend on the ratio of diameters of the large and minor apertures; the higher the ratio the wider the range.

When the device is in its set state there is no danger that a large 'interrogate' field will switch the flux round the large aperture. The flux always tends to switch round its shortest available switching path, thus when the device is set, it will switch round the centre minor aperture. When the device is set, any increase of the interrogate field, above its required switching magnitude will not change its switching path but only its switching time. This point, however, has no practical importance. In practical circuits, a large 'interrogate' field will result in large 'noise' output pulses which would consequently reduce the signal/noise ratio.

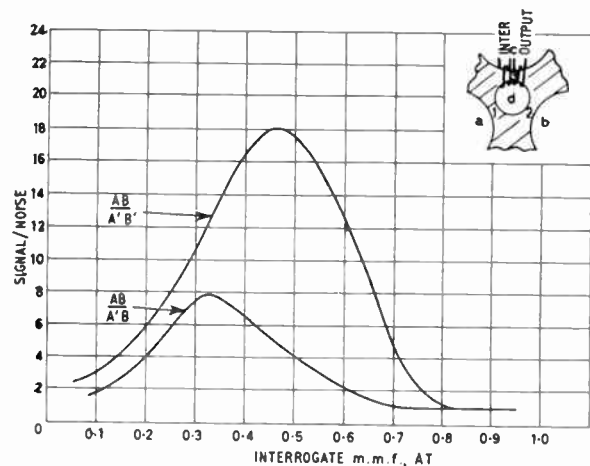


Fig. 4. Signal/noise ratio of the non-destructive read-out pulses.

Figure 4 shows the signal/noise ratio of the output pulses as a function of the 'interrogate' m.m.f., where the signal is the output after both inputs have been applied ( $AB$ ) and the noise is the output when no input has been applied ( $A'B'$ ). The signal/noise ratio increases with the increase of the 'interrogate' m.m.f., till it reaches a peak. Then, with further increase of the 'interrogate' m.m.f., the signal/noise ratio starts to decrease till it reaches the value of unity. The peak of the signal/noise curve corresponds to the threshold field of the large aperture  $c$ , thus any increase of the 'interrogate' m.m.f. above the peak point, will switch the flux round the large aperture.

The results given in Fig. 4 show that this device could be operated with very wide tolerances and giving reasonably high signal/noise ratio of about 18/1 (the upper curve). This encouraging result may be misleading, as it only shows the extreme conditions. In practice it was found that the worst noise output

pulses are not obtained for the blocked condition (input combination  $A'B'$ ), but when it is partially set, that is, for the input combination of one of the two inputs ( $AB'$  or  $A'B$ ). The signal/noise ratio of this condition is also given in Fig. 4 by the lower curve. The result now is much less than the previous result, by nearly a third, as now it is down to 7.5/1. The reason for these 'poor' results is that in the case of  $A'B'$  the device is fully blocked but in the case of  $A'B$  or  $AB'$  the device is partially set. The direction of the flux in leg 3 (where the 'interrogate' m.m.f. is applied), in the case of  $A'B'$  (Fig. 4, upper curve), is opposite to that of legs 1 and 2, while in the case of  $AB'$  (Fig. 4, lower curve), the flux in leg 3 is in an opposite direction only to leg 2. This will allow some exchange of flux round the minor aperture which will reduce the signal/noise ratio.

The signal/noise ratio may be improved by having a different wiring pattern, round the minor aperture, of the 'interrogate' and output windings. It was shown that the danger of unwanted switching occurs when the field induced in leg 3 is large enough to switch round the large aperture, when it is in its blocked state. By reducing the field induced in leg 3, this danger will also be reduced. This can be made possible by sharing the interrogate winding equally between the three legs (1, 2 and 3), hence causing the effective field induced in leg 3 to be reduced by a factor of three, whilst the effective field round the minor aperture, i.e. the additive of the three fields induced in the three legs, will be of the same magnitude as before. Furthermore, by sharing the output winding between the three legs, the noise output is further reduced, since the noise is due mainly to the unwanted flux changes in leg 3. The results obtained from the device, with the modified wiring pattern of the windings round the minor aperture, are given in Fig. 5. The peak signal/noise ratio in its worst operating conditions, has risen now to 15/1 (the lower curve).

Although the results of the signal/noise ratio for the blocked state have no practical value, they are interesting theoretically. A comparison of the curves of  $AB/A'B'$  for the new wiring pattern (Fig. 5, upper curve) with the previous results (Fig. 4, upper curve) shows that now a much higher signal/noise ratio has been achieved, the peak of the curve is less pronounced, and the range of the curve is far wider. The reason for this is that, due to the new wiring pattern, the field induced in leg 3 has been reduced by a factor of three as it is now equally shared by legs 1, 2 and 3. Thus the danger of the 'interrogate' field switching round the larger aperture c, during the blocked state, has been reduced by a factor of three. This would also result in the widening of the 'interrogate' field range.

The signal/noise ratio of the output pulses may be improved by decreasing the frequency of the alternating-interrogate field. For the curves presented in Figs. 4 and 5, 50 kc/s alternating pulses were used. The signal/noise ratio may be further improved by using sine waves instead of alternating pulses. However, taking advantage of these points will reduce the amplitude of the output pulses. Although a higher signal/noise ratio may be achieved, a greater number of turns will be needed in the output winding. The better signal/noise ratio of the output pulses with the decrease of the 'interrogate' frequency is a phenomenon of the ferrite material and not of the shape of the multi-aperture device. The slower the rise-time of a pulse applied to a ferrite core, the less pronounced will be the elastic switching of the material.

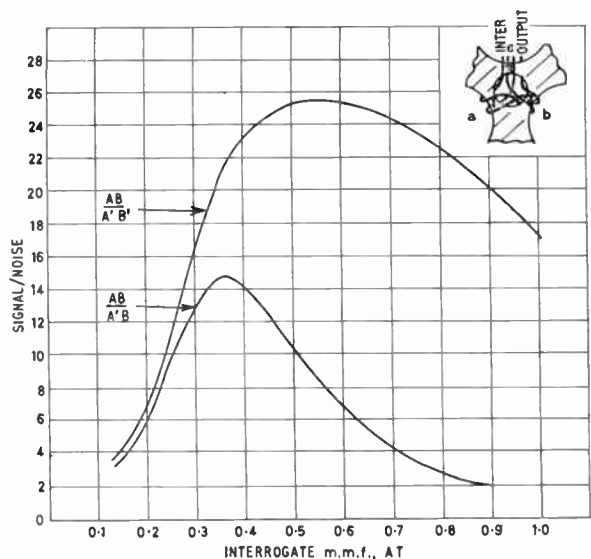


Fig. 5. Signal/noise ratio of the non-destructive read-out pulses with equal turns on legs 1, 2 and 3.

Figure 6 shows the setting characteristics of the device, where the setting m.m.f. refers to the input m.m.f.'s applied simultaneously to the two large apertures a and b, having the same magnitude applied to both apertures. The device is continuously interrogated by a constant interrogate m.m.f., while the set m.m.f. is varied, and after each set pulse the device is fully blocked by the maximum required field. This test was repeated for different values of interrogate m.m.f.'s. It can be seen from these curves that any increase in the input m.m.f., above the threshold m.m.f., will not change the amplitude of the output pulses which will remain constant. Any increase in the input m.m.f. will not change the point where the device is fully set but will change the switching time required for the device to set. The maximum amplitude of the output pulses obtained from the minor

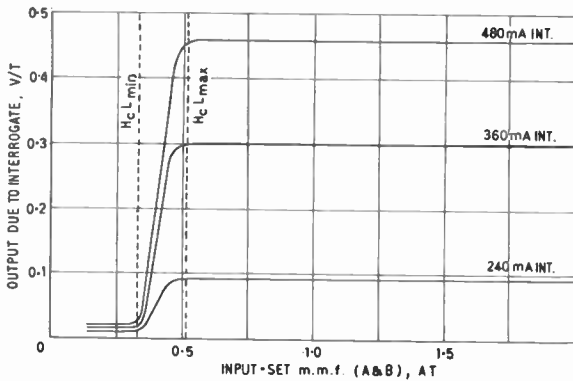


Fig. 6. Degree-of-setting as a function of the 'interrogate' m.m.f.

aperture will depend on the magnitude of the interrogate m.m.f. (provided that the interrogate m.m.f. is within its operation limits) and not on the magnitude of the set m.m.f.'s.

The minimum m.m.f. required to start the switching round the large aperture will be  $F_{min} = H_c L_{min}$  having  $L_{min} = 2\pi r$  where  $r$  is the radius of the large aperture. The minimum m.m.f. required fully to switch the material along a path round the large aperture will be  $F_{sat} = H_c L_{max}$  having  $L_{max} = 2\pi(r+d)$  where  $d$  is the minimum width of a leg. Any increase of the set m.m.f. above  $F_{sat}$  will not change the amount of material switched along the path but will reduce the switching time required for the domains to change their orientation. These two points,  $F_{min}$  and  $F_{sat}$ , can be easily seen in Fig. 6.

As the output pulses from the minor aperture remain constant for any amplitude of the set m.m.f.'s, provided they are above the threshold m.m.f., it is possible to apply any number of separate input m.m.f.'s on each input aperture. Hence, the characteristics of the device enables each aperture to operate as an OR gate, and the final output from the device will represent the following function:

$$out = (A_1 + A_2 + A_3 + \dots + A_n) \times (B_1 + B_2 + B_3 + \dots + B_n)$$

### 5. Destructive Read-out

The output pulses from the multi-aperture device may be produced in two forms, non-destructive read-out which can be produced at any given time and may be repeated indefinitely, or destructive read-out, where the output pulses are synchronous with the clock driving pulses. There are two destructive read-out pulses which are induced each time the device is switched from one state to another, one pulse when the device is set and another pulse when the device is reset to its blocked state. When trans-

ferring information from one device to another, it is usual to take the output at the time the device is reset.

On the assumption of the validity of the flux patterns shown in Fig. 3, it would first be necessary to switch the flux round the minor aperture after the device had been set in order to obtain the destructive read-out pulses from leg 3 of this device. This could be done by applying a single positive interrogate pulse round the minor aperture, which will reverse the flux in leg 3, in a manner shown by the change from Fig. 3(c) to Fig. 3(d). This method is often used in other shaped multi-aperture devices and this single pulse is known as the 'prime' pulse. The 'prime' pulse could easily be supplied by a d.c. m.m.f. which would eliminate the need for an extra clock pulse, provided the same amplitude limitations given to the interrogate m.m.f. are also given to the prime m.m.f.

According to the flux pattern given in Fig. 3, no output pulse can be obtained from leg 3 unless it has first been set by the two input m.m.f.'s (Fig. 3(c)), and then primed (Fig. 3(d)). In actual fact it was found that an output pulse is obtained from the winding round leg 3 even without the 'prime' m.m.f. being applied. This unpredicted result called for further investigation into the flux patterns of the device which proved that the initial flux patterns given in Fig. 3(c) and (d) were completely wrong. Although all the curves given in the previous section indicated that the predicted behaviour of the device was the correct one, these results were only misleading. The curves, which give a true picture of the non-destructive operation of the device, could also be explained by completely different flux patterns which are more complex than the original predicted flux patterns.

In order to investigate the flux switching path in the device, three separate windings were wound round the minor aperture, one on each of the three legs as shown in the wiring diagram given in Fig. 7. It was found that output 1 on leg 1 gave an output pulse only for an input combination of  $AB'$  but no

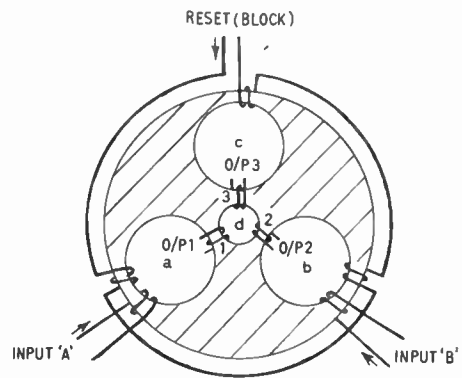


Fig. 7. Wiring diagram of test.

output for the input combinations of  $AB$ ,  $A'B'$ ,  $A'B$ . Output 2 gave an output only for  $A'B$  but not for  $AB$ ,  $A'B'$ ,  $AB'$ . Output 3, which according to the initial assumed flux patterns should not have given any output, gave an output pulse for an input combination of  $AB$  but no output for  $A'B'$ ,  $AB'$ ,  $A'B$ . From these experimental results it can be seen that when the two input m.m.f's are applied to each of the two input large apertures, they do not switch round each large aperture separately, as had been anticipated, but the two induced fields add up together and switch along a single longer path which is round both the large input apertures as shown in Fig. 8.

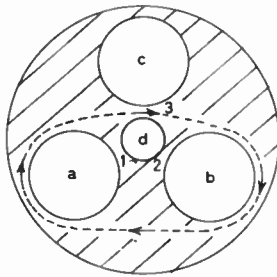


Fig. 8. Flux switching path during 'input-set'.

The remanence flux pattern of the device, after the termination of the two input fields, is of a complex nature and has no relevance to the operation of the device. In order to maintain flux continuity in the device, there will be further domain motion in the device, after the termination of the driving fields. The extra domain motion will not affect the flux pattern in the three legs round the minor aperture which will remain saturated, after the termination of the pulses, in the direction of the previous induced fields. Figure 9 shows the flux patterns in the three legs for different switching modes of the device.

With the true flux patterns of the device it is still possible to read the device non-destructively and this will correlate with all the curves given in the previous section. When the device is interrogated, no output can be obtained from the minor aperture when the device is in its blocked state (Fig. 9(a)), or when only one input is applied (Fig. 9(b)). This is because in both these cases, the flux in leg 3 is saturated in an opposite direction to the flux in leg 2 or leg 1 or to both of them. Only after both have been applied, when the device is in its set state as shown in Fig. 9(c), can the interrogate field switch the flux round the minor aperture. This is possible, as now the directions of the flux in all the three legs are in the same direction in relation to a field induced round the minor aperture. The first negative interrogate pulse will reverse the

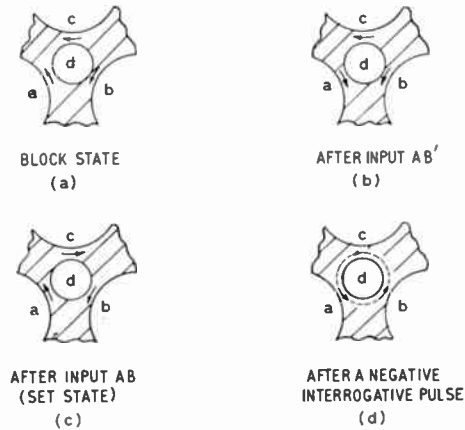


Fig. 9. Flux patterns round the minor aperture in different modes of operation.

flux round the minor aperture, as shown in Fig. 9(d), and the first positive pulse will reverse it back again.

The guidance of the flux round a longer switching path, when both inputs are applied (as was shown in Fig. 8), could be explained by two different hypotheses. Both of these sound plausible although the second seems more feasible. It may probably be a function of both hypotheses.

For the first explanation, it is assumed that although the switching of the flux is controlled by the minimum cross-sectional area of the path, the induced field could still have some effect on the whole cross-sectional area. That is, there will be remanent switching in the area controlled by the minimum cross-sectional area of the path, and there could be some elastic switching round the boundary of the path. When both 'input-set' m.m.f's are applied to apertures a and b of the device, two opposing fields are induced in the material between the two apertures (Fig. 3(c)). Although the cross-sectional area of the material between the two apertures is wide enough to accommodate both opposing switching paths, the elastic effect along the boundary of both paths will oppose any switching in the neighbouring path. As leg 3 provides an alternative switching path, which will have a lower reluctance in relation to the reluctance of the material between the two large input apertures, the switching will be along this leg and round the two outer legs of the two large apertures (Fig. 8).

The second explanation is simpler. When both input m.m.f's are applied simultaneously, the two induced fields will add up to one combined field and will switch along its effective shortest available path. Although the shortest available path for each individual input is round each large aperture separately, the sum of the two path lengths round each of the two

apertures is much longer than the effective path which is round the outer legs of both large apertures.

The flux switching path, along leg 3 and round the outer legs of the two input apertures, may occur only when both input fields are induced simultaneously. If both inputs are induced sequentially, i.e. first *A* and then *B* (or vice versa), then the flux will switch first along leg 1, due to input *A*, and then along leg 2, due to input *B*, whilst leg 3 will not be affected at all. Thus, when the inputs are applied sequentially the flux switching pattern will be as given in Fig. 3(c).

The fact that the switching of the flux follows a different pattern from that anticipated does not prevent the use of the destructive read-out pulse, from the device, for logical operations. Indeed, the new flux pattern enables the use of the device for a wider range of combinational logical operations. When taking the output from a winding on leg 3, the device will operate as a two input AND gate (*AB*) and when taking the output from legs 2 or 3 the device will operate as an inhibit gate (*AB'* or *A'B*). Furthermore, by taking the output from legs 2 and 3 together, i.e. a combined output round both legs, the device will operate as an exclusive-OR gate (*AB' + A'B*).

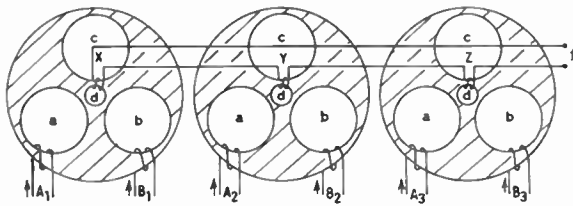


Fig. 10. AND-OR operation.

$$f = X + Y + Z = A_1B_1 + A_2B_2 + A_3B_3.$$

By suitably connecting different combinations of the input and output windings, it is possible to extend further the logical applications of this device. For example, by connecting in series the output windings of a number of these devices as shown in Fig. 10. As the output winding on each device is on leg 3, each device will function as an AND gate and the common serial output will represent an AND-OR combination. Any voltage pulse which is induced in any of the output windings will appear across the common-output terminals. However, the noise output pulses from each device will add up and the summed noise would also appear across the common output terminals, consequently reducing the signal/noise ratio of the common output pulse. Hence, the number of devices that may be connected in series must be limited. The common serial output will represent the following function, where *X*, *Y*, *Z* represent the output from each device:

$$f = X + Y + Z = A_1B_1 + A_2B_2 + A_3B_3$$

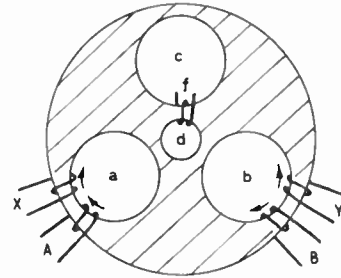


Fig. 11. OR-inhibit-AND operation.

$$f = (A + X)(BY')$$

Similar to the non-destructive read-out pulses, the amplitude of the destructive read-out pulses will remain approximately constant with variation of the applied m.m.f.'s, provided they are larger than the threshold m.m.f.'s. Thus each large input aperture could be the OR function and the output from each of the three legs could represent the following combinational logical operation:

$$\text{Output leg 1} = (A_1 + A_2 + \dots + A_n)(B'_1 + B'_2 + \dots + B'_n)$$

$$\text{Output leg 2} = (A'_1 + A'_2 + \dots + A'_n)(B_1 + B_2 + \dots + B_n)$$

$$\text{Output leg 3} = (A_1 + A_2 + \dots + A_n)(B_1 + B_2 + \dots + B_n)$$

An inhibit operation may be obtained in any one of the input large apertures, by inducing a field in a direction opposing the input-set field. Consequently no switching can occur in that aperture while the inhibit field is induced. An example of such an operation is shown in Fig. 11, where the input aperture *b* is inhibited by the field *Y*. Input aperture *a* of the device shown in Fig. 11 operates as an OR function, so the output from this device, when the output is taken from leg 3, will represent the following function:

$$f = (A + X)(BY')$$

The most interesting application of this device is that one single device may operate as a half-adder, as shown in Fig. 12. In this application, advantage is taken of the flux switching paths in all the three

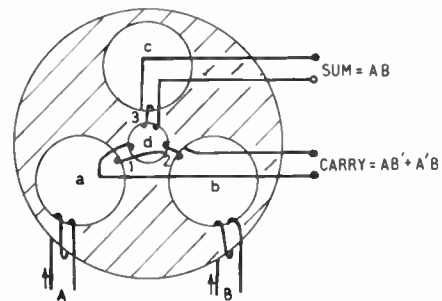


Fig. 12. Half-adder.

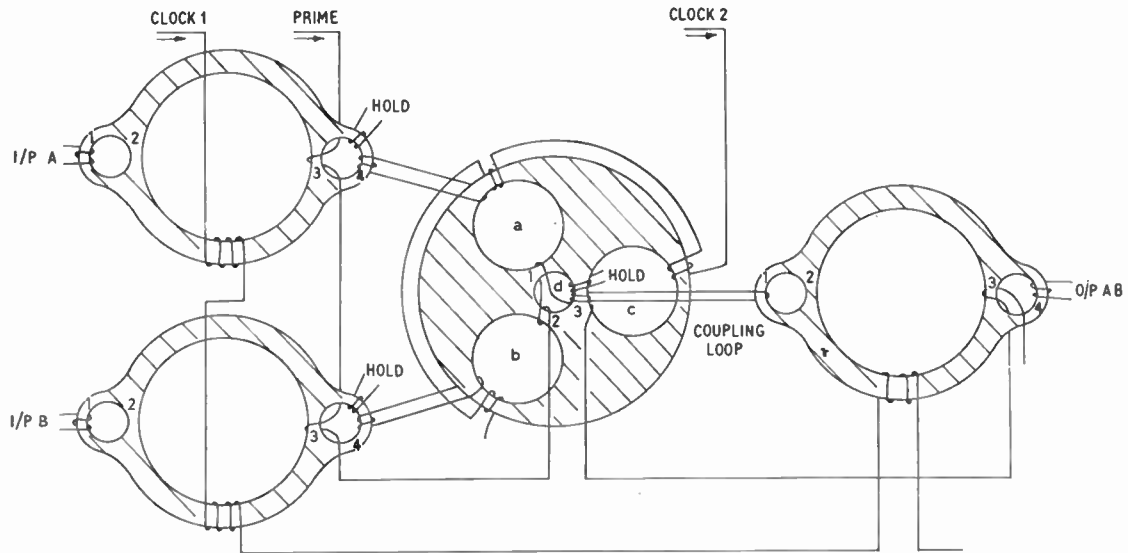


Fig. 13. AND operation in all-magnetic logic.

legs round the minor aperture. The sum output ( $AB$ ) is taken from a winding round leg 3 whilst the carry output ( $AB' + A'B$ ) is taken from the combined winding round legs 1 and 2.

**6. Operation in All-Magnetic Circuits**

One of the early major disadvantages of using magnetic materials, whether ferrite cores or multi-aperture devices, for logical applications is the necessity for transistors, or other components, as buffers between stages. In recent years considerable development has been concentrated on 'all-magnetic' logic circuits<sup>3-8</sup> where the connection between components is of wire only with no extra components required. Multi-aperture devices are ideal for all magnetic logic circuits, since the various switching paths within these devices can provide the isolation between the input and output circuits. Thus, it is possible to load the devices heavily by very low impedance coupling loops, without reflecting the output load to the input circuits. Once a device is set, a prime field, which is usually induced by a d.c. m.m.f., transfers the information from the input switching path to the output circuit. Because of the low impedance imposed on the output circuit, the prime operation will be relatively slow. Both input and output circuits in each device are controlled by the reset-block field.

The AND shape multi-aperture device could easily be used in all-magnetic logical applications, but only in its AND mode with no other logical operations possible. The devices connected to the input and output may be of any shape, provided that these devices can exhibit the feature of input and output

isolation. The connection between the AND device with other devices, in all-magnetic application, is demonstrated in Fig. 13. The operation of the input and output devices is not important for the operation of the AND device and is only included in Fig. 13 for demonstration purposes.

The sequence of operations of the AND device is similar to that explained before, although the flux switching paths will be different. When the two input devices are blocked by clock 1 pulse, there will be flux switching in leg 4 of both input devices, provided they were both previously in their set state. This change of flux in leg 4 of both input devices will induce an output voltage which will cause a current to flow in the input coupling loops in a direction to set the AND device. The prime field will switch the flux in the output leg and then when the device is blocked by the clock 2 pulse, the flux in that leg is switched back. This in turn will cause a current to flow in the output coupling loop which will consequently set the output device. Clock 1 and clock 2 are pulsed alternately.

The coupling loop between the devices is of wire only and its resistance, which will be only a fraction of an ohm, is controlled by the wire gauge and length. The low impedance of the coupling loop will have no effect on the input circuit of the AND device, except that a much larger m.m.f. would be required to reset the device into its blocked state. However, the low impedance imposed on the output circuit, i.e. on leg 3, will heavily damp the device which will cause the flux to switch along a different switching path from what was shown in Fig. 8. As this device can provide a number of switching paths, the damping of leg 3 by

the coupling loop will not prevent the device from being used in all-magnetic applications. Indeed, the existence of an alternative switching path, other than leg 3, when the input is applied, provides the required input/output isolation.

When both input fields are induced in the two input apertures a and b they will seek a path with a minimum energy state, i.e. a path which presents the lowest reluctance. In the absence of the low impedance imposed on the device, the lowest energy path will be along leg 3, but by loading this leg the reluctance along the leg is increased. An alternative switching path can be provided by leg 1 and leg 2, since the direction of the flux in these legs, when the device is in the block state, is the same as the flux direction in leg 3 in relation to fields round the input aperture, as can be seen in Fig. 3(a) and in Fig. 9(a).

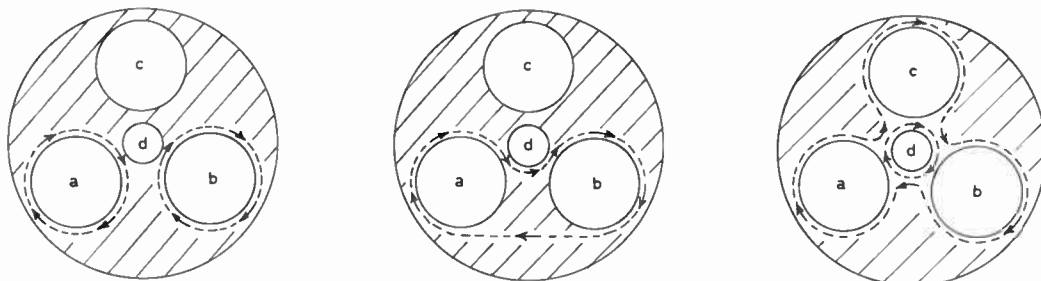
When the two input-set fields are induced in the two input apertures with the device heavily loaded, they may switch along two possible paths; however, in each of these alternative cases the path is along leg 1 and leg 2 and not along leg 3. There is no experimental evidence which can distinguish between the two different switching paths as the flux pattern round the minor aperture will be the same in both cases. The switching paths, when both input fields are induced, could be round each input aperture separately, as shown in Fig. 14(a). Alternatively, the switching path may be round the outer arms of the two input apertures and along legs 1 and 2 of the centre aperture as shown in Fig. 14(b). There is no way of defining which one of these switching paths is the actual one, but from a practical point of view there is no difference between the two paths, as the aim of the input operation is to switch the flux in legs 1 and 2 but not in leg 3. A winding, round the arm between the apertures a and b, will reveal no flux change for either of the two theories of the flux switching paths. In the case shown in Fig. 14(b) there is no flux switching in the centre arm whilst in the case shown in Fig. 14(a) flux switching does occur in

that arm but the resultant flux change will be equal to zero. If only one input field is applied, the switching path will be round one input large aperture; this applies to both switching theories.

The final flux pattern round the centre aperture is only achieved if leg 3 is heavily loaded by the coupling loop. If this low impedance load is removed, the flux switching path, when both input fields are applied, will be along leg 3 whilst legs 1 and 2 will not be affected as shown previously in Fig. 8. Furthermore, loads in the range of tens of ohms will still cause switching as outlined in Fig. 8. Only if the load is a fraction of an ohm, as with the impedance of the coupling loop, will the flux switch as outlined in Fig. 14.

The prime field, after the device is set, can switch the flux round the minor aperture, along legs 1, 2 and 3. Although leg 3 is heavily loaded, the prime field may still switch the flux in that leg, provided sufficient time is given for this operation to occur. The pattern in the device after the prime operation is shown in Fig. 14(c) which is the same as given in Fig. 3(d). As in the case of the 'interrogate' field, the widest operational range for the prime field is obtained when the prime m.m.f. is shared between the three legs.

Care must be taken to prevent back-flow of information from the output-device back into the AND device. When the output-device is switched by a clock 1 pulse (Fig. 13) there will be a change of flux in leg 1 of this device, causing back flow of current in the coupling loop which is in a direction to switch flux in the output leg of the AND device. To avoid this danger, it is possible to 'hold' the output leg of the AND device by inducing a field in that leg which is in a direction opposing the back flow of current. This hold field must be induced only on leg 3 of the AND device and only when the output device is driven, so as not to change the flux pattern round the minor aperture. These limits apply only to the AND device and not to multi-aperture devices where the control



(a) and (b) Alternate switching paths during 'input-set' when the device is heavily loaded. (c) After prime operation.

Fig. 14. Flux patterns in the device when it is heavily loaded.

of operation is from one large aperture. In the AND device the control is from three large apertures. Examples of such multi-aperture devices with centre control are the input and output devices shown in Fig. 13. The coupling loop, too, must only be on leg 3 of the AND device so as not to load any other leg which may change the flux switching paths.

If only one input m.m.f. is applied, there will be switching round only one of the two input large apertures. Thus with only one input field induced, only leg 1 or leg 2 will switch but not both legs. The prime field, when only one field is applied, will not be able to switch any flux round the minor centre aperture, as the direction of flux in leg 1 or leg 2 will be saturated in an opposite direction to that of leg 3.

### 7. Conclusions

The features of this special-shaped device are attractive for logical applications. One single device may produce a wide range of complex combinational logic functions, whereas if semiconductors are used, then a number of diodes and/or transistors are required for the same operation. Furthermore, the device can store the result obtained from the logical operation, whilst with other components, an extra store (usually a flip flop) must be added.

The device may also be used in all-magnetic logic circuits along with other shapes although it can then only operate in its AND mode. In these all-magnetic circuits, where the semiconductors are dispensed with, a higher reliability of operation is achieved.

The tolerances of the driving currents are extremely wide and are not as limited as in ferrite toroidal cores, but must exceed a threshold in order to switch the flux round a selected path.

It has been shown in this paper that the flux patterns are necessary for understanding the performance of multi-aperture devices. In addition, it has been demonstrated that the consideration of the various flux switching paths within the device enable it to be used for different logical applications.

Future development should be concentrated on different configurations mainly for all-magnetic logical circuits.

### 8. Acknowledgments

The author wishes to thank English Electric-Leo Computers Limited for permission and facilities to publish this paper.

### 9. Bibliography

1. J. A. Rajchman and A. W. Lo, "The transfluxor", *Proc. Inst. Radio Engrs*, **44**, p. 321, March 1956.
2. F. Schrieber, "Der Transfluxor als Verstärker", *Nachrichtentechn. Fachberichte*, **21**, pp. 76-92, 1960.
3. N. S. Prywes, "Diodeless magnetic shift registers utilizing transfluxors", *Trans. Inst. Radio Engrs (Electronic Computers)*, **EC-7**, p. 316, December 1958.
4. H. D. Crane, "High speed logic system using magnetic elements and connecting wire only", *Proc. Inst. Radio Engrs*, **47**, p. 63, January 1959.
5. D. R. Bennion, "MAD-resistance type magnetic shift register", *Proceedings of Special Technical Conference on Non-linear Magnetics and Magnetic Amplifiers*, (A.I.E.E., T-121), p. 96, October 1960.
6. V. F. Gianola, "Integrated magnetic circuits for synchronous sequential logic machines", *Bell Syst. Tech. J.*, **39**, p. 295, March 1960.
7. V. F. Gianola, "Computer devices, possibilities of all-magnetic logic", *J. Appl. Phys.*, **32**, Supplement, p. 27S, March 1961.
8. D. R. Bennion, H. D. Crane and D. C. Englebart, "A bibliographical sketch of an all-magnetic logic system", *Trans. Inst. Radio Engrs (Electronic Computers)*, **EC-10**, p. 203, June 1961.
9. A. W. Vinal, "The development of a multi-aperture reluctance switch", *Proceedings of Western Joint Computer Conference*, p. 443, May 1961.
10. V. F. Gianola and T. H. Crowley, "The laddic—a magnetic device for performing logic", *Bell Syst. Tech. J.*, **38**, p. 45, January 1959.
11. H. H. Georgens and L. I. Duthie, "Multi-aperture core logic: new reliability for industrial telemetry", *Control Engineering*, **9**, p. 75, March 1962.
12. S. M. Chalmers and L. Norde, "Digital telemetering and control for an irrigation system using multi-aperture magnetic logic", *Communication and Electronics*, **32**, No. 66, p. 163, May 1963.

*Manuscript first received by the Institution on 19th September 1963 and in final form on 7th November 1963. (Paper No. 885/C67.)*

© The British Institution of Radio Engineers, 1964

# Radio Engineering Overseas . . .

The following abstracts are taken from Commonwealth, European and Asian journals received by the Institution's Library. Abstracts of papers published in American journals are not included because they are available in many other publications. Members who wish to consult any of the papers quoted should apply to the Librarian, giving full bibliographical details, i.e. title, author, journal and date, of the paper required. All papers are in the language of the country of origin of the journal unless otherwise stated. Translations cannot be supplied. Information on translating services will be found in the Institution publication "Library Services and Technical Information".

## MODULATION OF LIGHT WAVES

The most significant wide-band modulation methods for light waves are described in a recent paper by a German engineer, and it is shown that the control of emission processes (internal modulation) in light sources has gained practical importance due to the semiconductor laser. Modulators in which suitable optically-active solid bodies or fluids act on the light waves are described; controlled electrical, magnetic or mechanical processes produce the necessary variations of the optical characteristics (external modulation).

"Light modulators for wide frequency bands", W. Klockhaus. *Nachrichtentechnische Zeitschrift*, 16, No. 11, pp. 561-568, November 1963.

## DIRECTIONAL AERIALS FOR SHARED TELEVISION CHANNELS

In a paper which was presented at an Australian I.R.E. Convention two practical examples were described of the design of two-element directional aerial systems for operation in the 525-1605 kc/s band. They were designed to give directional characteristics which are suitable for night-time restrictive services on common frequencies. The methods used to obtain the characteristics of individual theoretical matching networks and feeder systems have proved to be very accurate in practice. Procedures for adjusting directional systems in both azimuth and elevation are described in detail with a derivation of practical figures for the individual radiator and mutual impedances. These measured values may be substituted for those assumed in the preliminary theoretical investigations and working values are obtained for the components of the various networks.

"Directional aerials for medium-frequency broadcasting", N. J. Medlin. *Proceedings of the Institution of Radio Engineers Australia*, 24, No. 10, pp. 734-748, October 1963.

## ERROR PROBABILITIES IN BINARY TRANSMISSION

In a paper by a German engineer the error probabilities of binary transmission systems are calculated for Rayleigh fading and optimum diversity reception of  $n$ -th order and shown as a function of the error probability with non-diversity reception. Although the error probability of non-coherent transmission methods is reduced more by diversity reception than in the case of coherent methods, the coherent systems remain decidedly superior in diversity

reception. Under the assumption of a uniform information flow an expression is given for the bit error probability of protected codes for Rayleigh fading and  $n$ -tuple diversity reception. An example explains the application of these results. The influence of the fading correlation in the diversity channels is calculated and shown in diagrams as a function of the signal/noise ratio. The paper finally studies the effects of frequency-selective fading with the different methods of modulation. With amplitude and phase keying the error probabilities are accordingly not changed by frequency-selective fading as compared to the case of non-selective fading. With frequency shift keying, however, the error probability is increased less by selective fading than from uniform fading affecting all the frequencies of a transmission channel.

"The error probabilities of binary transmission with diversity reception and frequency-selective fading", P. Besslich. *Archiv der Elektrischen Übertragung*, 17, No. 6, pp. 271-277, June 1963.

## APERTURE-CORRECTION IN FACSIMILE TRANSMISSION

Methods of compensation of two-dimensional imaging errors, caused in the scanning of original picture copy, are described in a German paper. The transfer constants and block diagrams of suitable networks are communicated for sequential and interlaced scanning. A particular feature of these networks are delay elements giving the picture signal with a delay corresponding to multiples of the duration of one scanning line. The necessary conditions for quantitative dimensioning of the equalizer networks are communicated. Also discussed are different models of the scanning diaphragm to get a lead on the practical realizability of the explained compensation. Particular clarity of the discussions is obtained for the case that the scanning diaphragm has a radial transparency function that follows a Gaussian bell curve. In such a case the equalizer network can be divided in two sections effecting respectively the compensation in horizontal and vertical direction. On the whole it seems that two-dimensional imaging errors produced in the transmission of picture copy can be theoretically compensated for within wide limits in the amplifier channel. Technically however great difficulties are encountered so far in the generation of the required long delays during which the picture signal must be stored.

"Basic principles and limitations of two-dimensional aperture correction in picture scanning", F. Arp. *Archiv der Elektrischen Übertragung*, 17, No. 6, pp. 295-309, June 1963.